New Q-Enhanced Planar Resonators for Low Phase-Noise Radio Frequency Oscillators

By

Morteza Nick

A dissertation submitted in partial fulfillment
of the requirements for the degree of
Doctor of Philosophy
(Electrical Engineering)
in The University of Michigan
2011

Doctoral Committee

Professor Amir Mortazawi, Chair
Professor Kamal Sarabandi
Associate Professor Anthony Grbic
Associate Professor Jerome P. Lynch

To my parents.

ACKNOWLEDGEMENTS

The completion of this dissertation would not have been possible without the help and encouragement of many people. First, I would like to sincerely thank my research advisor Professor Amir Mortazawi for his continuous support and encouragement, and for the opportunity he provided for me to conduct independent research. I also sincerely thank my other committee members, Professor Kamal Sarabandi, Professor Anthony Grbic, and Professor Jerome Lynch for their interest and valuable expertise, time, and effort in advising my dissertation work.

I also would like to thank all my friends with whom my relationship expands beyond the circle of professional acquaintances. Specially thanks to my very good friends, Dr. Ali Nazari and Dr. Alireza Tabatabaeenejad, for their invaluable friendship and support since the very first days I came to the United States. My special thanks also to my other good friend Sepehr Entezari with whom I spent wonderful times during the past three years. Also my gratitude to all my other friends in the Radiation Laboratory and EECS department, and my friends in Ann Arbor, who made my stay in Michigan enjoyable.

Finally, I am most grateful to my family in Iran, whose unconditional love and support has lit my way through the life. Specially, I thank my father Gholam-Abbas and my mother Najmeh, who were my first teachers and their love and encouragement inspired my passion for learning. It is to commemorate their love that I dedicate this thesis to them.

Morteza Nick

June 2011

TABLE OF CONTENTS

List of Tables

List of Figures

ABSTRACT

New Q-Enhanced Planar Resonators for Low Phase-Noise Radio Frequency Oscillators

by

Morteza Nick

Chair: Amir Mortazawi

Low phase-noise oscillators are key components of high-performance wireless transceivers. Traditional oscillator designs employ *single resonators* whose quality-factors are limited and depend on the resonator fabrication technology. In particular, planar resonators suffer from excessive conductor and substrate losses, limiting their achievable quality-factor. This work investigates *complex resonant structures*, capable of overcoming the limited quality-factors of planar circuits. The proposed methods can be applied to design miniaturized, very low phase-noise, voltage-controlled-oscillators at microwave and millimeter-wave frequencies.

The application of elliptic filters as frequency stabilization elements in the design of low phase-noise oscillators is introduced. By taking advantage of the large quality-factor peaks formed at the pass-band edges of elliptic filters, significant phase-noise reductions are achieved. Active resonators are incorporated in the design of elliptic filters to compensate for the losses and boost their quality-factors. The problem of added

noise in active resonators is addressed and a design procedure is presented that allows for active resonators' full loss compensation with minimum noise-figure degradation. An X-band oscillator is designed employing a four-pole active elliptic filter as a frequency stabilization element within its feedback network. The high-Q and low-noise properties of the active elliptic filter enable the oscillator to achieve a record low phase-noise level of -150 dBc/Hz at 1 MHz frequency offset in planar microstrip circuit technology.

The thesis concludes with a novel voltage-controlled-oscillator that achieves a state-of-the-art phase-noise performance while having a compact and planar structure. The oscillator's core is an active elliptic filter which provides high frequency-selectivity and, at the same time, initiates and sustains the oscillation. The elliptic filter is implemented using a dual-mode square-loop resonator. This technique not only helps reduce the VCO's size, but also eases the frequency-tuning mechanism. The proposed VCO structure occupies a small area making it suitable for integrated circuit fabrication at millimeter-wave frequencies.

Chapter 1

Introduction

1.1 Motivation

The wireless communication market has been experiencing tremendous growth and will continue to do so in the next decade. Innovations in this area have not only provided easy access to information through cell phones and other wireless networks but are also opening new possibilities in other areas such as remote health monitoring for patience, remote sensing of the environment, etc. Future wireless communication units will require higher speed for faster data transmit rate, higher operation frequency to accommodate more channels and users, more functionality, light weight, lower power consumption, and low cost. To meet these requirements, the development of high-performance wireless transmitter and receiver systems at microwave and millimeter-wave frequencies has been accelerated.

Oscillators are vital components of any radio frequency (RF) communications system. They are necessary for the operation of phase-locked loops commonly used in frequency synthesizers and clock recovery circuits, and are also present in digital electronic systems which require a reference clock signal in order to synchronize operations. Noise is of major concern in oscillators because introducing even a small amount of noise into an oscillator leads to dramatic changes in its frequency spectrum and timing properties. This phenomenon is known as *phase-noise* or *timing jitter*. Oscillator phase-noise in wireless transceivers limits the overall performance of communication systems in a variety of ways. Phase-noise directly affects adjacent-channel interference and bit-error-rate. Phase-Noise of the local oscillator in a radio

receiver down-converts the adjacent channels into intermediate frequency thereby limiting receiver's immunity to nearby interference and jamming. With complex modulation schemes such as OFDM, the requirement of spectral purity is even more stringent [1], [2]. Phase-noise in wireless transmitters can also overwhelm the adjacent weak channels. In general, an oscillator's phase-noise determines the overall communication system's capability and places stringent requirements on the performance of other transceiver blocks such as the noise-figure of low-noise amplifiers, rejection factor of filters and the output power of power amplifiers. Since the number of wireless subscribers and thus, the amount of RF interference continue to increase, modern communication standards demand excellent phase-noise performance from local oscillators in transceivers.

The design of low phase-noise oscillators faces many challenges at microwave and millimeter-wave frequencies. The main limiting factor in designing low phase-noise oscillators at these frequencies is the low quality-factor of resonators due to high conductor and dielectric losses. Therefore in current microwave and millimeter-wave systems, dielectric resonator oscillators (DROs) are widely employed [3]. Dielectric resonators (DRs) provide high unloaded quality factors. However, DROs suffer from several major drawbacks. The main drawback of DRs is their large sizes as compared to the rest of the oscillator circuit. Furthermore DRs are not amenable to integration and not suitable for mass production because of their 3-D structures and the need for fine post-fabrication tuning.

Presently, microstip/stripline resonators are the most common choice for planar oscillator designs. Due to their small size and low fabrication cost, many microwave and millimeter-wave oscillators utilize microstrip/stripline resonators as their frequency stabilization elements. Moreover, the most attractive feature of these resonators is that they can be easily integrated with active circuits such as MMICs and RFICs because they can be manufactured by photolithography of metalized film on a dielectric substrate. Unfortunately, a major drawback of using planar resonators is their low quality-factors, which makes it difficult to design low phase-noise oscillators. This problem is more prominent in integrated circuits (ICs) where high degrees of thin conductor losses reduce

TABLE 1.1
Performance summary of several microwave and millimeter-wave oscillators made using different fabrication technologies

Device	**Resonator**	**Technology**	**Size***	**F_0 GHz**	**P_0 dBm**	**Efficiency**	**L(f)† dBc/Hz**	**FOM dBc/Hz**
GaAs HBT [4]	DRO	Nonplanar Hybrid	2.4×2.4×1.1 mm^3	23.8	3.3	3.4%	-146	-215.6
InGaP/GaAs HBT [5]	DRO	Nonplanar Hybrid	-	6.7	14	3.1%	-155	-202.5
---- [6]	DRO	Nonplanar Hybrid	6×6×3 mm^3	8	14.5	2%	-162	-208.6
HEMT [7]	Microstrip ring	Planar Hybrid	λ/4 × λ/4	12	5.3	48.7%	-116.2	-189.3
Si BJT [8]	Microstrip hair-pin	Planar Hybrid	λ/6 × λ/6	9	9	4.5%	-129	-185.6
SiGe BiCMOS [9]	Above-IC FBAR	Quasi-Integrated	0.35×0.30 mm^2	2.4	-2.5	1.9%	-144	-195.7
CMOS [10]	Ring	CMOS Integrated	λ/8 × λ/8	10	-15	1%	-110	-185.2
SiGe HBT [This Work, Chapter 6]	High-Q negative-resistance	Planar Hybrid	λ/8 × λ/8	8.2	7	12.5%	-149.5	-211.7

* Size of resonator, λ is the wavelength † Phase-Noise at 1MHz frequency offset.

the quality factor by orders of magnitude compared to hybrid circuit technologies.

Table 1.1 summarizes the performance of several microwave and millimeter-wave oscillators made using different fabrication technologies. Since oscillators operate at different frequencies and output power levels, in order to make a fair comparison, an oscillator figure-of-merit, *FOM*, is usually defined as following [11]

$$FOM = L(\Delta f) - 20log_{10}\left(\frac{f_0}{\Delta f}\right) + 10log_{10}\left(\frac{P_{DC}}{1mW}\right) \quad (1.1)$$

Here f_0 is the oscillation frequency, $L(\Delta f)$ is the phase-noise at the offset frequency Δf, and P_{DC} is the total consumed DC power in milli-watts. The *FOM* normalizes the phase-noise to the oscillation frequency and power consumption, providing a measure to compare the performance of various oscillators. As shown in Table 1.1, planar

oscillators' *FOM*s are worse by approximately 20 dB or more, compared to DROs, due to low quality-factor of their resonators.

1.2 Thesis Overview

The work carried out during the course of this thesis has been directed toward the design of high-Q planar resonators intended for low phase-noise applications. The proposed methods can be applied to design miniaturized very low phase-noise voltage-controlled-oscillators at microwave and mm-wave frequencies using hybrid or integrated circuit fabrication technologies. It is a common-practice to design oscillators using *single resonators*. However, in this case, the achievable oscillator Q is determined and limited by the resonator technology used. In particular, planar resonators suffer from excessive conductor and substrate losses limiting their achievable quality-factor. Therefore, conventional low phase-noise oscillator design techniques rely on reducing the losses in single resonators by manipulating their circuit designs and layouts. This work investigates *complex resonant structures*, including active and high-order resonant circuits, capable of overcoming the limited quality-factor of current planar hybrid and IC fabrication technologies. The high-Q properties of the proposed resonant structures allows for the design of oscillators with state-of-the-art phase-noise performance, close to the phase-noise of the DROs (shown in Table 1.1), while providing compact and planar structures compatible with hybrid and integrated circuit fabrication technologies.

The organization of this thesis is as follows.

Following the introduction, Chapter 2 provides an overview of phase-noise in oscillators, starting with the definition of phase-noise and moving on to describing the existing phase-noise models. The famous Leeson's phase-noise model is revisited and generalized to oscillators with complex resonant tanks as they are the subject of this thesis. Lesson's phase-noise formula employs the term "loaded quality factor", the definition of which is critical to understanding resonator design for low phase-noise oscillators. This issue is addressed in Chapter 3 where different definitions of resonator quality-factor are discussed and compared to each other. A figure-of-merit for resonators is introduced in order to evaluate their overall effect on the phase-noise of oscillators.

This figure-of-merit also serves as a basis for optimizing the design of various resonators for low phase-noise applications.

In chapter 4, a quality-factor enhancement technique based on employing high-order elliptic-response band-pass filters is introduced. The resonant properties of elliptic filters are described showing that they can achieve significantly higher quality-factors compared to single resonators. The filter optimization for low phase-noise applications is discussed. For experimental verification, an 8 GHz microstrip oscillator employing a four-pole elliptic filter as its frequency stabilization element is demonstrated.

Chapter 5 discusses active resonators and their application for low phase-noise oscillators. Active resonators are analyzed and a design procedure is presented to optimize their performance for low-noise applications. Analytical expressions are derived for the noise-figure and power consumption of active resonators providing a good understanding of the trade-offs involved in low phase-noise oscillator design using active resonators. In particular, it is shown that oscillators using single active resonators demonstrate low DC-to-RF power efficiencies. To mitigate this problem, it is suggested to use active elliptic filters in the feedback-loop of the oscillators, since they can achieve high quality-factors at lower noise-figures and power consumptions. An 8 GHz oscillator is designed and tested using a four-pole active elliptic filter. The oscillator demonstrates a state-of-the-art phase-noise performance compared to other reported planar oscillators.

Chapter 6 describes the resonant properties of dual-mode resonators and it shows that a compact high-Q active elliptic filter can be realized using a dual-mode square-loop microstrip resonator. The dual-mode elliptic filter is then used to design a miniaturized low phase-noise voltage-controlled-oscillator (VCO) at X-band. The oscillator consists of a reactively-terminated dual-mode active elliptic filter and a load matching network. In this configuration, the active filter not only provides high frequency-selectivity but also it initiates and sustains the oscillation. The new oscillator structure shows significant advantages in terms of size, power consumption and frequency tunability, while achieving similar state-of-the-art phase-noise performance compared to the oscillator described in Chapter 5. This makes the proposed VCO design technique attractive for integrated circuit designers at millimeter-wave frequencies.

Chapter 7 concludes the thesis with a summary of the work presented herein and suggests some future works regarding the IC fabrication of the proposed techniques at millimeter-wave frequencies.

Chapter 2
Fundamentals of Phase-Noise in Electrical Oscillators

2.1 Introduction

The output of an ideal sinusoidal oscillator can be expressed as $V_{out}(t)=A\cos(\omega_0 t+\varphi)$ where, A is the amplitude, ω_0 is the frequency, and φ is an arbitrary and fixed phase reference. Therefore, the spectrum of an ideal oscillator with no random fluctuations is a pair of impulses at $\pm\omega_0$. However, the existing noise sources in electronic systems cause random amplitude and phase fluctuations. The output of a noisy oscillator can be represented by

$$V_{out}(t) = \big(A + a(t)\big)\cos\big(\omega_0 t + \varphi(t)\big) \tag{2.1}$$

where $a(t)$ and $\phi(t)$ are random amplitude and phase-noise. As a consequence of the fluctuations, the spectrum of a practical oscillator is broadened in the vicinity of the carrier frequency. In practice, amplitude noise is much smaller than phase-noise due to the amplitude-restoring mechanism in oscillators [12]-[15]. This is illustrated in Fig. 2.1 where it shows the limit cycle of an ideal LC oscillator. The current noise perturbs the signal and causes its phasor to deviate from the stable trajectory, producing both amplitude and phase-noise. The amplitude deviation is resisted by the stable limit cycle, whereas the phase is free to drift. Therefore, oscillators almost exclusively generate phase-noise near the carrier.

In analog circuits, phase-noise is usually characterized in the frequency domain. It is expressed in units of dBc/Hz, representing the noise power relative to the carrier contained in a 1 Hz bandwidth centered at a certain frequency offset from the carrier

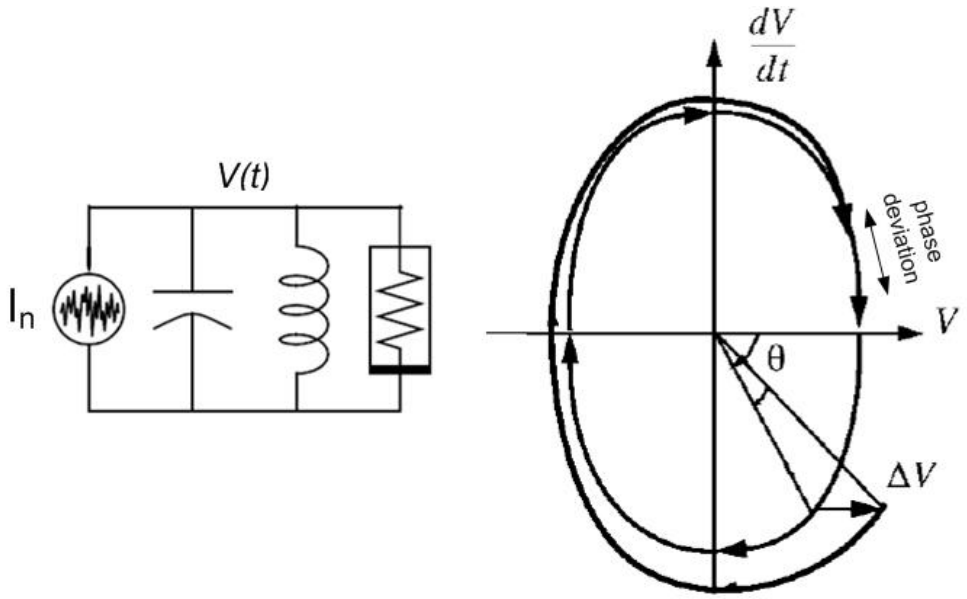

Fig. 2.1 Limit cycle of an ideal LC oscillator [14]. The current noise perturbs the oscillator's voltage by ΔV. The perturbed signal restores its stable amplitude whereas its phase is free to drift, causing strong random phase variations.

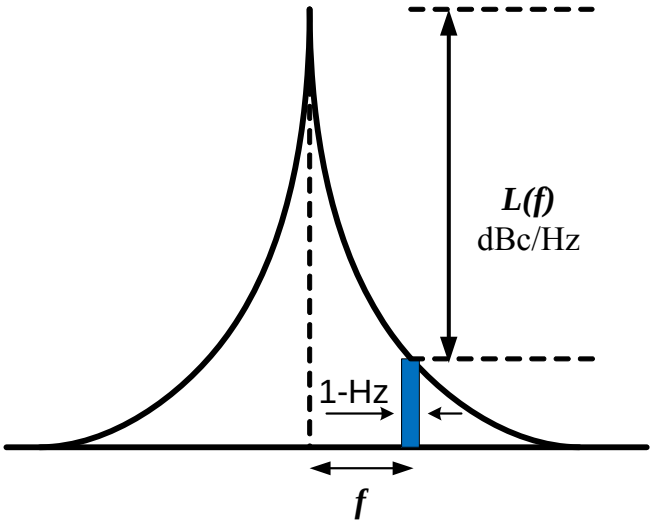

Fig. 2.2 Definition of the single-side-band phase-noise, *L(f)*.

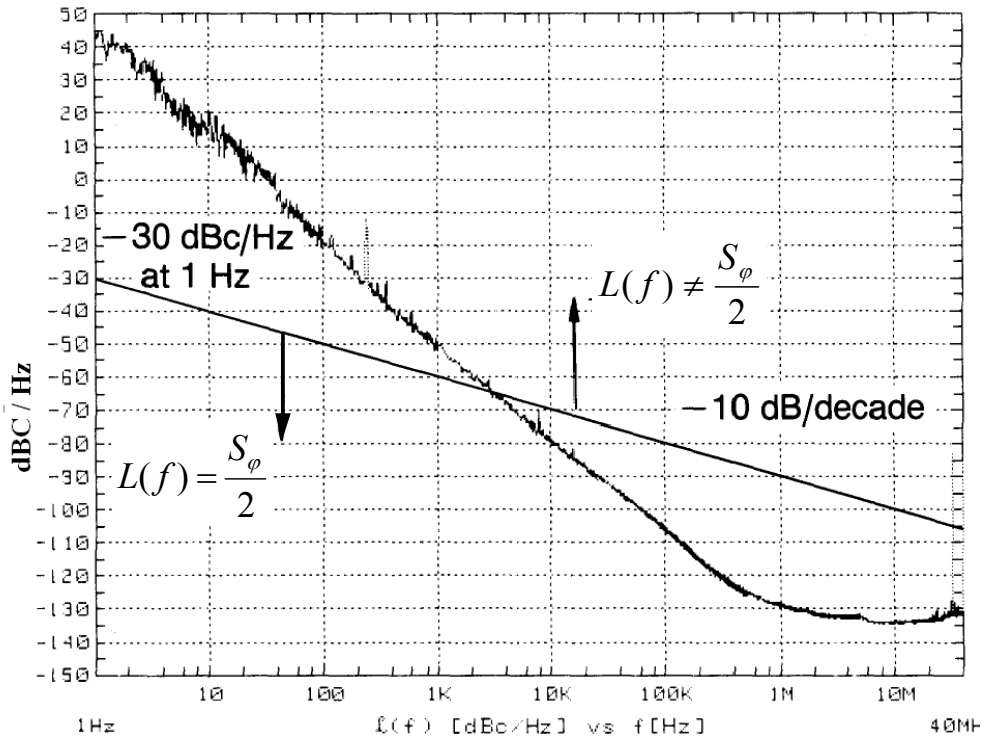

Fig. 2.3 The region of validity of (2.3) [15].

$$L(f) = \frac{\text{single-side-band power density per Hz at offset } f}{\text{carrier power}} \quad \frac{dBc}{Hz}. \tag{2.2}$$

The definition of *L(f)* is graphically shown in Fig. 2.2. It is noteworthy that *L(f)* uses the power spectral density of the output signal, which should be distinguished from the power spectral density of signal's phase-noise $S_\phi(f)$. From phase modulation theory and for small phase deviations it follows that [12]

$$L(f) = \frac{S_\varphi(f)}{2}. \tag{2.3}$$

This equation holds for most of the practical oscillators. However, one should be aware of its inaccuracy in case of high phase-noise levels where the phase deviations are not small. Fig. 2.3 shows the region of validity of (2.3). In particular, it fails for very close-to-carrier frequencies, where the phase-noise is strong and small angle assumption is invalid [15].

2.2 Phase-Noise Models

Oscillators are nonlinear time-varying systems due to the presence of large and periodic signals within their circuits. This makes the phase-noise analysis in oscillators a challenging task which has been the area of investigation for several decades. There are three major approaches to the problem. The simplest approach to the phase-noise analysis uses a linear time-invariant model for oscillators. The well-known Leeson's model for phase-noise is based on this method [16]. Assuming the phase-noise as a small perturbation, Leeson linearizes the oscillator circuit around the steady-state point in order to obtain a closed-form formula for phase-noise. While often of great practical importance, the Leeson's formula has two major defects. One is that it cannot correctly describe the upconversion of the low-frequency flicker noise components to around-carrier phase-noise, and the other is that it predicts an infinite phase-noise power. Using a linear time-variant model for the oscillator, Hajimiri and Lee [14] have proposed a phase-noise analysis method which explains this upconversion phenomenon, but it fails to correctly predict the phase-noise at frequency offsets very close to carrier. To overcome this problem, a nonlinear analysis is required such as harmonic-balance and Monte Carlo methods which are widely used in CAD simulations [17], [18]. Recently, Demir [19] presented a general method that can correctly predict the spectrum of the phase-noise; however, it is more suitable for numerical calculations.

Despite its simplicity, Leeson's phase-noise model is of great practical importance, giving useful design insights for low phase-noise oscillators. In this section, the Leeson's phase-noise model is discussed and generalized to oscillators using complex resonant circuits as they are the subject of this thesis.

2.2.1 Leeson's Phase-Noise Model Generalized to Oscillators with Complex Resonant Tanks

Consider the block diagram of a parallel-feedback oscillator, Fig. 2.4(a), which shows clearly the two basic elements: the amplifier with the gain of G, and the selective filter with the band-pass transfer function of $H(j\omega)$. The Barkhausen's condition for oscillator startup implies that, at frequency of oscillation ω_0 [20]

$$G\,H(j\omega_0) = 1\angle 0\,. \tag{2.4}$$

Namely, the total phase shift around the loop must be an integer multiple of 360°, with a steady-state gain of unity. It is worth noting that the general block diagram used for this analysis does not deal with the details of the oscillator, and thus the results are general.

Let us assume all the noise sources can be referred at the input of the amplifier with the power spectral density of

$$S_n(\Delta\omega) = \overline{|e_n(t)|^2} = FKT\left(1 + \frac{\omega_c}{\Delta\omega}\right) \tag{2.5}$$

consisting of a white-noise component (independent of frequency) and a flicker-noise component (inversely proportional to frequency). In the above equation F is the noise figure of the amplifier, K is Boltzmann constant, T is ambient temperature, $\Delta\omega$ is the frequency offset from the carrier, and ω_c is the frequency at which flicker and white noise components are equal, as known as flicker-noise corner frequency.

The additive noise source $e_n(t)$ modulates the oscillator's signal, as shown in Fig. 2.4(b), thereby generating phase uncertainty represented by

$$\Delta\theta(t) = \text{atan}\left(\frac{e_n(t)}{V_{in}(t)}\right) \approx \frac{e_n(t)}{V_{in}(t)} \tag{2.6}$$

$$S_{\Delta\theta}(\Delta\omega) = \frac{\overline{|e_n(t)|^2}}{\overline{|V_{in}(t)|^2}} = \frac{GFKT}{P_0}\left(1 + \frac{\omega_c}{\Delta\omega}\right) \tag{2.7}$$

where P_0 is the output power of the amplifier. According to the signal transmission theory, band-pass filtering of a phase-modulated carrier is identical to filtering of the modulating signal in the equivalent low-pass filter, $\hat{H}(j\Delta\omega)$ [21]. Therefore, one can use the low-pass equivalent of the oscillator's model (Fig. 2.4(c)) to find its phase-noise spectral density. This approach was first introduced in [22]. By writing the loop equation in Fig. 2.4(c) one obtains

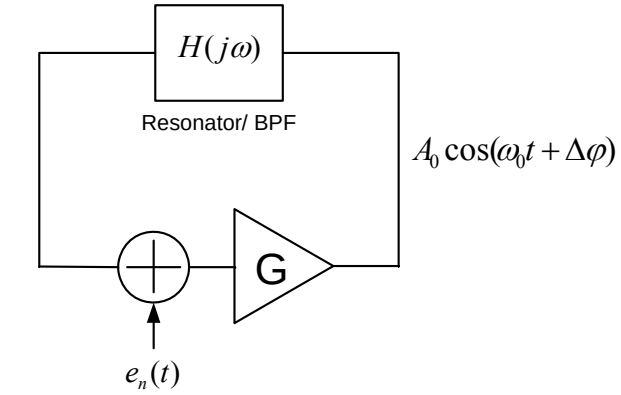

(a)

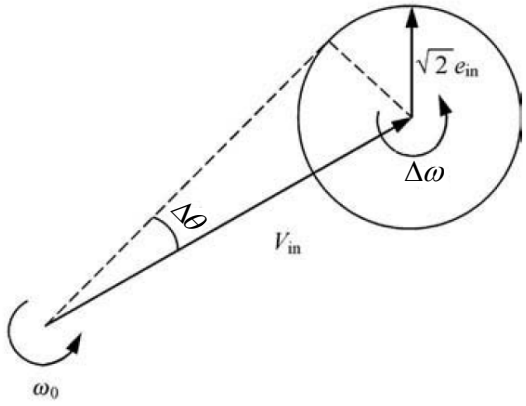

(b)

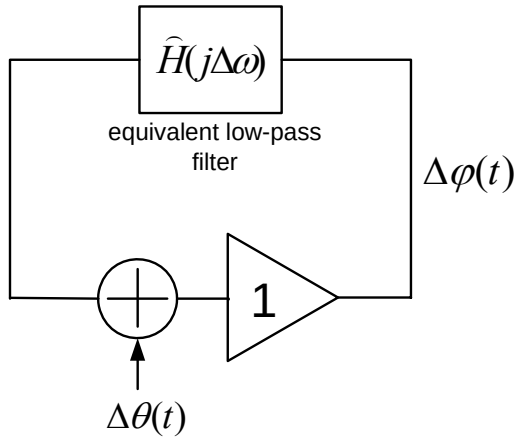

(c)

Fig. 2.4 (a) Linear model of a parallel-feedback oscillator. (b) Vector representation of the relationship between signal, added-noise and phase-noise. (c) Low-pass equivalent of the oscillator's model used for phase-noise analysis

$$\Delta\varphi(\Delta\omega) = \frac{\Delta\theta(\omega)}{1 - \widehat{H}(\omega)} \tag{2.8}$$

$$\boxed{S_{\varphi}(\Delta\omega) = |\Delta\varphi(\Delta\omega)|^2 = \frac{S_{\Delta\theta}(\omega)}{\left|1 - \widehat{H}(\Delta\omega)\right|^2}.} \tag{2.9}$$

The above expression is a more general form of the Lesson's phase-noise model which can be used for oscillators with complex resonant tanks.

Microwave oscillators are usually designed by using single resonators as the frequency-selective elements, as shown in Fig. 2.5. The original Leeson's formula was derived for oscillators using single resonators in their feedback loops. The equivalent low-pass transfer function for a single resonator is given as

$$\widehat{H}(\Delta\omega) = \frac{1}{1 + j2Q_L\dfrac{\Delta\omega}{\omega_0}} \tag{2.10}$$

where Q_L is the loaded quality-factor of the resonator. By combining (2.9.) and (2.10), one obtains the phase-noise spectral density as

$$S_{\varphi}(\Delta\omega) = \left[1 + \left(\frac{\omega_0}{2Q_L\Delta\omega}\right)^2\right] S_{\Delta\theta}(\omega). \tag{2.11}$$

Finally, phase-noise is represented by

$$\boxed{\mathrm{L(f)} = \frac{\mathrm{S_{\varphi}(\Delta\omega)}}{2} = \frac{\mathrm{GFKTB}}{2\mathrm{P_0}}\left[1 + \left(\frac{\omega_0}{2\mathrm{Q_L}\Delta\omega}\right)^2\right]\left(1 + \frac{\omega_c}{\Delta\omega}\right)} \tag{2.12}$$

which is known as the Leeson's formula for single-resonator oscillators. in the above equation *G* is the gain of the amplifier which according to (2.4) can be replaced with the insertion loss of the resonator (*I.L.*). The predicted phase-noise spectral density is graphically depicted in Fig. 2.6 where three different regions can be identified. Close to carrier, $1/f^3$ phase-noise behavior is a result of random frequency modulation of the oscillator due to the *1/f* flicker noise. In the region of $1/f^2$ phase-noise behavior, white

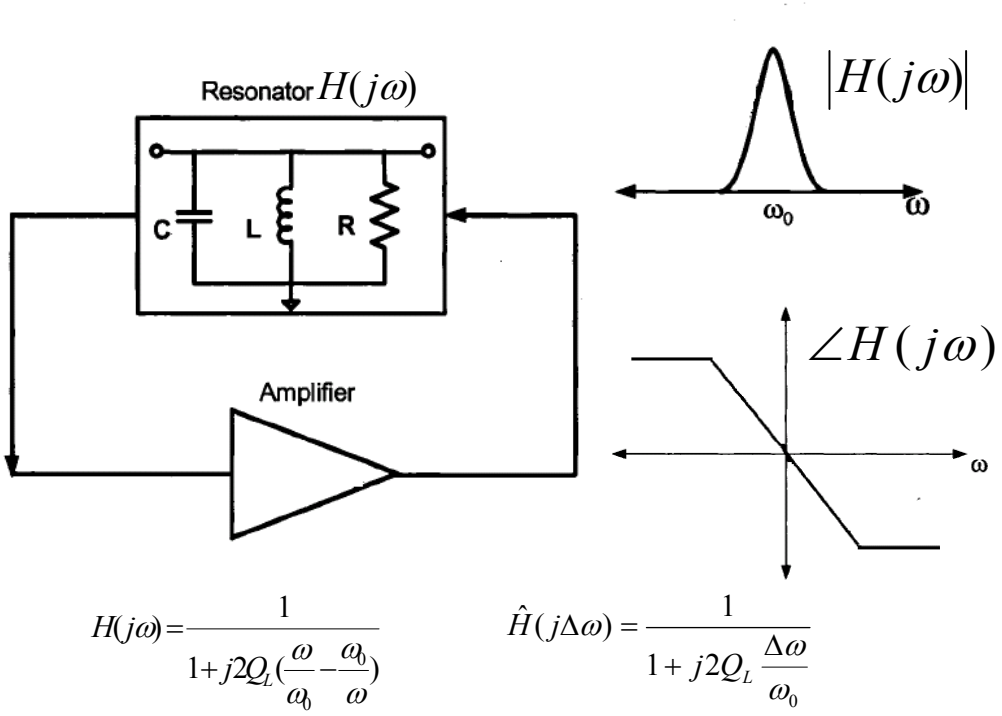

Fig. 2.5 Block diagram of an oscillator designed using a single resonator. *H(jω)* is the band-pass transfer function of the resonator and $\tilde{H}(j\Delta\omega)$ is its low-pass equivalent.

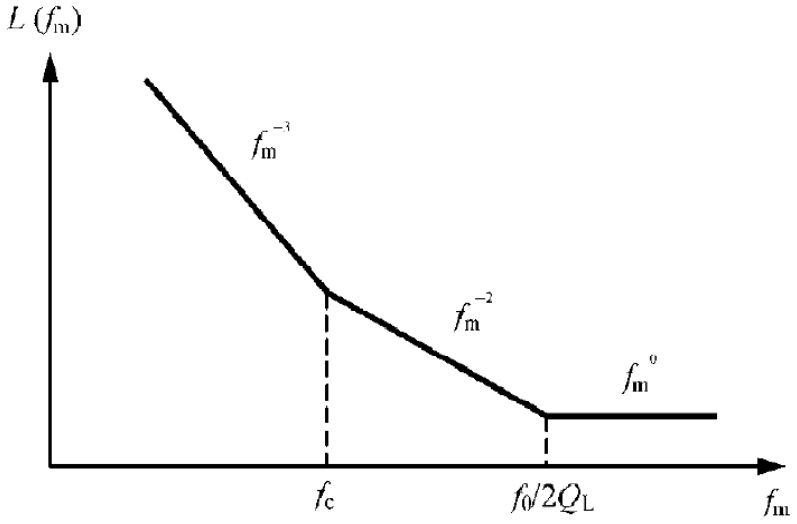

Fig. 2.6 Phase-noise behavior of a typical oscillator.

noise causes random frequency modulation. Finally, at far offset frequencies phase-noise becomes flat which is due to the additive noise effect.

In general, oscillators' feedback networks can contain multiple-resonator structures such as band-pass filters. Leeson's phase-noise formula was derived for an oscillator using a single resonator with the transfer function given in (2.10); thus one might question its validity for oscillators using more complex resonant structures with different $\hat{H}(j\Delta\omega)$. In fact, by replacing $\hat{H}(j\Delta\omega)$ in (2.9) with its Taylor series expansion around the resonant frequency, one can easily show that the Lesson's phase-noise formula remains valid and can be applied to oscillators with complex resonant tanks, provided that the loaded quality-factor is defined as

$$Q_L = \frac{\omega_0}{2}\sqrt{\left(\frac{dA(\omega)}{d\omega}\right)^2 + \left(\frac{d\emptyset(\omega)}{d\omega}\right)^2}\Bigg|_{\omega_0} \tag{2.13}$$

where $A(\omega)$ and $\varphi(\omega)$ are the amplitude and phase of the filter's transfer function $H(j\Delta\omega)$. Therefore, the application of (2.12) is justified when we design oscillators with complex resonant tanks in the rest of this thesis. The above definition for loaded quality-factor was first proposed by Razavi [23]. We will discuss more about the quality factor of resonators in Chapter 3.

2.2.2 Design Implications and Limitations of Leeson's Phase-Noise Model

Despite its simplicity, the Leeson's formula gives a sense of the phase-noise performance for oscillators. In addition, it indicates the basic factors and provides the necessary design rules to minimize the oscillators phase-noise [20]:

- Choose an active device with low-noise properties. SiGe heterojunction bipolar transistors (HBTs) with low noise-figures and low flicker-noise corner frequencies are the most popular devices for a low phase-noise oscillator design.
- Increase the oscillator's output power (P_0) through a proper feedback loop design
- Reduce the resonator's insertion loss, or equivalently, reduce the amplifier's gain (G).

- Choose a resonator with a high loaded quality-factor. This is the most effective step in the design of low phase-noise oscillators.

Although Leeson's phase-noise model provides a valuable insight into the oscillator design from engineering perspectives, it cannot explain some of the important phase-noise phenomena. This is due to simplifying assumptions made about the linearity and time-invariant behavior of the system. Some of the important shortcomings of the Leeson's model are listed below:

- The model includes a noise factor, *F*, which is an empirical fitting parameter and therefore must be determined from measurements; diminishing the predictive power of the phase-noise equation.
- Leeson's model observes the asymptotic behavior of phase-noise at close-to-carrier offsets, asserting that phase-noise goes to infinity with $1/f^3$ rate. This is obviously wrong as it implies an infinite output power for oscillator. For noisy oscillators it could also suggest that $L(f) > 0$ dBc/Hz! This singularity arises from linearity assumption for oscillator operation around steady-state point. In fact, the linear model breaks down at close-to-carrier frequencies where the phase-noise power is strong.

  Several authors have resolved this issue by using a nonlinear model for the oscillator. In the absence of the flicker noise, it has been shown that phase-noise takes the form of a Lorentzian [19]

$$L(\Delta\omega) \propto \frac{c^2}{c^2 + (\Delta\omega)^2} \tag{2.14}$$

  where c is a fitting parameter. The above model nicely avoids any singularity at $\Delta\omega = 0$ while maintains the same asymptotic behavior (Fig. 2.7). It also has the property that the total power of phase-noise from minus infinity to plus infinity is 1. This means that phase-noise doesn't change the total power of the oscillator; it merely broadens its spectral peak. There is no closed-form expression for the phase-noise spectrum in the presence of $1/f$ noise. In the past few years some

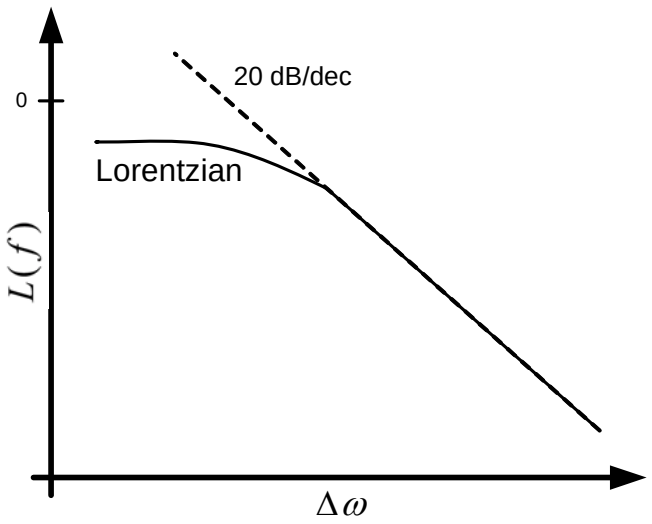

Fig. 2.7 Close-In phase-noise behavior due to white noise sources. Leeson's model predicts phase-noise monotonically increases by approaching the carrier whereas in reality it takes the form of a Lorentzian.

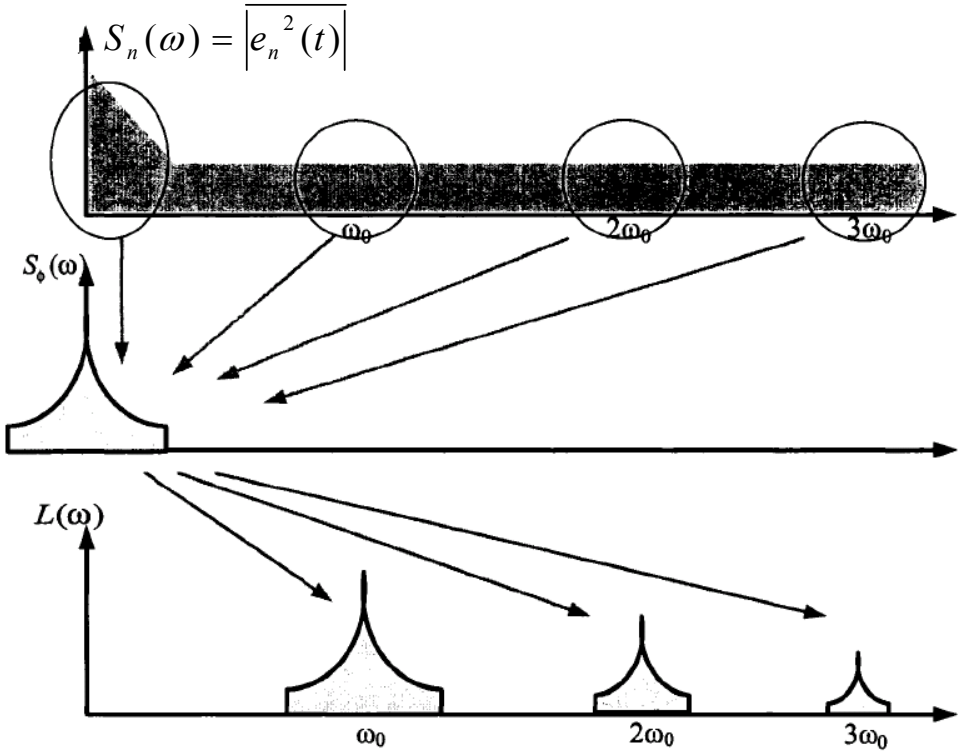

Fig. 2.8 Conversion process from noise ($S_n(\omega)$) to phase-noise ($L(\omega)$). Noise components from harmonically-related frequencies are up/down-converted to around carrier phase-noise. Leeson's model fails to address this phenomenon [14].

analytical models for phase-noise with flicker noise has been proposed. Herzel [24] decomposes the model into a Lorentzian for white-noise and a Gaussian for flicker-noise sources. The final spectrum is a convolution of a Lorentzian with a Gaussian spectrum, for which there is no closed-form expression and it has to be numerically calculated.

- The Leeson's model fails to properly describe the up-conversion and down-conversion of noise components from harmonically related frequencies to around-carrier frequency (Fig. 2.8). Particularly, the effect of the low-frequency flicker-noise components on close-in phase-noise is not well characterized in Leeson's model. The model asserts that the phase-noise $1/f^3$ corner frequency is exactly equal to the amplifier's flicker-noise corner frequency, ω_c. However, measurements frequently show no such equality. This is because Leeson models the oscillator as a time-invariant system, whereas oscillators are in general cyclo-stationary time-varying systems due to the presence of the periodic large-signal oscillation. This issue has been addressed by several authors. Hajimiri has shown that the oscillator's phase-noise $1/f^3$ corner frequency can be significantly lower than the device's flicker corner frequency, provided that the oscillation signal is odd-symmetric [14].

2.3 The Effect of Phase-Noise in Wireless Communication and RADAR Systems

Oscillator phase-noise in wireless transceivers limits the overall performance of communication systems in a variety of ways. Phase-noise directly affects short-term frequency stability, bit-error-rate, and adjacent-channel interference. To understand the importance of phase-noise in wireless communications, consider a generic receiver as depicted in Fig. 2.9, where it consists of a low-noise amplifier, a band-pass filter, and a down-conversion mixer. The local oscillator (LO) providing the carrier signal for both mixers is embedded in a frequency synthesizer. If the LO output contains phase-noise, the down-converted is corrupted. Referring to Fig. 2.9, we note that in the ideal case, the

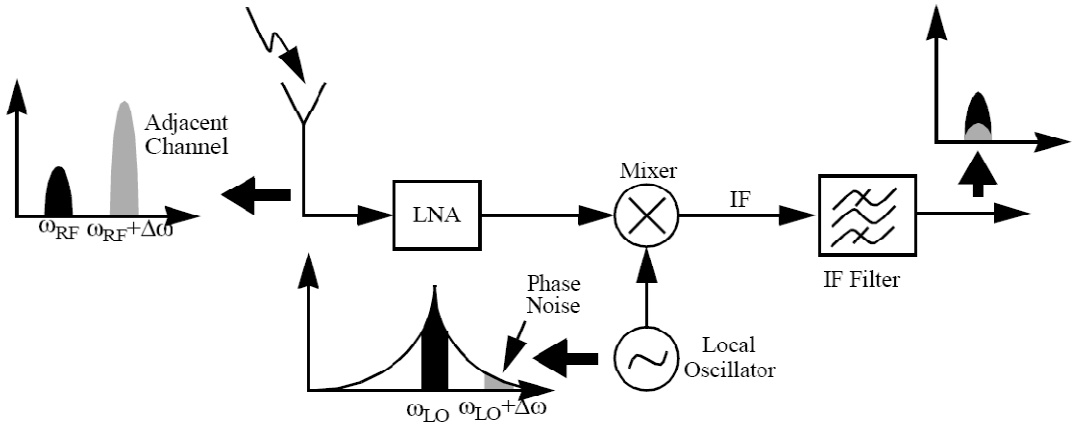

Fig. 2.9 The effect of phase-noise on wireless receivers [20]. The local oscillator's phase-noise down-converts the strong adjacent channel to IF band, causing destructive interference.

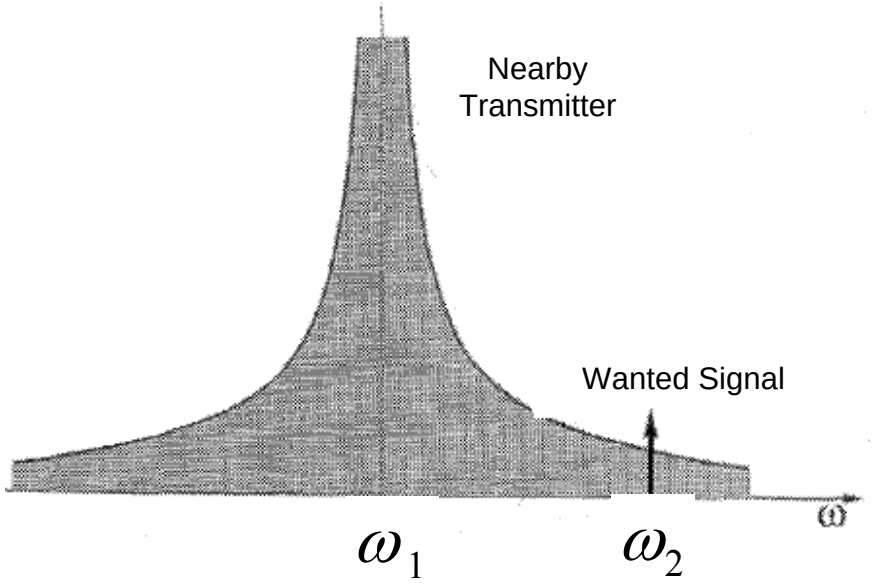

Fig. 2.10 The effect of phase-noise on transmit path [23]. The nearby transmitter's phase-noise might overwhelm the weak wanted signal.

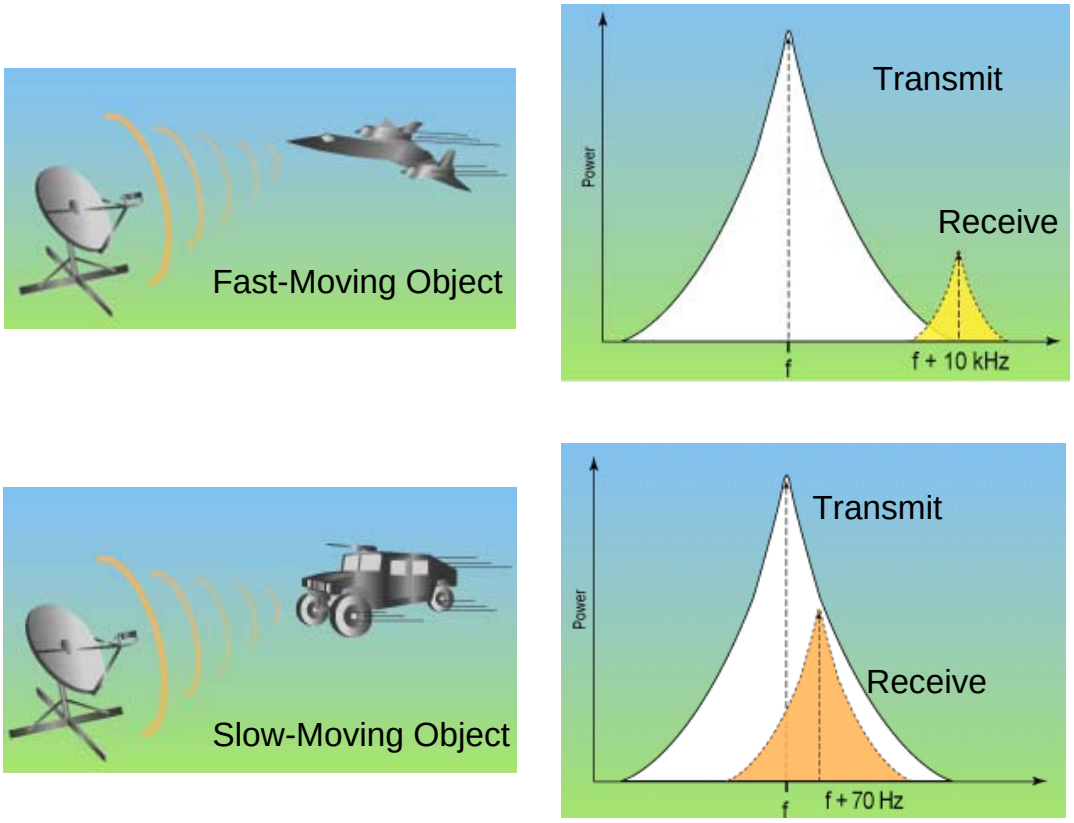

Fig. 2.11 The effect of the phase-noise in Doppler radar systems [20]. (Top) for a fast-moving object, the reflected signal is above the transmitted signal's phase-noise. (Bottom) For a slow-moving object the reflected signal is buried under the LO's phase-noise

signal band of interest is convolved with an impulse and thus translated to a lower frequency with no change in its shape. In reality, however, the wanted signal may be accompanied by a large interferer in an adjacent channel, and the local oscillator exhibits finite phase-noise. When the two signals are mixed with the LO output, the down-converted band consists of two overlapping spectra, with the wanted signal suffering from significant noise due to tail of the interferer.

Shown in Fig. 2.10, is the effect of phase-noise on the transmit path. Suppose a noiseless receiver is to detect a weak signal at ω_2 while a powerful, nearby transmitter generates a signal at ω_1 with substantial phase-noise. Then, the wanted signal is corrupted by the phase-noise tail of the interfering transmitter. The important point here is that the difference between ω_1 and ω_2 can be as small as a few tens of kilohertz while each of

these frequencies is around several GHz. Therefore, the output spectrum of the LO must be extremely sharp having a very low phase-noise.

Phase-noise of local oscillators also degrades the performance of the RADAR systems. It limits the RADAR's range as well as its minimum detectable Doppler shift. As shown in Fig. 2.11, for a fast moving target, the Doppler shift is around several kHz. Therefore, the reflected signal is well above the phase-noise level of the local oscillator in the receiver. However, for a slow moving target where the Doppler shift is around several tens of hertz, the reflected signal cannot be detected as it is buried in the phase-noise of the local oscillator.

Chapter 3

The Definition of Quality-Factor for Microwave Resonators

Resonators are one of the key components in RF communication systems. They provide high frequency-selectivity in filters and oscillators. The quality-factor is the most important parameter of a resonant circuit. Lesson's formula for phase-noise employs the term "loaded quality-factor", Q_L, the definition of which is critical to understanding resonator design for low phase-noise oscillators. Two common definition of quality-factor are discussed in this chapter. The first definition is based on the field theory which relates the quality-factor to energy storage and dissipation, whereas the second one is circuit-based relating the quality-factor to the resonator's frequency response. It is shown that the two definitions are equivalent and yield identical results for both single resonators and band-pass filters. A figure-of-merit for resonators, *R-FOM*, is defined to assess their overall effects on the phase-noise of oscillators. The *R-FOM* is useful for evaluating and comparing the performance of various resonators, and it is used throughout this thesis to optimize resonator designs for low phase-noise applications.

3.1 Quality Factor Definition

Energy view

Fields inside a resonator store energy at the resonant frequency where equal storage of electric and magnetic energies occurs. In practice, some of the stored energy is dissipated due to losses and input/output loads, thereby reducing resonator's frequency selectivity. Therefore one can define the loaded quality-factor as [20]:

$$Q_L = 2\pi \frac{\text{average energy stored}}{\text{energy dissipated during one cycle}} = \omega_0 \frac{W_T}{P_T} \tag{3.1}$$

where ω_0 is the resonant frequency, W_T is average stored energy, and P_T is total power loss in watts. The above definition includes both internal and external energy losses. One can separate the effect of internal and external energy losses and define the "unloaded" and "external" quality-factors, Q_u and Q_e, respectively, as followings

$$Q_u = \omega_0 \frac{W_T}{P_i} \tag{3.2}$$

$$Q_e = \omega_0 \frac{W_T}{P_e} \tag{3.3}$$

where P_i and P_e are the dissipated energies due to the resonator's internal losses and the external loadings, respectively. Since $P_T=P_e+P_i$, one can show that

$$\frac{1}{Q_L} = \frac{1}{Q_u} + \frac{1}{Q_e}. \tag{3.4}$$

It should be emphasized that it's the loaded quality-factor, Q_L, which appears in the phase-noise calculations. The loaded quality-factor is limited by the resonator losses and external loadings. In a "loosely-coupled" resonator, the internal losses are dominant and thus $Q_L \approx Q_u$. Conversely, in a "tightly-coupled" resonator, the external loadings are dominant and in this case $Q_L \approx Q_e$

Transfer function view

An alternative definition of the quality-factor uses the resonator's transfer function in the frequency domain. The transfer function is a complex function which governs the relationship between the input and output

$$H(j\omega) = A(\omega)e^{j\emptyset(\omega)} \tag{3.5}$$

where $A(\omega)$ and $\varphi(\omega)$ are the amplitude and phase response of the system. The quality-factor in terms of the resonator's transfer function is defined as [23]

$$Q_L = \frac{\omega_0}{2}\sqrt{\left(\frac{dA(\omega)}{d\omega}\right)^2 + \left(\frac{d\emptyset(\omega)}{d\omega}\right)^2}\Bigg|_{\omega_0} \approx \frac{\omega_0}{2}\frac{d\emptyset(\omega)}{d\omega}\Bigg|_{\omega_0}. \tag{3.6}$$

The approximation is due to the fact that, in most resonant circuits, phase variations are more significant than the amplitude variations. This definition has an interesting interpretation in the context of low phase-noise oscillator design. Recall that for steady oscillations, the total phase shift around the loop must be precisely 360^o. Now, suppose the oscillation frequency slightly deviates from ω_0. Then, if the phase slope is large, a significant change in the phase shift arises, violating the condition of oscillation and forcing the frequency to return to ω_0. In other words, the quality factor is a measure of how much the closed-loop system opposes variations in the frequency of oscillation. This concept proves useful in our subsequent analyses and methods for low phase-noise designs.

The energy-based definition of the quality-factor in (3.1) is ambiguous when a system has no energy storing element, as in the case of ring or distributed oscillators. Furthermore, it is difficult to use when the system contains multiple resonators, such as high-order band-pass filters. Also, the original form of the Leeson's phase-noise formula contains the right-hand side of (3.6), which is then replaced with Q_L by definition. Due to these reasons, we use the definition of the quality factor introduced in (3.6) throughout this thesis.

3.2 Comparison between Different Definitions of Quality-Factor

In this section we investigate the relation between different definitions of quality-factor. It is shown that, for single resonators and high-order band-pass filters, the energy-based definition of quality-factor given in (3.1) yields identical results as the general definition introduced in (3.6).

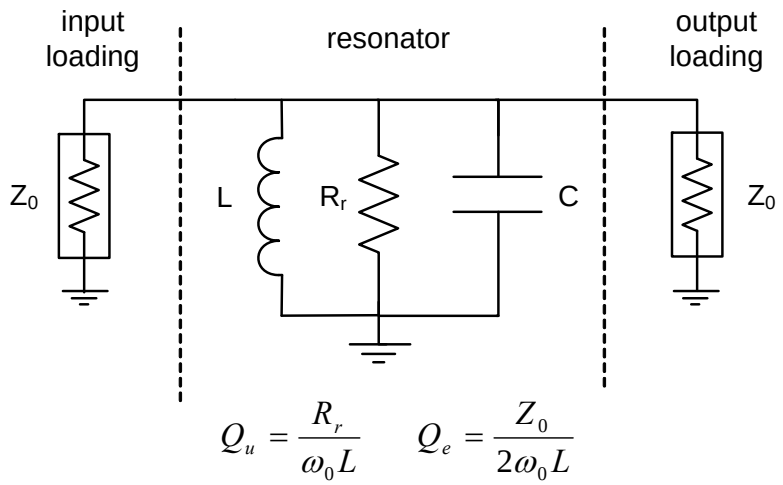

Fig. 3.1 A doubly-loaded shunt resonator.

Single resonator

Consider the resonator shown in Fig. 3.1 where the resistor R_r models the internal losses and the terminations Z_0 represent input/output loadings. Assume the resonator's (tank's) node voltage is at some certain value, V_0. The stored and dissipated energies are calculated as

$$W_T = W_m + W_e = 2W_e = \frac{1}{2}CV_0^2 \tag{3.7}$$

$$P_T = \frac{1}{2}\frac{V_0^2}{(R_r \| Z_0 \| Z_0)} \tag{3.8}$$

The loaded quality-factor is determined by inserting (3.7) and (3.8) into (3.1)

$$Q_L = \omega_0 C\ (R_r \| Z_0 \| Z_0). \tag{3.9}$$

The second definition of quality factor is based on the resonator's transfer function between input and output ports. In the circuit of Fig. 3.1 it can be shown that

$$S_{21}(j\omega) = \frac{2}{\frac{Z_0}{R_r \| Z_0 \| Z_0} + jZ_0\left(\omega C - \frac{1}{\omega L}\right)}. \tag{3.10}$$

Calculating the phase derivative of the transfer function at resonance, one can obtain the loaded quality-factor

$$Q_L = \frac{\omega_0}{2}\frac{d(\angle S_{21})}{d\omega}\bigg|_{\omega_0} = \omega_0 C\ (R_r \| Z_0 \| Z_0). \tag{3.11}$$

Comparing the results in (3.9) and (3.11), it is clear that the two definitions of quality factor are compatible and yield the same results for a single resonator.

Multiple-Resonator band-pass filters

To determine the quality-factor of a high-order filter using the energy-based definition given in (3.1), the total stored and dissipated energies must be calculated. The energy calculations require finding the voltages across the capacitors and resistors, and the currents through the inductors in a multiple-order filter's equivalent circuit. This is a tedious task which makes it impossible to find a closed-form expression for the loaded-quality factor in general case. Instead, circuit simulations are performed to find the loaded quality-factor.

Fig. 3.2(a) shows the circuit schematic of a four-pole Chebyshev band-pass filter consisting of four resonators coupled to each other through quarter-wave impedance inverters. The circuit is excited with a power source and simulated in Agilent's ADS to determine the voltages at the nodes and the currents through the inductors. The total stored energy can then be calculated by the following equations

$$W_T = W_m + W_e \tag{3.12}$$

$$W_e = \frac{1}{4} C_0 \sum_{i=2}^{5} V_i^2 \tag{3.13}$$

$$W_m = \frac{1}{4} L_0 \sum_{i=2}^{5} I_i^2 \tag{3.14}$$

where V_i is the voltage, and I_i is the current through the inductor, at node i. The total dissipated energy is obtained from

$$P_T = \frac{1}{2}\sum_{i=2}^{5}\frac{V_i^2}{R_0} + \frac{1}{2}\left[\frac{V_1^2}{Z_0} + \frac{V_6^2}{Z_0}\right] \tag{3.15}$$

in which the first term is due to the internal energy loss, and the second term is the energy dissipated by the input and output loads. The quality factor can now be calculated by inserting (3.12) and (3.15) into (3.1) and the results are plotted in fig. 3.2.c.

The filer's quality-factor can also be determined based on its simulated transfer function according to (3.6). The results are superimposed in Fig. 3.2.c where they very closely match the quality factor values obtained from the energy-view definition. The above procedure was performed for several other filters with different frequency responses and different number of resonators. In all cases the same conclusion was drawn, indicating that the two definitions of quality factor introduced in this section yield almost identical results for multiple-order band-pass filters.

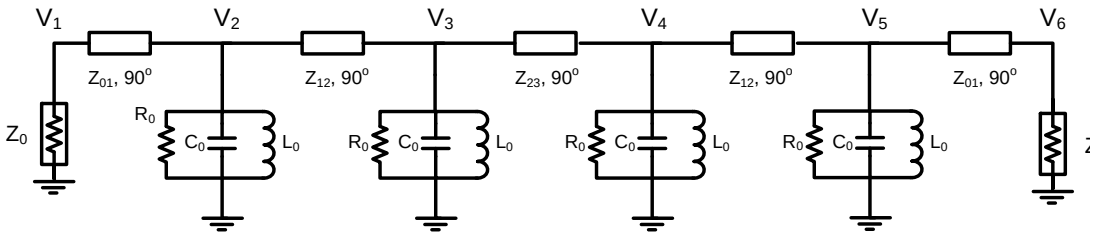

(a)

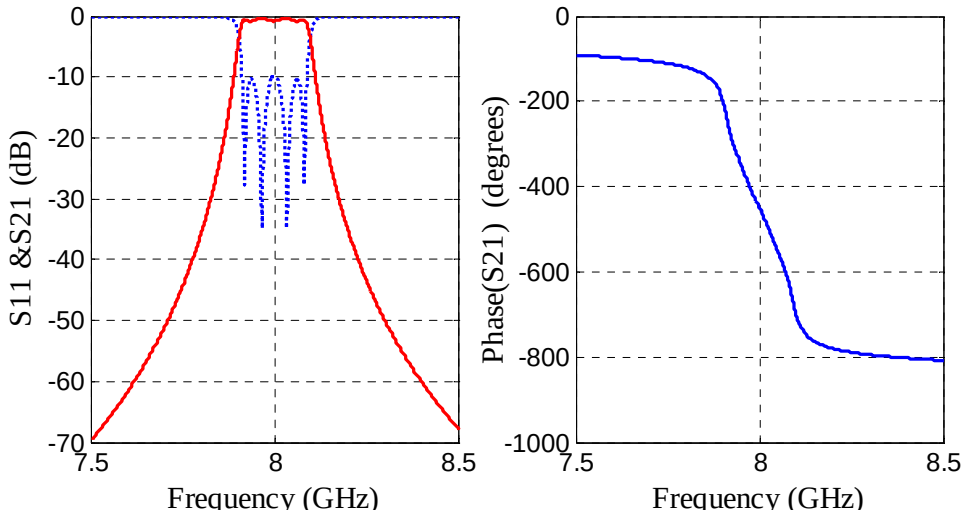

(b)

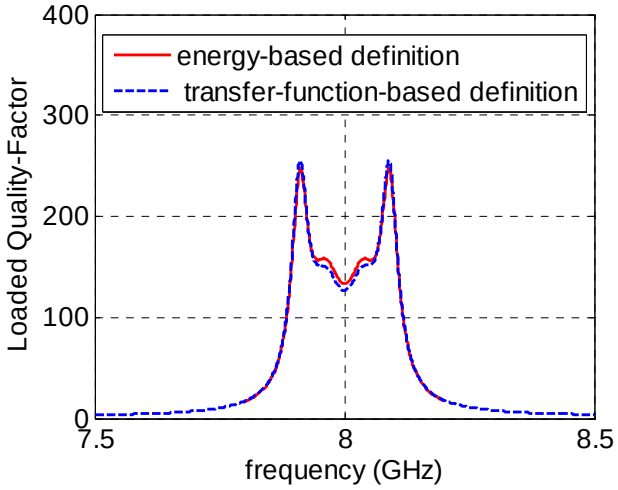

(c)

Fig. 3.2 Comparison between different definitions of loaded quality-factor for a four-pole band-pass Chebyshev filter. (a) The filter's circuit diagram (b) simulated frequency-response, and (c) loaded quality-factor.

3.3 Resonator Design for Low Phase-Noise Applications

According to Leeson's formula, phase-noise in oscillators is inversely proportional to the inverse-square of the resonators' loaded quality-factor. Furthermore, the insertion loss of the resonators also appears in the Leeson's formula (2.12) indicating that phase-noise proportionally degrades by increasing the resonator's insertion loss, *I.L*. Therefore, to evaluate the overall effect of resonators on oscillators' phase-noise, a resonator figure-of merit, *R-FOM*, can be defined as

$$R - FOM = 10\log\left(\frac{\mathrm{I.L}}{\mathrm{Q_L^2}}\right). \tag{3.16}$$

To reduce the phase-noise of an oscillator, one needs to decrease (more negative) the *R-FOM* of its resonator. In other words, resonators should be designed for their minimum *R-FOM* when considering low phase-noise applications. In this section we discuss single resonators and find their optimum coupling for lowest phase-noise. The definition of *R-FOM* can also be applied to band-pass filters to optimize their design for low phase-noise applications. This will be further discussed in the incoming chapters.

In single resonators, the loaded quality-factor and insertion loss are two inter-related parameters both depending on the resonator's unloaded (Q_u) and external (Q_e) quality-factors. To determine the relation between the insertion loss and the quality-factors, consider the resonator shown in Fig. 3.1. It is a straightforward task to show that at resonance

$$\mathrm{I.L.} = \frac{1}{|\mathrm{S_{21}}|^2} = \left(1 + \frac{\mathrm{Z_0}}{2\mathrm{R_r}}\right)^2 = \left(1 + \frac{\mathrm{Q_e}}{\mathrm{Q_u}}\right)^2 \tag{3.17}$$

Therefore, one can express the resonator figure-of-merit in terms of the quality-factors by inserting (3.4) and (3.17) into (3.16)

$$\mathrm{R - FOM} = 10\log\left[\left(1 + \frac{\mathrm{Q_e}}{\mathrm{Q_u}}\right)^2\left(\frac{1}{\mathrm{Q_e}} + \frac{1}{\mathrm{Q_u}}\right)^2\right]. \tag{3.18}$$

In the above equation, the unloaded quality-factor, Q_u, is a predetermined parameter depending on the resonator structure and fabrication technology. Therefore, phase-noise is minimized by finding the optimal value of Q_e resulting in the minimum of *R-FOM*

$$\frac{\mathrm{d}}{\mathrm{d}(\mathrm{Q_e})}(\mathrm{R-FOM}) = 0 \quad \longrightarrow \quad \boxed{\mathrm{Q_e} = \mathrm{Q_u} \quad \text{or equivalently} \;\; \mathrm{Q_L} = \frac{\mathrm{Q_u}}{2}} \qquad (3.19)$$

The above equation shows how to couple the resonator to the amplifier in the feedback loop for phase-noise minimization. Everard [25] was the first person to determine such an optimum value for a resonator's loading. According to (3.19) the insertion loss of a resonator tuned for optimum loading is 6 dB. This indicates that the amplifier should have a power gain of more than 6 dB to guarantee oscillation start-up.

Chapter 4

The Application of High-Order Band-Pass Filters as Frequency Stabilization Elements

Microwave oscillators commonly use a single resonator in their series or parallel feedback networks. The quality-factor of a resonator is limited due to the conductor, dielectric and radiation losses. In particular, planar resonators exhibit low quality-factors due to high degrees of losses in planar circuits. Therefore, despite numerous efforts [7], [8], [26-29], the design of a low phase-noise planar oscillator has remained a serious challenge.

The frequency selectivity in an oscillator can be improved by employing multiple resonators in its feedback network. This approach has been rarely addressed in the literature despite its promising benefits. The first demonstration of a low phase-noise oscillator design using multiple resonators was presented in [30] where four cells of resonator-amplifiers are cascaded to increase the frequency-selectivity in the oscillator loop, Fig. 4.1. In this configuration, both the quality-factor and the noise level are increased by a factor of 4, resulting in 6 dB of phase-noise reduction. However, the phase-noise reduction comes at the cost of 4 times increase in the power consumption due to the use of multiple amplifiers. In this chapter, we employ high-order elliptic-response band-pass filters to design low phase-noise oscillators. It is shown that elliptic-response filters can provide higher quality-factors compared to single resonators and other types of band-pass filters. This is due to their use of multiple resonators and their close-to-passband transmission zeros which help increase frequency-selectivity. A design procedure is presented that allows for optimum filter design for low phase-noise applications. As a proof of concept, an 8 GHz low phase-noise oscillator is

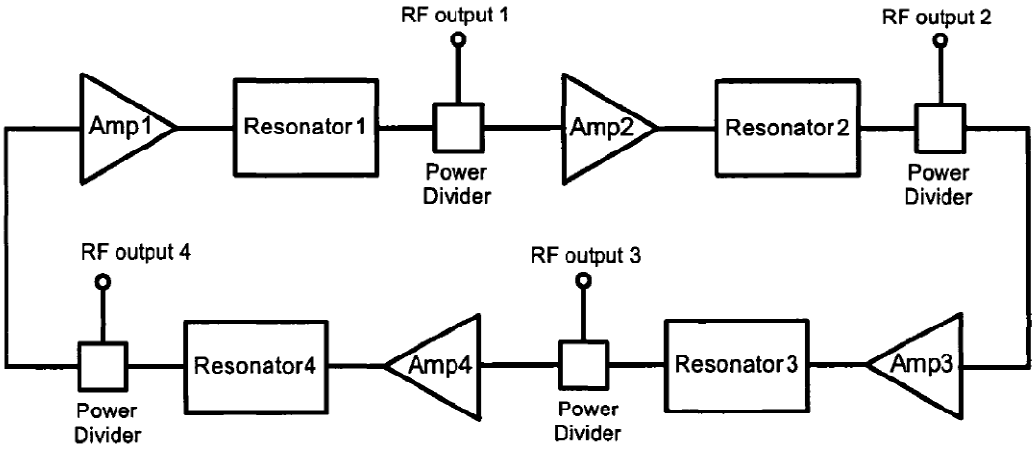

Fig. 4.1 circuit diagram of a cascaded multiple-resonator oscillator [29].

designed using a four-pole elliptic band-pass filter in its feedback loop. The oscillator achieves a phase-noise of -143 dBc/Hz at 1-MHz offset which is the lowest phase-noise value among planar oscillators reported in the literature.

4.1 High Quality-Factor Band-Pass Filter Design

4.1.1 Theory

Band-Pass filters consisting of multiple resonators can provide significantly higher quality-factors as compared to single resonators because frequency-selectivity can be improved by adding more resonators. The frequency response of a filter can be determined by finding the number and the location of the poles and zeros of its transfer function. Transfer functions of Butterworth and Chebyshev filters have only poles while those of elliptic filters have the same number of poles and zeros. Due to the existence of zeros, elliptic filters are capable of providing sharper roll-offs and higher selectivity than Butterworth and Chebyshev filters and, thus, they can provide larger quality-factors. Fig. 4.2 compares the frequency response and the quality-factor of a Butterworth, a Chebyshev and an elliptic four-pole band-pass filter. These filters have the same center frequency of 8 GHz, a bandwidth of 100 MHz, and are designed using similar resonators with unloaded quality-factors of 300. Large quality-factor peaks at the edges of the pass-

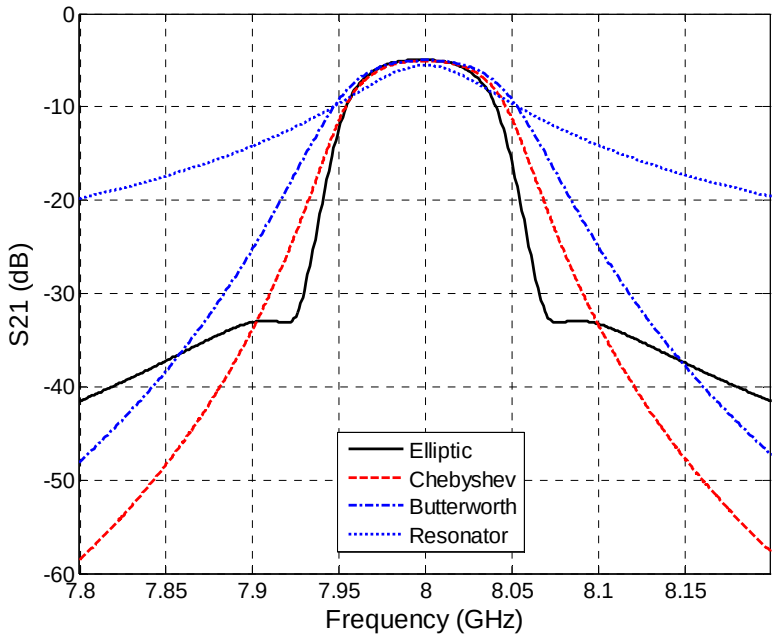

(a)

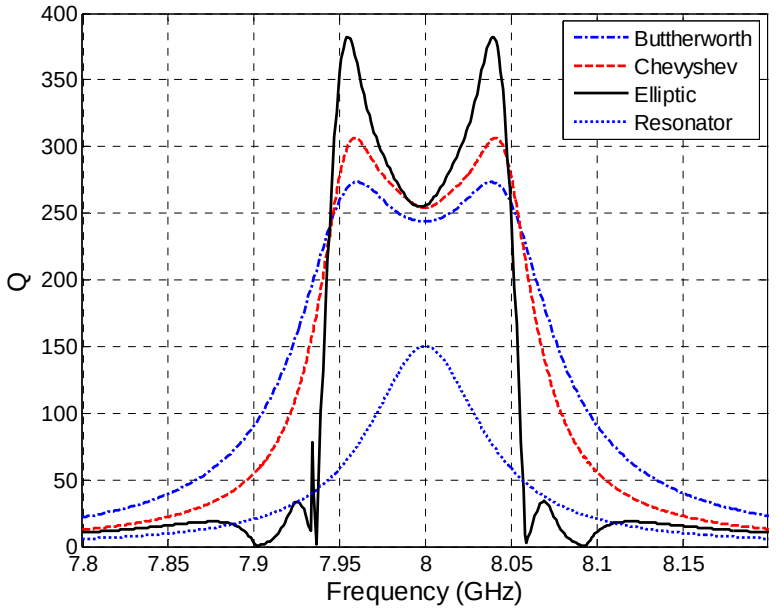

(b)

Fig. 4.2 Comparison between (a) insertion loss and (b) quality-factor of four-pole band-pass filters with different frequency responses. The filters are designed using resonators with unloaded quality-factors of 300. The frequency response of a doubly-loaded resonator is also included for comparison.

band are observed in the elliptic filter response; due to its close-to-passband transmission zeros.

The quality-factor of the described elliptic filter is also compared with that of a single resonator. It should be noted that (Section 3.3) when a single resonator is used for an oscillator design, its loaded quality-factor drops by half due to the external loading effects. In this example, the loaded quality-factor of the single resonator drops to 150 which is about 2.5 times lower than the loaded quality-factor of the four-pole elliptic filter. Therefore, it can be concluded that by using an elliptic filter in the feedback loop of an oscillator a significant phase-noise reduction can be expected. In general the sharp quality-factor peaks of elliptic filters are problematic due to the distortion they cause in communication systems. However, in this work we show that one can take advantage of this characteristic of elliptic filters to design low phase-noise oscillators.

4.1.2 Filter Design and Optimization

In microwave circuits, the elliptic-response filter is mainly realized with a selective quasi-elliptic function having only one pair of transmission zeros, providing an intermediate response between elliptic and Chebyshev filters. Fig. 4.3 shows the coupling structure of a four-pole quasi-elliptic filter. Resonators 1 & 2, 2 & 3, and 3 & 4 are directly coupled while resonators 1 & 4 are cross-coupled. Directly coupled resonators have a positive coupling coefficient while the cross coupling coefficient between resonators 1 and 4 is negative. The cross coupling introduces a single pair of transmission zeros, leading to filter's elliptic response. Elliptic filters in conventional applications are designed to meet some pre-determined specifications such as bandwidth, return loss, out-of-band rejection etc., whereas in low phase-noise oscillators, the resonator figure-of-merit, *R-FOM*, is the performance criterion. The *R-FOM* was introduced in Section 3.3 to evaluate the overall effect of resonators on oscillators' phase-noise. Equation (3.16) can be modified to express the *R-FOM* in terms of the S_{21} of the filters

$$R - FOM = 20\log(|S_{21}|) - 20 * \log\left(\frac{\omega_0}{2}\frac{d(\angle S_{21})}{d\omega}\right). \qquad (4.1)$$

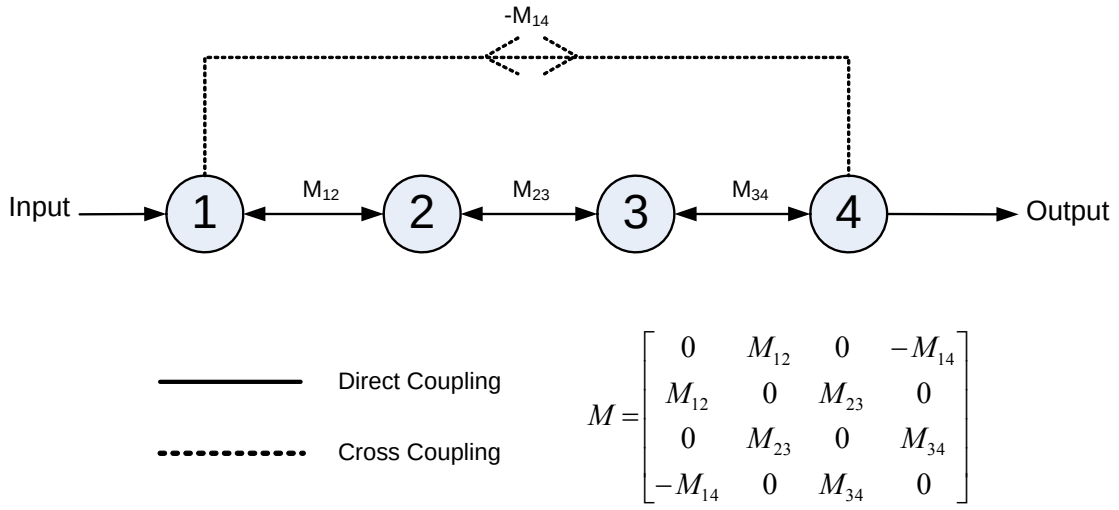

Fig. 4.3 Coupling scheme of a four-pole elliptic-response band-pass filter. The circles represent the resonators and *M* is the coupling matrix.

Since S_{21} of the quasi-elliptic filter is a function of number of poles (*N*), pass-band bandwidth (*BW*), location of zero (Ω_t) and return loss (*RL*), the *R-FOM* is consequently a function of these parameters. Therefore, the design optimization goal would be to find proper values for number of poles, bandwidth, return loss and location of transmission zero, to minimize the *R-FOM*.

The optimization procedure is detailed here. First, the coupling matrices (*M*) and the input and output coupling coefficients (Q_e) are calculated for various filter orders, bandwidths, return losses, and locations of zeros. Utilizing these design parameters, an Agilent ADS schematic circuit as shown in Fig. 4.4 is simulated to obtain the S_{21} of various filters. Here, the lumped RLC elements represent the four synchronously tuned resonators and are determined in terms of the filter design parameters [31]

$$C_0 = \frac{Q_e}{\omega_0 Z_0} \times 10^{12}\ (pF) \qquad L_0 = \frac{Z_0}{Q_e \omega_0} \times 10^{9}\ (nH) \qquad R_0 = \frac{Q_u}{Q_e} Z_0\ (ohms) \quad (4.2)$$

where ω_0 is the angular frequency at the midband frequency of the filter and Q_e is the external quality factor of resonators at the input and output. Q_u is the resonators' unloaded quality-factor signifying the resonators' losses. The unloaded quality-factor for the

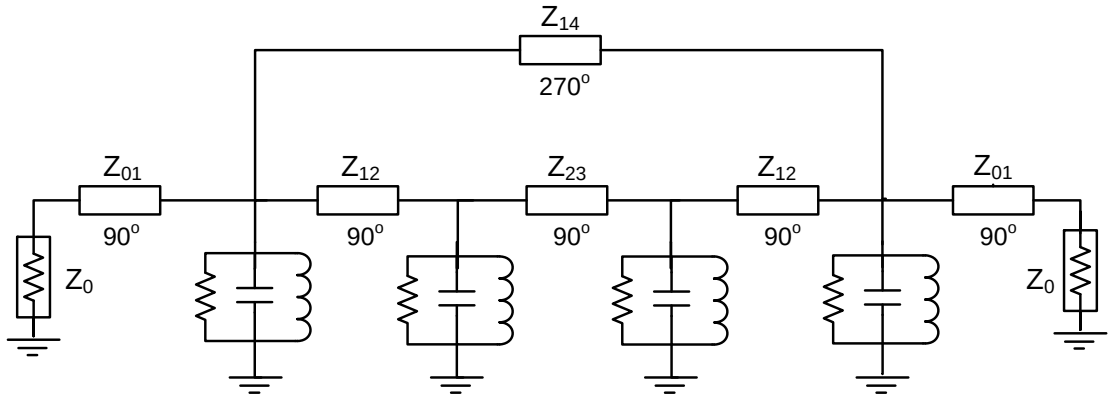

Fig. 4.4 Agilent ADS circuit schematic for filter simulation.

resonators used in this work was determined by simulating an 8 GHz microstrip open square-loop resonator on a Rogers RT/Duroid 5880 substrate (ε_r = 2.2, Height = 31 mils) using IE3D^{TM} software package. The simulated Q_u for the resonators is 200. The quarter-wavelength transmission lines are used to represent the couplings and their characteristic impedances are determined by [31]

$$Z_{01} = Z_0 \qquad Z_{12} = \frac{Z_0}{Q_e M_{12}} \qquad Z_{23} = \frac{Z_0}{Q_e M_{23}} \qquad Z_{14} = \frac{Z_0}{Q_e |M_{14}|} \tag{4.3}$$

where $Z_0 = 50\Omega$ is the I/O terminal impedance.

Fig. 4.5 depicts the *R-FOM* versus frequency for several values of *BW*, Ω_t and *RL* for a four-pole elliptic filter. It is observed that for each case there is a minimum *R-FOM* occurring at a particular frequency. The oscillator utilizing the filter in its feedback loop should be designed at this frequency to achieve the lowest phase-noise. Furthermore, Fig. 4.5 shows that the minimum *R-FOM* of the filter depends on the filter parameters. To determine the best values for these parameters, the minimum *R-FOM*s were plotted versus parameter variations for each case as shown in Fig. 4.6. Referring to Fig. 4.6(a), a filter with a narrower bandwidth has a lower *R-FOM* and, thus, is better suited for low phase-noise oscillator designs. This behavior can be attributed to the sharper selectivity of narrowband filters. Shown in Fig. 4.6(b), is the effect of the return loss on filter's *R-FOM*. A lower return loss results in a higher selectivity at the cost of higher insertion

loss. Due to this trade-off, there is an optimum value for the return loss which is *RL=10dB* for the filter studied in this work.

Fig. 4.6(c) shows the effect of the location of transmission zero, Ω_t, on *R-FOM*. Ideally, as Ω_t approaches the edge of the pass-band, the filter exhibits a sharper skirt and thus the group delay's peak value increases. In reality, resonators' losses degrade the performance of the filters with very close to pass-band zeros, causing the group delay peak value to drop. Therefore, after a certain point, the *R-FOM* does not decrease anymore as Ω_t is pushed closer to the filter's pass-band. This can be seen in Fig. 4.6(c) where R-FOM increases for transmission zeros less than Ω_t =1.6. Therefore the optimum value of the transmission zero location for the filter under study is Ω_t =1.6. In general, the location of transmission zero can be closer to the passband edge as the Q_u of the resonators increases, allowing lower *R-FOM* values to be achieved. This is demonstrated in Fig. 4.7 where the *R-FOM* of a filter with resonators' Q_u of 1000 is compared with the *R-FOM* of our filter with Q_u of 200. The optimum Ω_t value for the filter with higher Q_u resonators' is Ω_t =1.2 which is less than the optimum Ω_t value of the filter under study.

In summary, the optimum four-pole filter parameters for minimum *R-FOM* where determined to be *BW = 2.2%*, Ω_t = 1.6 and *RL = 10dB*. Bandwidth values of less than 2.2% were not considered because they require very small coupling coefficients which are not feasible due to the losses.

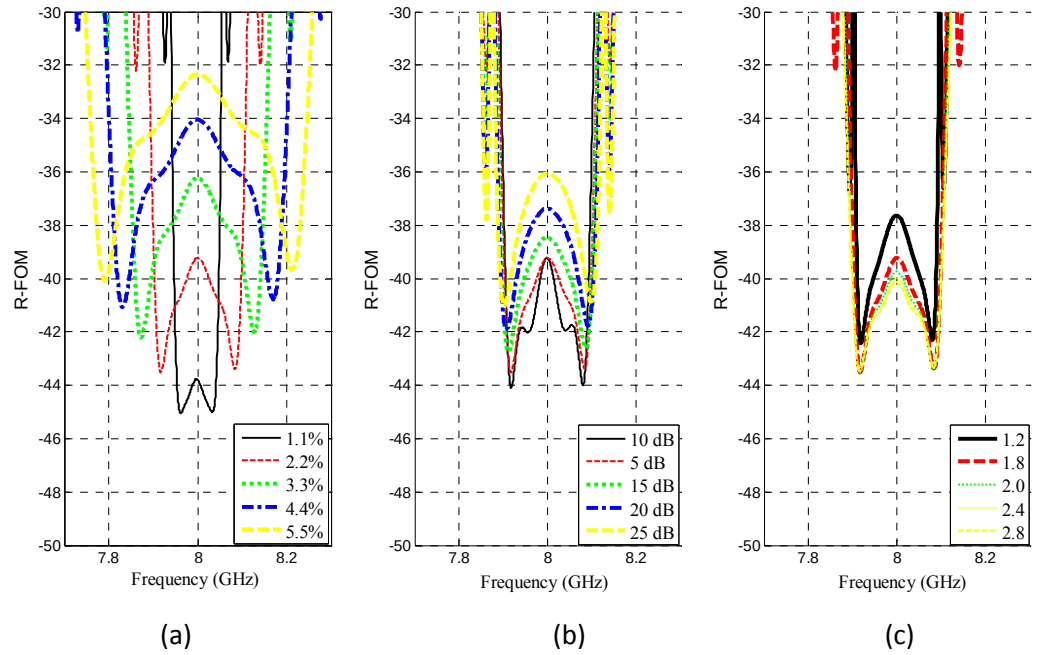

Fig. 4.5 Resonator figure-of-merit (*R-FOM*) versus frequency for different (a) bandwidths, (b) return losses, and (c) normalized location of transmission zeros of a four-pole elliptic filter.

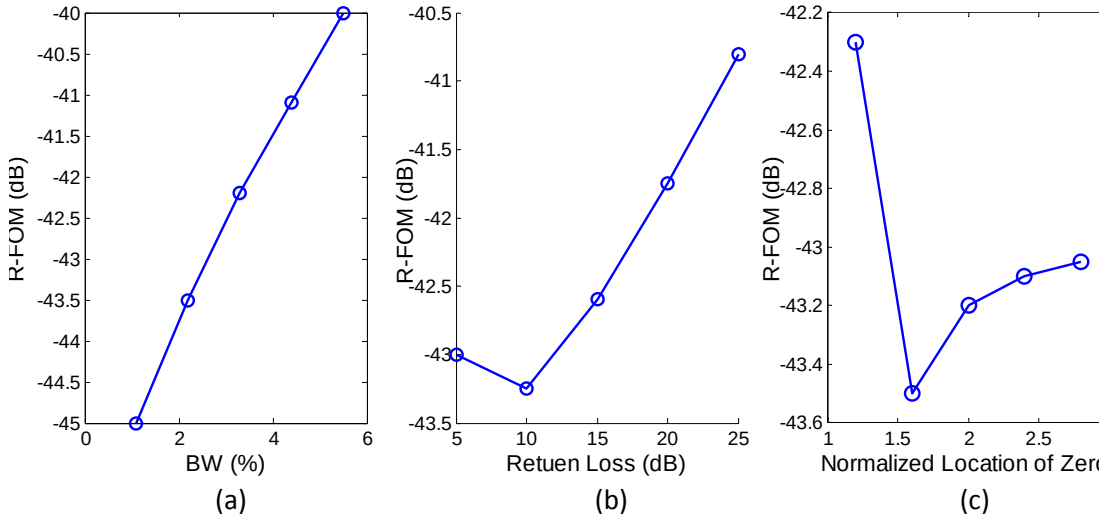

Fig. 4.6 Minimum *R-FOM* versus (a) bandwidths, (b) return losses, and (c) normalized location of transmission zeros of a four-pole elliptic filter.

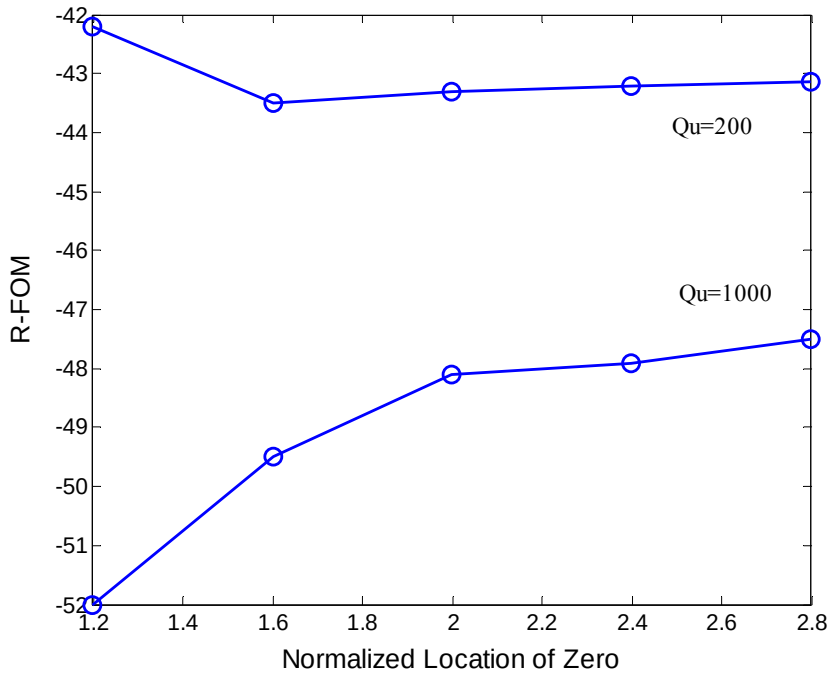

Fig. 4.7 Resonator figure-of-merit (*R-FOM*) of the four-pole elliptic filter versus the normalized location of transmission zero implemented on a low-loss (Q_u=*1000*) and a high-loss (Q_u=*200*) substrate.

Another important parameter of a filter that affects the *R-FOM* is its order (*N*). Ideally, an increase in the filter's order results in a higher quality-factor and thus reduces the *R-FOM*. However, in practice, increasing the band-pass filter's order causes a higher insertion loss and thereby can adversely affect the *R-FOM*. Therefore one needs to find the optimum order for a filter for achieving the lowest *R-FOM*. A similar analysis was performed on several six-pole filters with different values of bandwidth, location of transmission zero and return losse. As expected, the previously discussed results for four-pole filters similarly apply to the six-pole filters'. In fact, it was found that an optimized six-pole filter reduces the *R-FOM* by 2 dB, indicating that a six-pole filter would be a better candidate for low phase-noise oscillator applications as compared to a four-pole filter. Nevertheless, in this work, the optimized four-pole filter was utilized in the oscillator design since its *R-FOM* is low enough to achieve a low phase-noise operation of the oscillator. It also provides a lower insertion loss and a smaller size, making the oscillator design easier.

The optimized four-pole filter is implemented on a Rogers RT/Duroid 5880 substrate (ε_r =2.2, Height = 31 mils). The coupling matrix and the I/O coupling coefficients are

$$M = \begin{bmatrix} 0.00000 & +0.0137 & 0.0000 & -0.0031 \\ +0.0137 & 0.00000 & +0.0137 & 0.00000 \\ 0.00000 & +0.0137 & 0.00000 & +0.0137 \\ -0.0031 & 0.00000 & +0.0137 & 0.0000 \end{bmatrix}$$

$$Q_e = 73.5. \tag{4.4}$$

Based on the above coupling matrix and I/O coupling coefficients, full wave EM simulations using IE3D® are performed to determine the exact physical layout for the filter as shown in Fig. 4.8. The overall physical size of the filter is 12.6 mm by 12.4 mm. Fig. 4.9 shows the measured frequency response of the filter where it shows similar performance compared to simulation results. The simulated and measured quality-factor and R-FOM of the elliptic filter are shown in Fig. 4.10. The R-FOM minimum value occurs at the frequency of 8.07 GHz. At this frequency the loaded quality-factor of the filter was measured to be Q_L=*185*. The feedback oscillator utilizing the R-FOM-optimized filter is designed to operate at this frequency to achieve a low phase-noise performance.

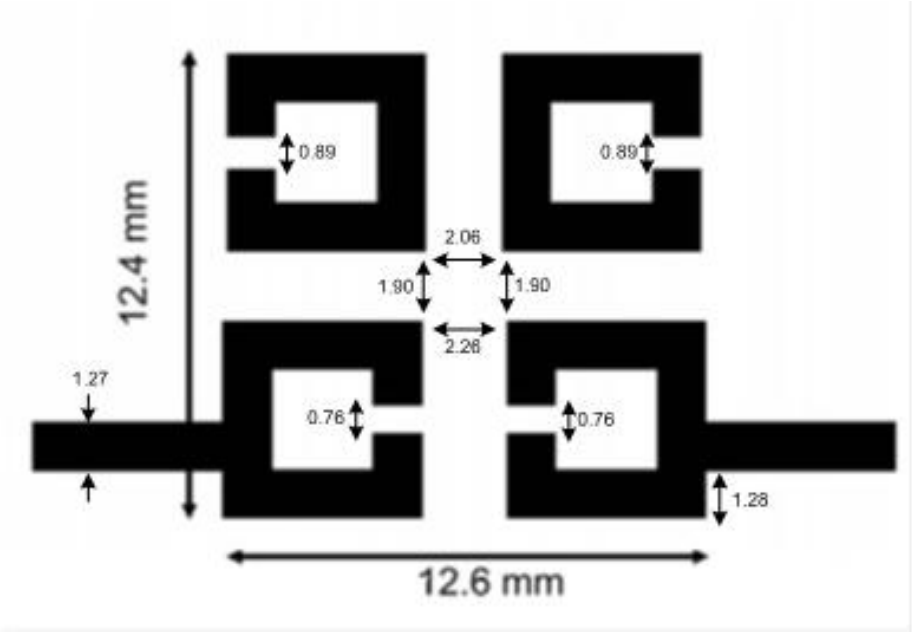

Fig. 4.8 Layout of the optimized four-pole elliptic filter. All the dimensions are in millimeters

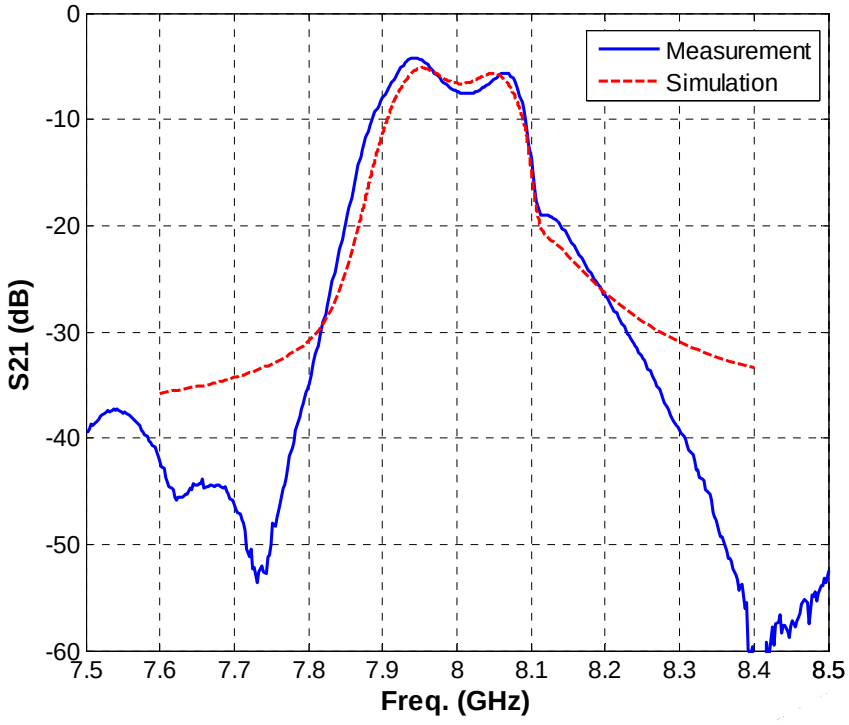

Fig. 4.9 Insertion loss of the optimized four-pole elliptic filter.

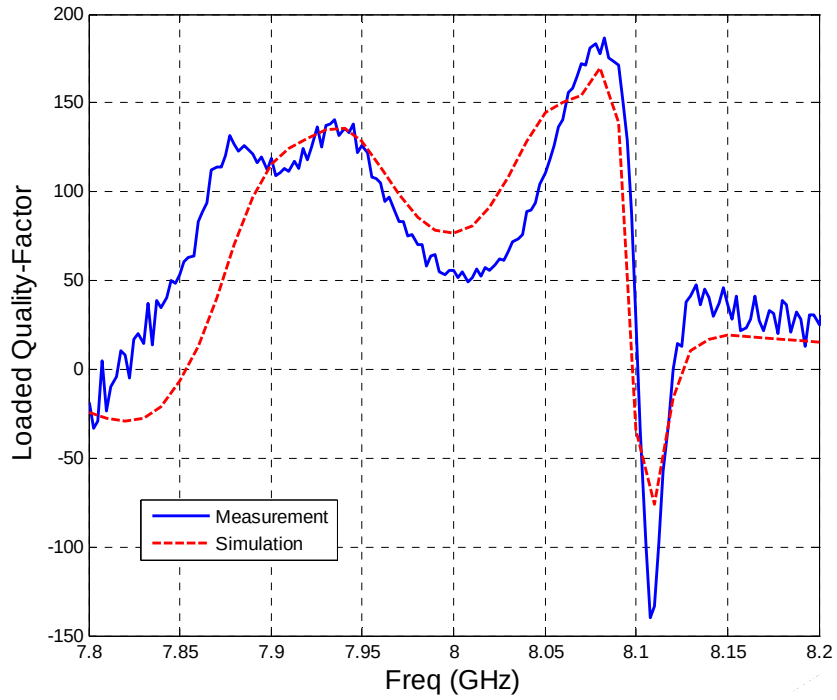

(a)

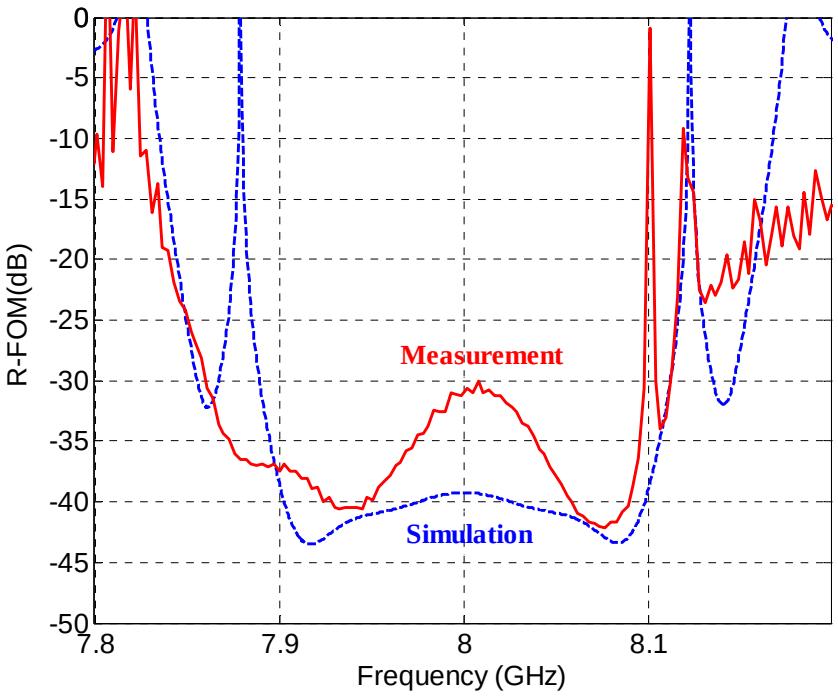

(b)

Fig. 4.10 Simulated and measured (a) quality-factor and (b) R-FOM of the four-pole elliptic filter optimized for low phase-noise oscillator applications.

4.2 An X-band Low Phase-Noise Oscillator Employing a Four-Pole Elliptic Band-Pass Filter

4.2.1 Oscillator Design

An X-band microwave oscillator is designed based on the four-pole elliptic band-pass filter described in the previous section. The oscillator consists of an amplifier to provide enough loop-gain for oscillation start-up, the elliptic filter acting as the frequency stabilization element, and a parallel feedback network. The circuit schematic of the oscillator is shown in Fig. 4.11.

The oscillator is designed based on the substitution theory [32]. The design procedure is summarized here. First, the amplifier is designed by conjugate-matching the input and output of the transistor to 50 Ω. The elliptic filter is then connected to the amplifier's input, and the resulting filter-amplifier circuit is excited with a signal source at the input and simulated using the harmonic balance method in Agilent ADS (Fig. 4.12). The voltages and currents at the input and output terminals of the filter-amplifier (V_1, V_2, I_1, I_2) are determined at a specific RF input power level. Then the feedback network element values are determined based on the following equations [33]

$$Y_{out} = G_{out} + jB_{out}$$

$$G_{out} = (Y_1 + Y_3 A_r + Y_4 A_i)/|A|^2$$

$$B_{out} = \left[\frac{Y_1(A_r - |A|^2)}{A_i} - A_i Y_3 + A_r Y_4\right]/|A|^2$$

$$B_1 = \frac{Y_1}{A_i}$$

$$B_2 = \frac{Y_1(A_r - 1)}{A_i} + Y_2 \tag{4.5}$$

where

$$A = A_r + jA_i = V_2/V_1$$

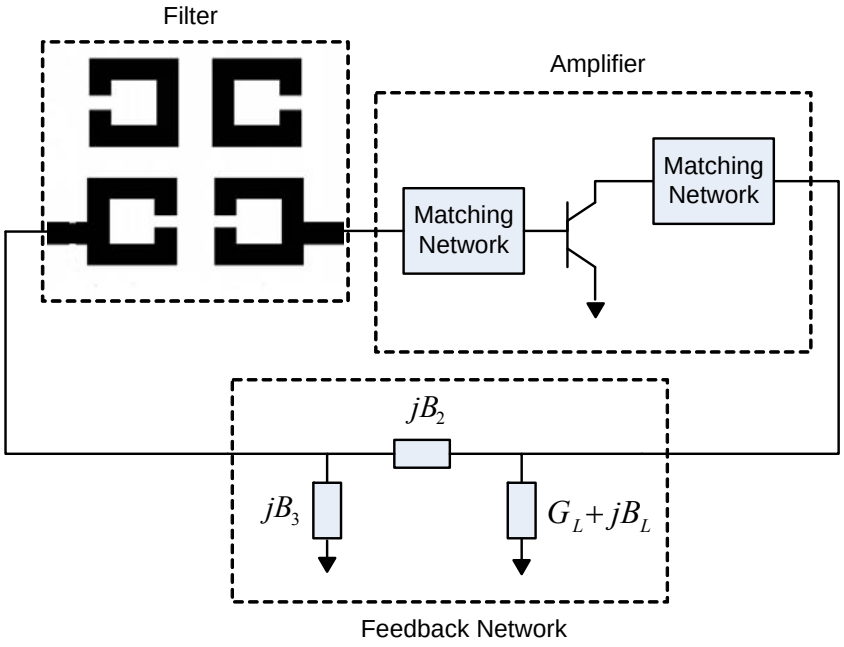

Fig. 4.11 Circuit schematic of the oscillator employing an elliptic filter as its frequency stabilization element.

$$Y_1 = -Re(I_1/V_1)$$

$$Y_2 = -Im(I_1/V_1)$$

$$Y_3 = Re(I_2/V_1)$$

$$Y_4 = Im\left(\frac{I_2}{V_1}\right) \tag{4.6}$$

Note that in the above equations only the fundamental frequency components of currents and voltages are used.

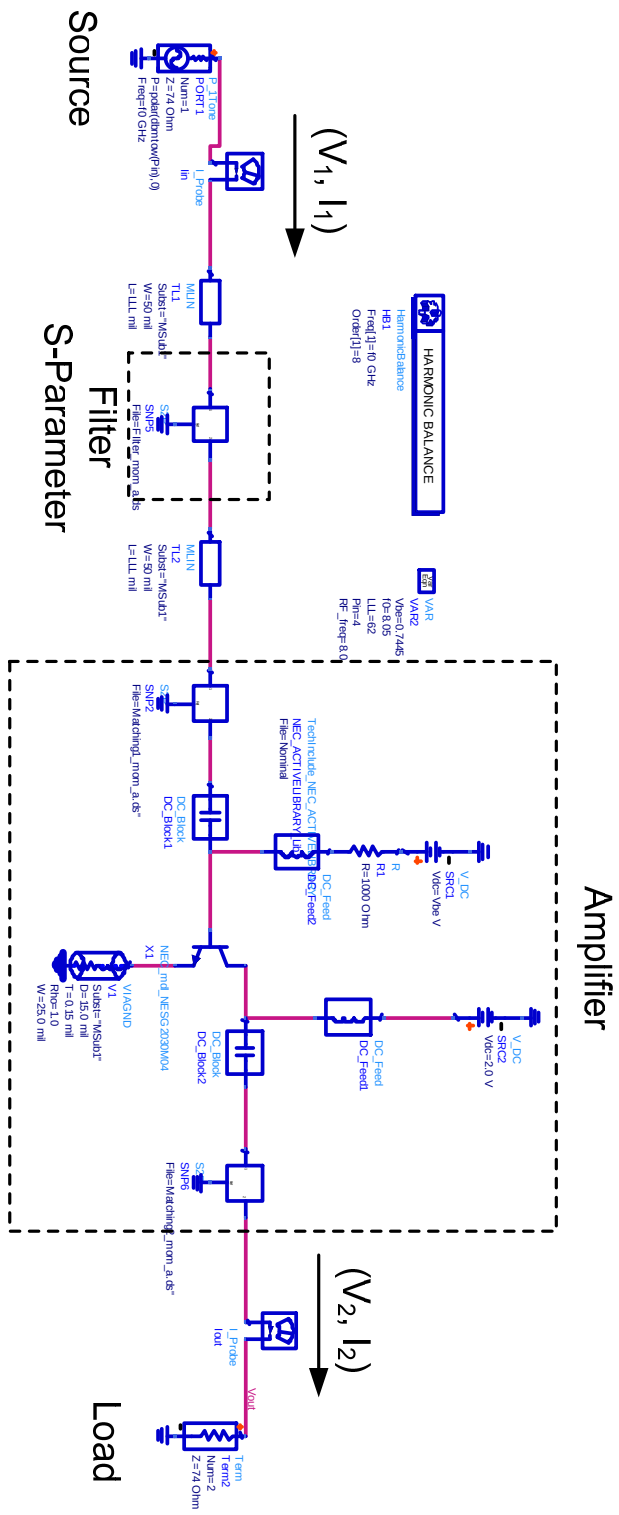

Fig. 4.12 Circuit schematic of the filter-amplifier unit. The circuit is simulated using harmonic balance nonlinear tool so as to find input/output currents and voltages for the oscillator's feedback network design.

4.2.2 Measurement Results

The oscillator was fabricated on a Rogers RT/duroid 5880 substrate. A circuit prototyping machine was used in the oscillator fabrication. Although the filter part of the oscillator is most sensitive to fabrication tolerances, it can tolerate fabrication errors of 25 μm or less without considerable loss of performance. The active device is a packaged SiGe HBT (NECNESG2030M04) biased at a collector-emitter voltage of 2 V with a collector current of 11 mA. The top view of the fabricated oscillator is shown in Fig. 4.13.

The measured oscillation frequency is 8.05 GHz with the output power of 3.5 dBm after de-embedding cable and bias tee. The amount of the consumed dc power is 22 mW, corresponding to a DC-RF efficiency of 10%. The oscillator's phase-noise is measured based on the FM discriminator technique with the phase-noise measurement system Agilent E5504A. As shown in Fig. 4.14, the measured phase-noise is -122.5 dBc/Hz and -143.5 dBc/Hz at 100 kHz and 1 MHz offset frequencies, respectively. The oscillator's phase-noise was simulated in Agilent ADS by taking into account the thermal noise sources. Since the transistor's noise model does not include flicker noise sources, the simulation results are invalid in the flicker frequency noise region. This can be observed in Fig. 4.14 where the simulation and measurement results are in good agreement except for the $1/f^3$ region caused by flicker noise sources. According to the measurement, $1/f^3$ corner frequency is around 100 kHz. Table 4.1 compares the performance of the SiGe HBT elliptic-filter oscillator with other reported microwave planar free-running oscillators. The oscillator presented in this paper demonstrates the lowest phase-noise due to the high loaded quality-factor provided by the elliptic filter.

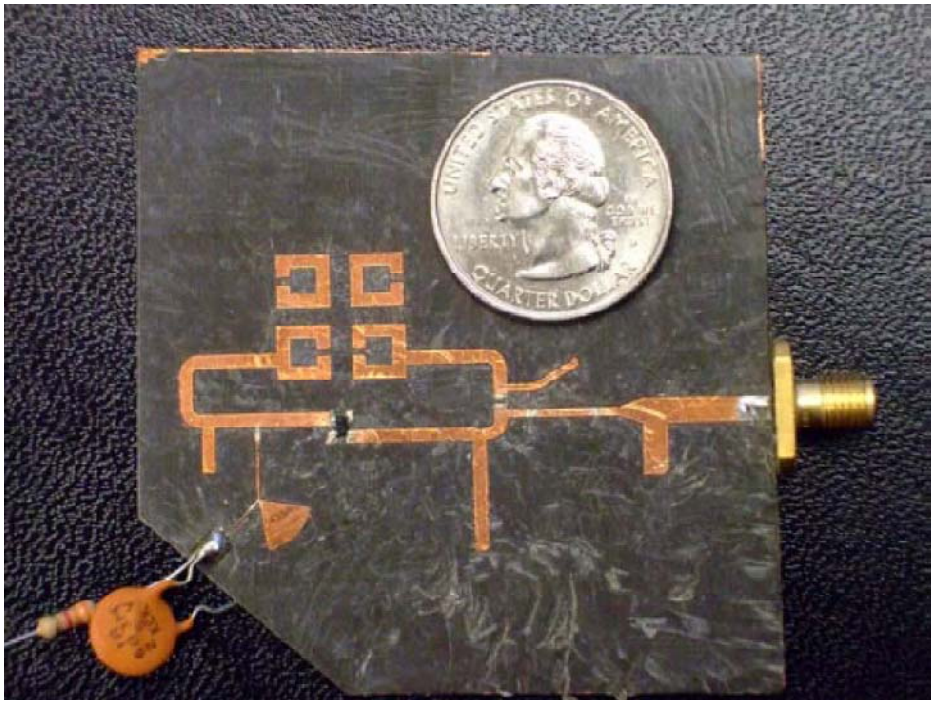

Fig. 4.13 A picture of the fabricated oscillator. The oscillator circuit diagram is shown in Fig. 3.11. The elliptic filter's dimensions are given in Fig. 4.8. The feedback network's element values are B_1=-0.037, B_2=-.025, B_{out}=0.0124 and G_{out}=0.0068 (Fig. 4.8).

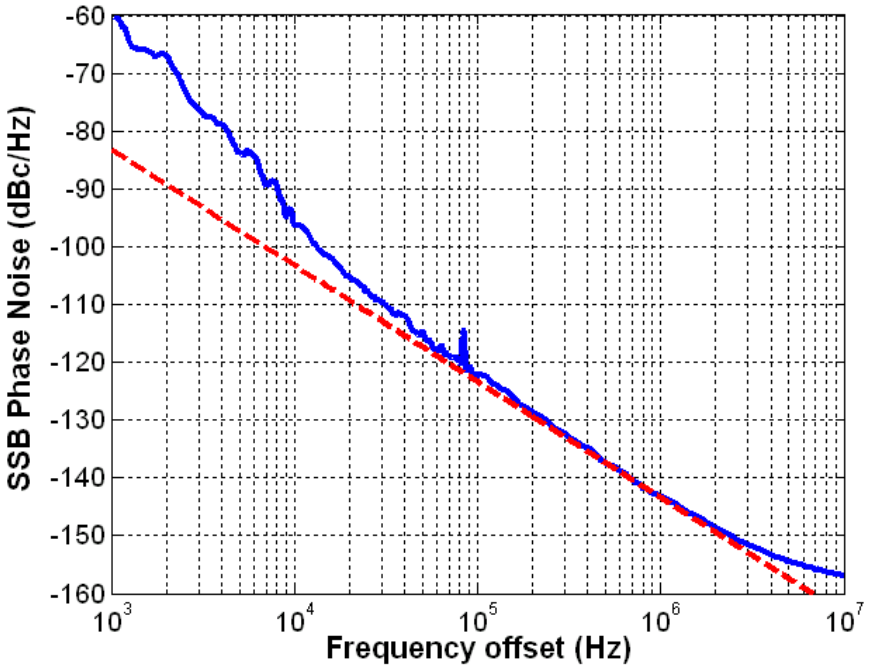

Fig. 4.14 Measured (solid) and simulated (dashed) phase-noise of the SiGe HBT X-band oscillator.

Table 4.1
Comparison with other reported microwave planar oscillators

Device	Resonator	F_0 (GHz)	P_0 (dBm)	Efficiency (%)	L(f) ‡ dBc/Hz	FOM dBc/Hz
HEMT [7]	ring	12	5	48.7	-116	-189.3
Si BJT [8]	hair-pin	9	9	4.5	-132	-185.6
HEMT [26]	active resonator	10	10	2.0	-134	-187.4
Si BJT [27]	Microstrip line	9.9	7	-	-133	-
SI BJT [28]	open-loop resonator	5.8	-0.5	-	-133	-
SiGe HBT [34]	extended-resonance	9.1	9.7	14	-139	-199.9
SiGe HBT [This work]	Elliptic filter	8	3.5	10	143.5	-207

‡ Phase-noise at 1 MHz offset frequency

The figure-of-merit of an oscillator is defined as following [11]

$$FOM = L(\Delta f) - 20log_{10}\left(\frac{f_0}{\Delta f}\right) + 10log_{10}\left(\frac{P_{DC}}{1mW}\right) \quad (4.7)$$

where Δf is the offset frequency, $L(\Delta f)$ is the phase-noise, and P_{DC} is the total consumed DC power in milli-watts. Oscillators with low phase-noise, low power consumption and, thus, low *FOM*s are desired. Table 4.1 compares the *FOM* of various oscillators. The oscillator presented in this work shows the lowest *FOM* among planar oscillators reported to date. This indicates that its phase-noise has been improved due to higher quality factor of the elliptic filter, rather than sacrificing the DC power consumption.

4.3 Conclusion

Elliptic-response band-pass filters can provide higher quality-factors compared to single resonators or other types of band-pass filters. This is due to their use of multiple resonators and the presence of close-to-passband transmission zeros in their frequency responses, which help improve frequency-selectivity. A low phase-noise oscillator was designed based on employing a four-pole elliptic filter in its feedback loop. In order to get the lowest phase-noise performance from the oscillator, the filter in the feedback loop is optimized for its minimum resonator figure-of-merit. The optimization method determines the optimum values for the order, bandwidth, location of zero, and return loss of the filter. As a result the presented oscillator shows the lowest phase-noise performance among planar oscillators reported in the literature. At 8 GHz, its measured phase-noise is -143 dBc/Hz at 1 MHz frequency offset. The output power level is 3.5 dBm with a 10% DC-RF efficiency and a *FOM* of -207 dBc/Hz. The oscillator's low *FOM* value indicates that the phase-noise has been improved without increasing the DC power consumption, thanks to the high quality-factor of the elliptic filter used in its feedback network.

Chapter 5

Theory and Design of Low-Noise Active Resonators and Their Application for Low Phase-Noise Oscillators

High-Q resonators are essential in designing low phase-noise oscillators. Transmission-line-based resonators such as ring [7], hair-pin [8] and spiral [29] resonators are widely used to design planar oscillators. Unfortunately, these resonators do not possess high unloaded-quality-factors and hence do not allow for low phase-noise oscillator design. One approach to decrease the phase-noise is to use high-order band-pass elliptic filters in the feedback loop of the oscillators, because such filters can provide higher quality-factors compared to single resonators. This approach was successfully implemented in the design of an X-band low phase-noise planar oscillator discussed in the previous chapter. Nevertheless, the filter's quality-factors are still limited by the unloaded quality-factor of their constituent resonators. Significant phase-noise improvements could be achieved by designing active resonators to enhance their unloaded quality-factors.

The unloaded-quality-factors of printed planar resonators are limited due to the dielectric, conductor and radiation losses. An active resonator can be designed to compensate for the energy losses in the passive resonator [35]-[40]. Active resonators have been widely used in the design of highly frequency-selective filters. Also, a few authors have used them as frequency stabilization elements in the feedback network of low phase-noise oscillators [26], [41], [42]. Although this approach has proved to be successful in reducing the phase-noise of oscillators, it has not been fully explored and some subtle design issues remain to be addressed. One important issue to investigate is the effect of the added-noise introduced by the active resonators. In fact, careful noise

design of active resonators is necessary in order to obtain the lowest phase-noise from the oscillators. Furthermore, previous works have mainly focused on designing *single* active resonators. The frequency-selectivity of the feedback network can be significantly improved by utilizing multiple active resonators in the form of a *band-pass elliptic filter*.

In Section 5.1 active resonators are analyzed and, for the first time, a design procedure is presented which simultaneously allows for resonators' full loss-compensation with minimum noise degradation. The procedure is general and can be applied to various resonators used for different applications. Analytical expressions are derived for the noise-figure and power consumption of active resonators. These equations provide a good understanding of the application of active resonators for low phase-noise oscillators, which is the subject of Section 5.2. Through analysis and simulations, it has been shown that active resonators can significantly reduce the phase-noise of oscillators, however, at the cost of increased power consumption. In fact, low phase-noise oscillator design using single active resonators results in poor DC-to-RF power efficiency. In Section 5.3 an active elliptic filter is used as the frequency stabilization element to design a low phase-noise oscillator. Active elliptic filters can provide high loaded quality-factors at lower noise-figures and power consumptions as compared to single active resonators. A four-pole active elliptic filter is designed and used in the feedback network of an 8 GHz oscillator. The oscillator demonstrates a measured phase-noise of -150 dBc/Hz at 1 MHz frequency offset with a DC-to-RF efficiency of 5%. To the best of our knowledge, the oscillator presented in this chapter achieves the lowest phase-noise among other planar oscillators reported to date.

5.1 Low-Noise Active Resonator Design

At microwave frequencies, active resonators are usually implemented by providing active feedback-loops or coupling negative-resistance devices to passive resonators [35]-[40]. Due to the presence of excess noise added by active devices (transistors), special attention should be paid to the noise design of the active resonator. In this section, the equations for the design of a low-noise lossless active resonator are

presented. Both the active feedback-loop and the negative-resistance methods are discussed. For the sake of clarity, we consider square loop microstrip resonators; however, the results are general and can be applied to various types of resonators intended for different applications.

5.1.1 Resonator Loss Compensation Using Active Feedback Loops

A square open-loop resonator along with its active feedback-loop is shown in Fig. 5.1. The external-quality-factor, Q_e, represents the resonator's input and output loadings. On the other hand, the external-quality-factors, Q_1 and Q_2, denote the loading effects due to the gain stage's input and output coupling, respectively. G is the voltage gain of the amplifier. The phase of the active feedback-loop should be an integer multiple of 360^o for loss compensation. The equivalent circuit of the active resonator is shown in Fig. 5.2, where the shunt RLC network models the passive resonator coupled to the amplifier through the transformers with turn ratios n_1 and n_2. The active resonator's input and output external couplings are represented by the transformers T_i and T_o. The amplifier is bilaterally conjugate matched at its input and output[1].

It can be shown that the active feedback-loop in the circuit of Fig. 5.2 is equivalent to a negative resistance with the following value:

$$R_{active} = \left(\frac{-50\, n_2^2}{2G\frac{n_2}{n_1} - 1} \right) \| 50 n_1^2 \,. \tag{5.1}$$

The resonator is fully loss-compensated when this negative resistance is equal in magnitude to the positive resistance of the passive resonator, R_r. This requirement is fulfilled when the gain of the amplifier is chosen such that

$$G = \frac{\sqrt{n_1 n_2}}{2}\left(\frac{1}{Q_1} + \frac{1}{Q_2} + \frac{1}{Q_u}\right) \tag{5.2}$$

where the Q definitions are shown in Fig. 5.2.

[1] In general, the amplifier can be matched to different impedances at its input and output. Through a similar analysis, it can be shown that the design equations (5.2), (5.3) and (5.4) remain valid in this case.

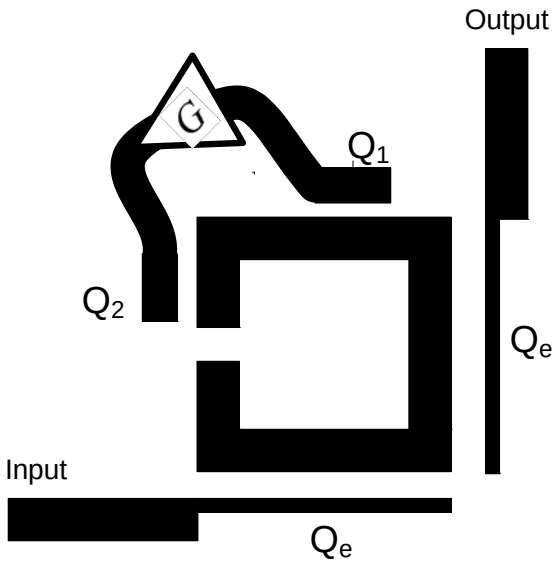

Fig. 5.1 A square open-loop resonator with an active feedback-loop for loss compensation. The active resonator is doubly-loaded through the input and output coupled-lines with external quality-factor of Q_e.

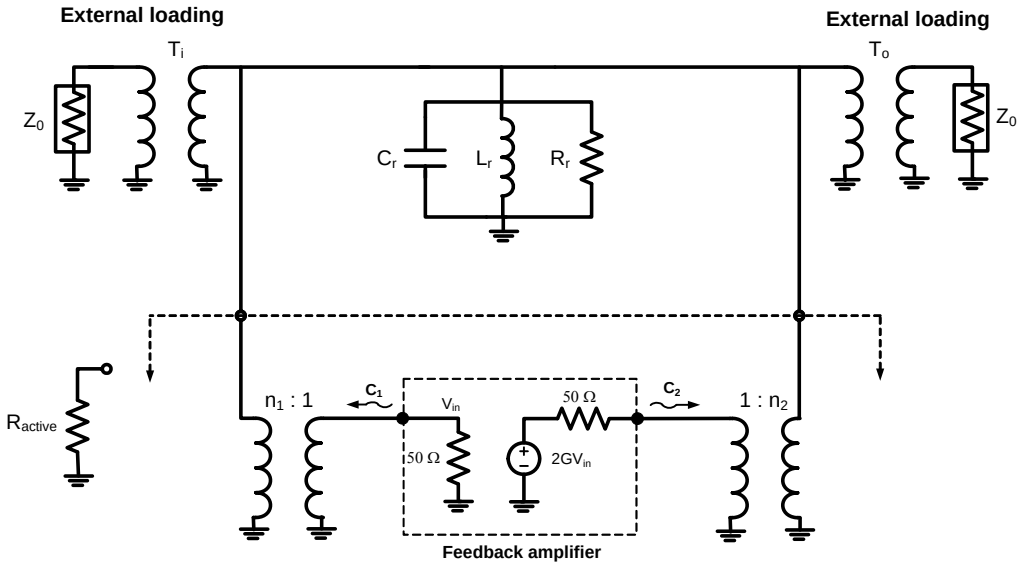

$$Q_1 = \frac{n_1^2 50}{\omega_0 L_r} \qquad Q_2 = \frac{n_2^2 50}{\omega_0 L_r} \qquad Q_u = \frac{R_r}{\omega_0 L_r}$$

Fig. 5.2 A doubly-loaded resonator employing an active feedback-loop for loss compensation. Q_u is the unloaded-quality-factor of the passive resonator. The amplifier is matched to 50 Ω at the input and output. C_1 and C_2 are the amplifier's input and output noise waves, respectively.

The noise sources of the amplifier in the feedback loop generate two noise-waves, C_1 and C_2 (Fig. 5.2), which degrade the doubly-loaded resonator's noise-figure. It is very important to minimize the effect of the added-noise introduced by the amplifier, especially when the active resonator is intended for low phase-noise oscillator applications. Noise analysis of active resonators has been performed in [43],[44], where it is shown that the contribution of the noise-wave C_1 to the noise-figure of the resonator is nullified when the active feedback-loop is designed such that:

$$Q_2 = G^2 Q_1 \tag{5.3}$$

By satisfying the above condition, the active resonator achieves its minimum noise-figure as given by

$$\boxed{F_{min} = F_{passive} + \left(\frac{2Q_e}{Q_u}\right) M}$$

$$\text{where} \qquad M = \frac{F_A - 1}{1 - \frac{1}{G^2}} \qquad \text{and} \qquad F_{passive} = 1 + \frac{2Q_e}{Q_u} \tag{5.4}$$

In the above equation, $F_{passive}$ is the noise-figure of the passive resonator; M and F_A are the noise-measure and noise-figure of the amplifier, respectively. Equation (5.4) clearly shows the effect of the noise of the amplifier on the active resonator's noise-figure and, more importantly, it indicates that low noise-measure transistors should be used in the design of active resonators. Since transistors with noise-measures as low as 0.1, at microwave frequencies, are readily available, active resonators could be designed with small noise-figure degradations compared to their passive counterparts.

To verify the above theory, several open-square active resonators with different feedback-loop parameters (Q_1, Q_2 and M) are designed and simulated. All these resonators satisfy the condition in (5.2) and, thus, are fully loss compensated. Fig. 5.3 shows the simulated frequency responses of the resonators, where they all achieve a similar lossless transfer function. The resonator's noise-figures are simulated at the resonance frequency and plotted in Fig 5.4 where they show different noise-

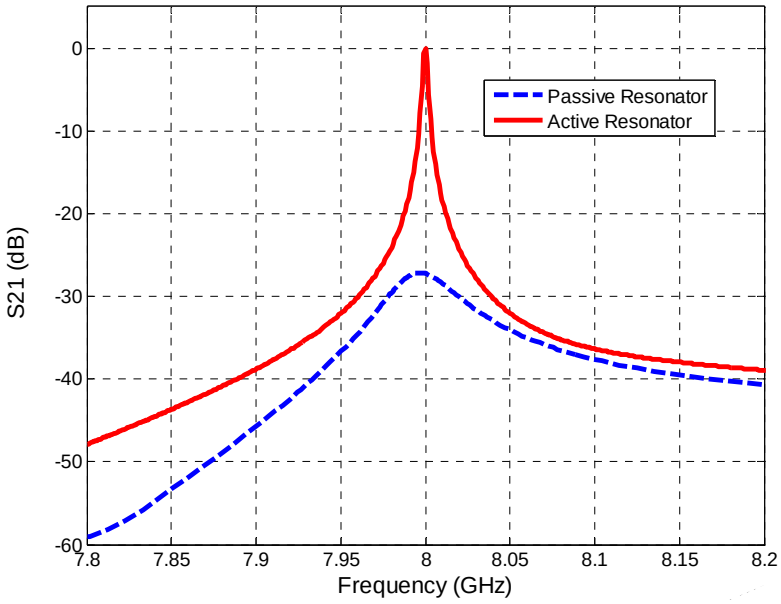

Fig. 5.3 Simulated frequency response of several active resonators with different feedback-loop parameters. The active resonators achieve the same transfer response since they all satisfy the loss compensation condition given in (5.2). The unloaded and external quality-factors of the resonators are $Q_u=200$ and $Q_e=200$, respectively.

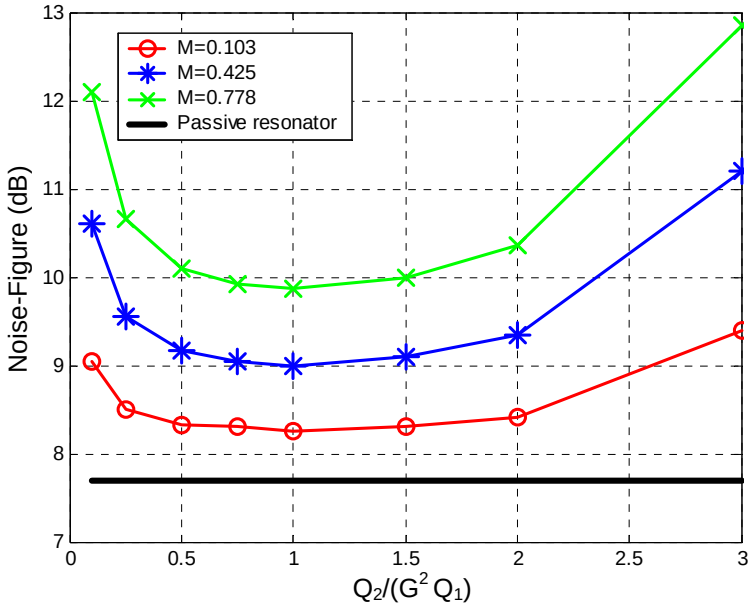

Fig. 5.4. Simulated noise-figures of several active resonators. The noise-figure is measured at the resonant frequency. Each marker represents an active resonator designed with different feedback-loop parameters. The unloaded and external quality-factors of the resonators are $Q_u=200$ and $Q_e=200$, respectively. M is the noise-measure of the amplifier used in the active feedback-loop.

figures. The minimum noise-figure is achieved when $Q_2/(G^2Q_1)$ equals unity, as also predicted by (5.3). In this case, the active resonator incurs less than 0.5 dB noise-figure degradation, compared to the passive resonator. Fig. 5.4 shows that if the active resonators are not designed properly significant noise-figure degradations could occur.

Equations (5.2) and (5.3) can be combined to find the optimum feedback loop's design parameters as

$$\boxed{Q_1 = \left(\frac{G^2 - 1}{G^2}\right) Q_u}$$

$$\boxed{Q_2 = (G^2 - 1) Q_u} \tag{5.5}$$

The above equations result in a lossless high-Q resonator with minimum noise-degradation.

5.1.2 Resonator Loss Compensation Using Negative-Resistance Devices

A square loop resonator along with a negative-resistance circuitry for its loss compensation is shown in Fig. 5.5(a). The external quality factor, Q_e, represents the input and output loadings, and Q_{-r} is the resonator's quality factor due to coupling to the negative–resistance device. The active resonator's equivalent circuit is shown in Fig. 5.5(b) where the shunt RLC network represents the passive resonator coupled to the input and output ports through the transformers with turn ratio n_e. The current source I_n models the extra noise introduced by the active device. The coupling to the negative-resistance device is modeled by the transformer with turn ratio n_r.

Resonator's losses are fully compensated when the negative resistance presented to the RLC network is equal in magnitude to the positive resistance R_r, namely

$$R_r = -50n_2^2 \quad \text{or equivalently} \quad Q_u = Q_{-r}\,. \tag{5.6}$$

Therefore, the negative-resistance coupling gap in Fig. 5.5(a) should be found through

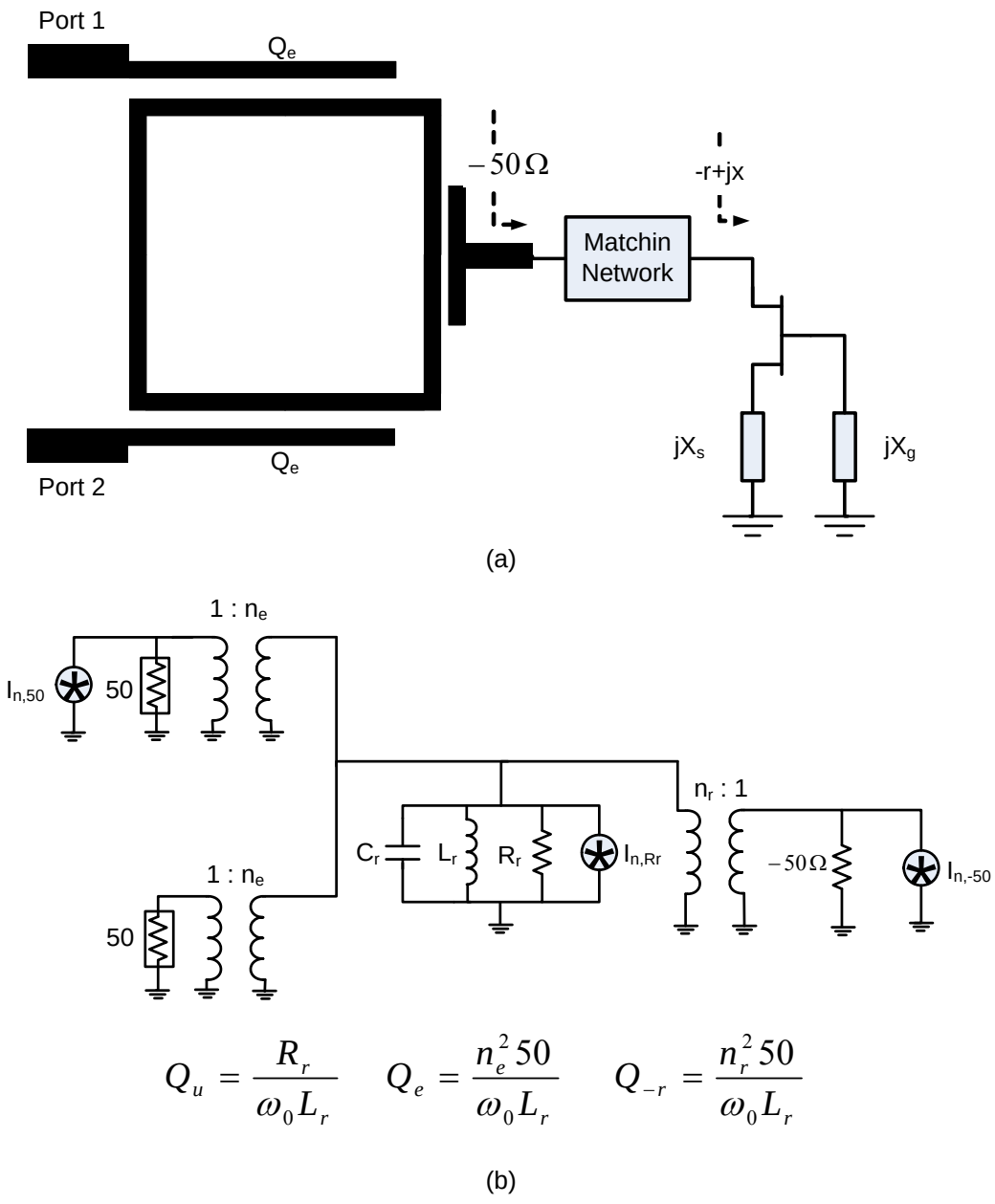

$$Q_u = \frac{R_r}{\omega_0 L_r} \qquad Q_e = \frac{n_e^2 50}{\omega_0 L_r} \qquad Q_{-r} = \frac{n_r^2 50}{\omega_0 L_r}$$

(b)

Fig. 5.5 (a) A microstrip square loop resonator along with its negative-resistance circuitry for loss compensation. (b) Equivalent circuit of the active resonator.

EM simulations such that $Q_{-r}=Q_u$, in order to fully compensate for the resonator's losses.

In microwave circuits, a negative-resistance is usually realized by providing series feedback to the gate and source terminals of a transistor [20]. In the circuit shown in Fig. 5.5(a), the gate and source reactances, X_g and X_s, act as series feedbacks. The negative-

resistance circuit is noisy due to the transistor's noise sources, where its noise level is determined through the equation for noise-measure defined as [45]

$$M = \frac{P_e}{KT_0B} \tag{5.7}$$

where K is the Boltzmann's constant, T_0 is the reference temperature and B is the bandwidth used to measure the exchangeable noise power of the active device, P_e. It is very important to design the negative-resistance device for the lowest minimum noise-measure, M_{min}, in order to minimize its noise effect on the resonator. Since the noise-measure of an one-port network is independent of the lossless network used at its input [46], in the negative-resistance circuit of Fig. 5.5(a), the noise-measure is independent of the drain matching network and it only depends on the source and gate reactive terminations. The optimum X_g and X_s values can be determined according to the procedure introduced in [47], in order to achieve the minimum noise measure at the drain port. The minimum noise-measure is given by

$$\mathrm{M_{min}} = \frac{\mathrm{F_{min}} - 1}{1 - \frac{1}{\mathrm{G_a}}} \tag{5.8}$$

where F_{min} and G_a are the transistor's minimum noise-figure and associated gain, respectively. The drain matching network is then designed to transform the impedance at the drain to the required value, -50 Ω in this example.

The minimum noise-figure of the active resonator can be derived in terms of the circuit and device parameters by analyzing the equivalent circuit of Fig. 5.5(b). The output noise contributions are from the input noise ($\mathrm{I_{n,50}}$), passive resonator losses ($\mathrm{I_{n,Rr}}$), and the negative-resistance device ($\mathrm{I_{n,-50}}$), with the power spectral densities of

$$\overline{\mathrm{I_{n,50}}^2} = \frac{4\mathrm{KT_0B}}{50} \qquad \overline{\mathrm{I_{n,R_r}}^2} = \frac{4\mathrm{KT_0B}}{\mathrm{R_r}} \qquad \overline{\mathrm{I_{n,-50}}^2} = \frac{4\mathrm{KT_0B}}{50}\mathrm{M_{min}}\,. \tag{5.9}$$

The last term in (5.9) is obtained by equating the exchangeable noise power of the

negative-resistance device given in (5.7) to that of the current source $I_{n,-50}$ in parallel with the -50 Ω resistor. By calculating the ratio of the total output noise power to the contribution from the input noise, one can show that the active resonator's noise-figure is

$$\boxed{F_{min} = F_{passive} + \left(\frac{2Q_e}{Q_u}\right) M_{min}}$$

$$\text{where} \qquad F_{passive} = 1 + \frac{2Q_e}{Q_u} \ . \tag{5.10}$$

In the above equations F_{active} and $F_{passive}$ are the noise-figure of the active and passive resonators, respectively. Equation (5.10) encapsulates the noise effect of the active device on the resonator's noise-figure, indicating that a low noise-measure transistor should be selected for the active resonator design. Since transistors with noise-measures as low as 0.1 at microwave frequencies are readily available, small noise-figure degradations could be achieved compared to the passive resonator. It is interesting that the above equation is similar to (5.4) which is the noise-figure of an active resonator designed using an active feedback-loop.

The negative-resistance device amplifies RF power in order to compensate for the energy loss within the passive resonator. The amount of the power added by the negative-resistance can be determined by analyzing the equivalent circuit shown in Fig. 5.5(b). Assuming the input power at port one is P_{in}, the voltage across the LC tank becomes

$$V_{tank} = \sqrt{2\omega_0 L_r Q_e P_{in}} \tag{5.11}$$

The amount of the power added by the negative-resistance device (P_{added}) is equal to the power dissipated by the tank's positive resistance:

$$P_{added} = \frac{V_{tank}^2}{2R_r} = \left(\frac{2Q_e}{Q_u}\right) P_{in}. \tag{5.12}$$

The above equation shows the relation between the power added by the negative-resistance device and the resonator's input power and quality-factors. Finally, it should be

mentioned that the above equation is general and can be applied to various types of active resonators. Following a similar procedure, one can show that it also holds for the active resonators designed using active feedback-loops.

5.1.3 Low-Noise Active Resonator Design, Final Remarks

Active resonators are designed by using active feedback-loops or negative-resistance devices to compensate for the losses within the passive resonators. Both loss compensation methods were discussed and their respective design procedures were presented that allow for resonators' full loss compensation with minimum noise-figure degradations. It was shown that the two methods yield a similar performance in terms of noise-figure and power consumption and their choice depends on the implementation constraints. A summary of the formulas for noise-figure and power consumption of active resonators are provided here for future reference.

Note that, in active resonators, the loaded and external quality-factors are equal since the unloaded quality-factor is infinity due to full loss compensation. Therefore one can rewrite (5.4), (5.10) and (5.12) as

$$\begin{cases} Q_{L,active} = Q_e \\ F_{passive} = 1 + \dfrac{2Q_e}{Q_u} \\ F_{active} = F_{passive} + \left(\dfrac{2Q_{L,active}}{Q_u}\right) M \\ \dfrac{P_{added}}{P_{in}} = \dfrac{2Q_{L,active}}{Q_u} \end{cases} \tag{5.13}$$

where $F_{passive}$ and F_{active} are the noise-figures of the passive and active resonators, respectively. $Q_{L,\,active}$, Q_e and Q_u are, respectively, the loaded quality-factor of the active resonator, the external quality-factor, and the unloaded quality-factor of the passive resonator. P_{in} is the power input to the resonator and P_{added} is the power added by the loss compensation network.

5.2 The Application of Active Resonators for Low Phase-Noise Oscillators

In this section it will be shown that one can take advantage of high loaded quality-factors of active resonators to design very low phase-noise oscillators. Both theoretical analysis and simulation results are presented, indicating that phase-noise monotonically decreases by increasing the active resonator's loaded quality-factor. Too large a value of quality-factor, however, significantly increases the power consumption and poses serious challenges to the design of the amplifier in the resonator's loss compensation network. In other words, the power efficiency is compromised for lower phase-noise in oscillators employing active resonators, as discussed in the following.

5.2.1 Theory

Active resonators can be designed for very high loaded quality-factors due to their lossless characteristics. This makes them attractive for the design of low phase-noise oscillators. On the other hand, the active resonator's excess noise sources increase the noise level in the oscillator's loops which adversely affects its phase-noise. A resonator figure-of-merit, *R-FOM*, was introduced in Section 3.3 in order to evaluate the overall effect of a resonator on an oscillator's phase-noise. The *R-FOM* definition is modified as following so that it can be applied to active resonators

$$R - FOM = 10log\left(\frac{F}{Q_L^2}\right). \tag{5.14}$$

Here, F is the resonator's noise figure. The above definition is based on the observation that F and $Q_L{}^2$ appear, respectively, in the denominator and numerator of the Leeson's formula for phase-noise. Note that (5.14) is a general form of (3.16) which can be applied to both active and passive resonators.

An active resonator's *R-FOM* can be expressed in terms of design parameters by inserting (5.13) into (5.14)

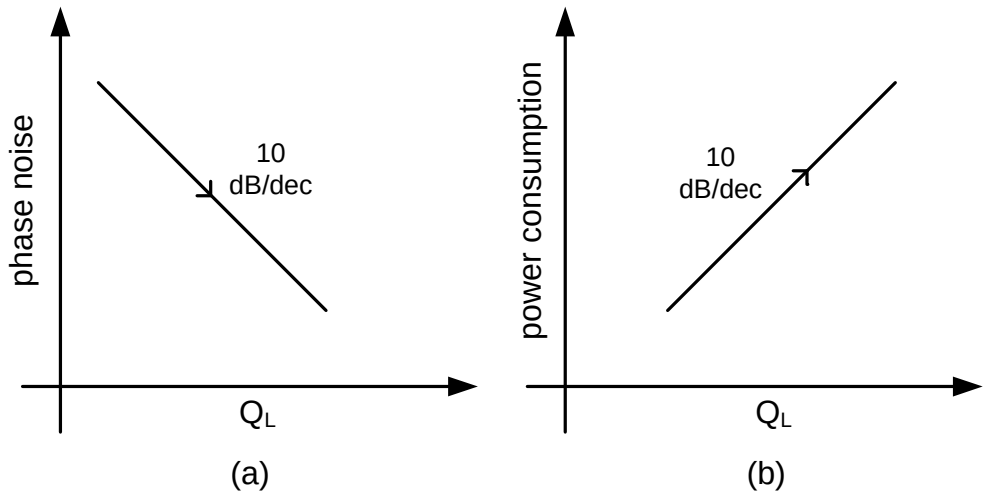

Fig. 5.6 (a) Phase-noise and (b) power consumption in oscillators versus the loaded quality-factor of the active resonators used as their frequency stabilization elements.

$$R - FOM = 10log\left(\frac{1 + (M+1)\frac{2Q_L}{Q_u}}{Q_L^2}\right). \tag{5.15}$$

Recalling from Section 3.3, low *R-FOM* values are desired for low phase-noise applications. According to the above equation, by increasing the loaded quality-factor of an active resonator (Q_L), its *R-FOM* and, equivalently, the oscillator's phase-noise monotonically decreases with an asymptotic rate of 10 dB/dec, as shown in Fig. 5.6(a). It should be mentioned that in active resonators, due to their lossless characteristics, very high loaded quality-factors can be achieved by decreasing the resonator's external coupling to the input and output loads. Therefore, despite their excess noise, high-Q active resonators can be used to design very low phase-noise oscillators.

Phase-noise reduction using active resonators comes at the cost of increased power consumption. The active device in a resonator's loss compensation network consumes DC power in order to generate RF energy to compensate for the energy dissipation within the resonator. The power added by the active device is given in (5.13) where it is proportional to the active resonator's loaded quality-factor. Therefore, increasing the active resonator's loaded quality-factor for lower phase-noise directly translates into higher power consumption with a rate of 10 dB/dec, as depicted in Fig.

5.6(b). This manifests itself as very low DC-to-RF power efficiency in low phase-noise oscillators employing active resonators.

Another important issue is the effect of the active resonators' flicker-noise sources on the oscillators' phase-noise. Ideally, the flicker noise sources of active resonators do not contribute to the oscillators' phase-noise. This is because the low-frequency flicker-noise components cannot reach to the oscillators' loops due to the band-pass characteristics of the resonators. However, the active resonators' nonlinearities can upconvert the flicker noise components to around-carrier frequencies, where they can then reach the oscillators' loops, degrading their close-in phase-noise. Therefore, one must ensure that the amplifiers in the active resonators are operating in their linear regime.

5.2.2 Simulation Results for an 8-GHz Oscillator Using an Active Resonator

An 8 GHz oscillator is designed using a microstrip square-loop active resonator, in order to verify the previous discussions. Fig. 5.7 shows the circuit schematic of the oscillator consisting of an amplifier, the resonator, and a π-feedback-network. The amplifier in the oscillator's loop is designed using a bilaterally conjugate-matched to 50 ohms SiGe HBT transistor, providing a small signal gain of 8 dB. The π feedback-network element values are determined based on the substitution theory, discussed in Section 4.2.1, to close the oscillator's loop.

The simulated unloaded quality-factor of the passive microstrip square-loop resonator implemented on a 32 mils thick RO4003C substrate is 72. The resonator is loss compensated with an active feedback loop using an ideal amplifier with 7 dB insertion gain and 2 dB noise-figure. The active feedback-loop is designed based on the procedure introduced in Section 5.1.1. The loaded quality-factor of the active resonator is controlled by adjusting the input/output coupling gaps (g). Several active resonators with different loaded quality-factors were designed, and their simulated noise-figures are depicted in Fig. 5.8(a). As it can be seen, the simulation results are in good agreement with the theoretical values calculated from (5.13). This validates the active resonators' noise

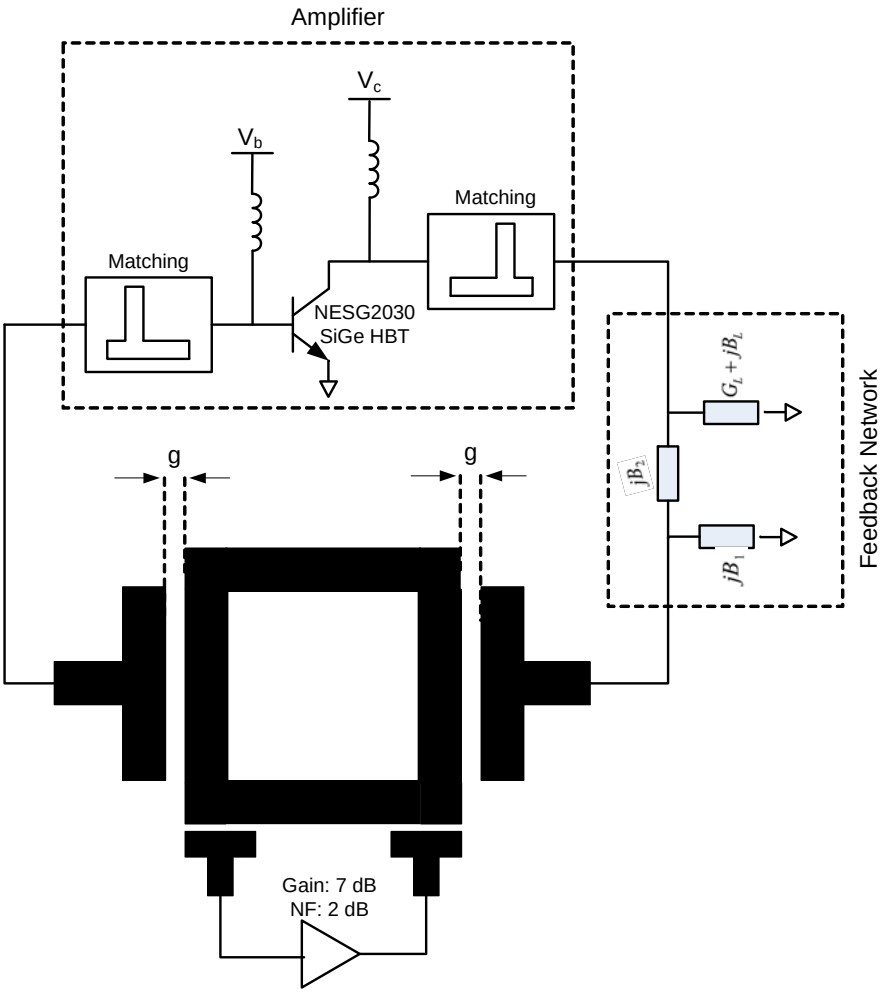

Fig. 5.7 Circuit schematic of an 8 GHz oscillator designed using a microstrip square-loop active resonator.

analysis presented in Section 5.1. It is also notable that noise-figure proportionally increases by increasing the loaded quality-factor.

The oscillator is simulated in Agilent's ADS. The oscillation frequency is 8 GHz with 7 dBm output power level. Fig. 5.8(b) shows the simulated oscillator's phase-noise versus the active resonator's loaded quality-factor. As it can be seen, the phase-noise monotonically decreases by increasing the resonator's loaded quality-factor (increasing g). The rate of the phase-noise improvement is close to 10 dB/dec as predicted by (5.15) obtained from theoretical analysis. Notably, the active resonator with the loaded quality-factor of 2000 reduces the phase-noise level to -150 dBc/Hz at 1 MHz frequency offset;

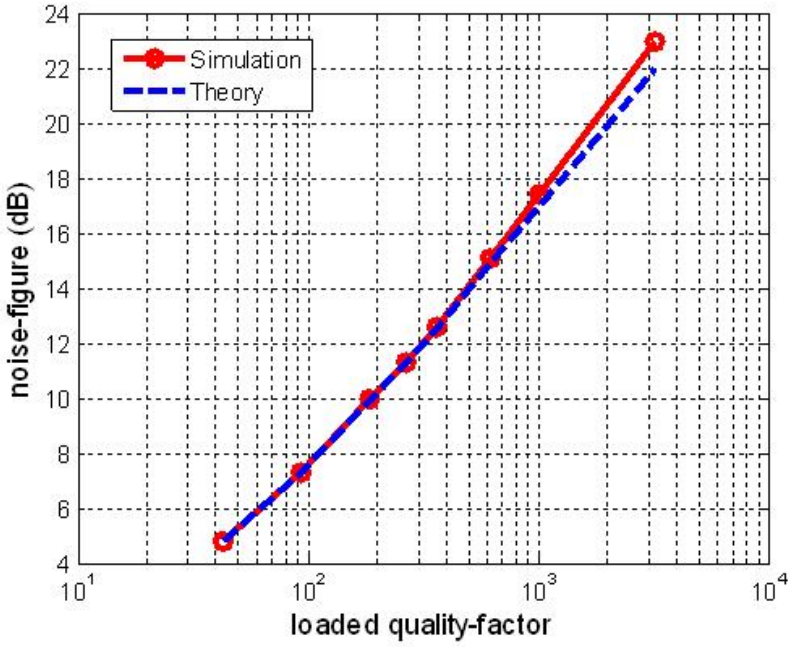

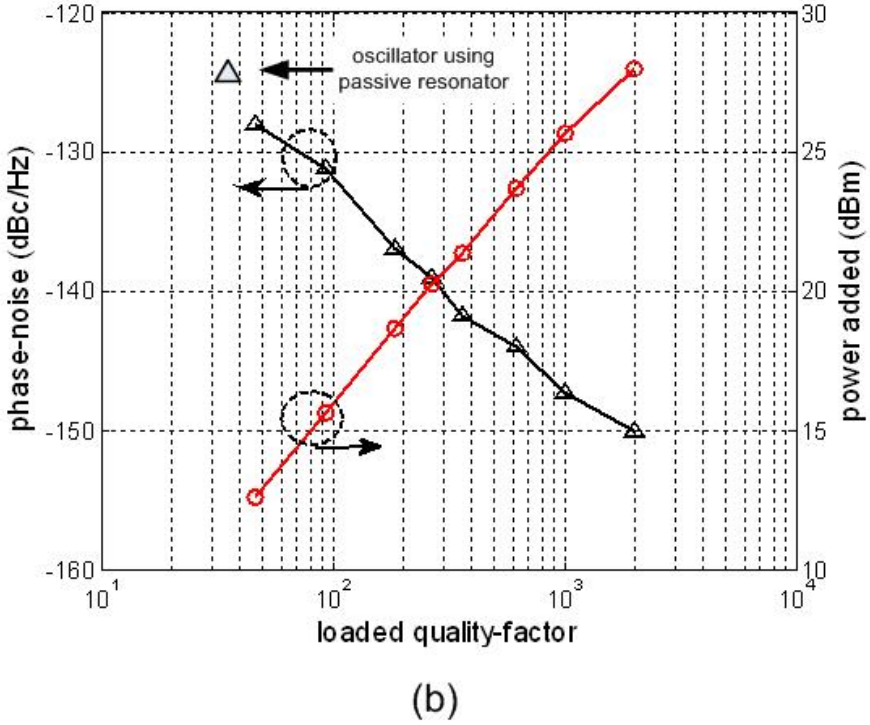

Fig. 5.8 (a) Simulated noise-figure of the square-loop active resonator for different loaded quality-factors. Noise-figure is calculated at the resonant frequency. (b) Simulated oscillator's phase-noise at 1 MHz frequency offset versus the loaded quality-factor of its active resonator. This graph also shows the amount of the power added by the amplifier (P_{added}) in the active resonator's loss compensation network.

namely, 25 dB lower than the phase-noise of a similar oscillator using a passive square-loop resonator. The compromise is the increased power consumption. As observed in Fig. 5.8(b), in order to achieve a loaded quality-factor of 2000, the amplifier in the resonator's loss compensation network should generate 28 dBm of RF power. This value is about 125 times higher than the oscillator's output power level! As a result, the DC-to-RF power efficiency is severely degraded and drops to less than 0.5%.

5.3 Low Phase-Noise Oscillator Design Employing Active Elliptic Filters

In the preceding section we showed that low phase-noise oscillator designed using a *single* active resonator suffers from a very low DC-to-RF power efficiency. This is due to the high power consumption of active resonators designed for high loaded quality-factors. One can mitigate this problem by employing active elliptic filters as the frequency stabilization elements in oscillators. In chapter 4, it was shown that elliptic filters can provide higher loaded quality-factors compared to single resonators, due to their higher frequency-selectivity caused by the presence of close-to-passband transmission zeros. This feature helps active elliptic filters to achieve high loaded quality-factors at lower noise figures and power consumptions compared to single active resonators. To demonstrate this approach, an 8 GHz oscillator using a four-pole active elliptic filter is designed and tested. The oscillator shows a measured phase-noise of -150 dBc/Hz at 1 MHz frequency offset from the carrier with a DC-to-RF efficiency of 5%. To the best of our knowledge, the presented oscillator achieves the lowest phase-noise among planar oscillators reported to date.

5.3.1 Active Elliptic Filter Design

This section presents the procedure used to design an active four-pole elliptic-response filter for implementation in a low phase-noise oscillator. Elliptic filters are best suited for this application since they demonstrate higher quality-factors compared to the Butterworth and Chebyshev filters (as mentioned in Chapter 4). First, an open-square active resonator as shown in Fig. 5.9(a) is designed at 8 GHz based on the procedure outlined in Section 5.1.1. The resonator is implemented on a Rogers' RO3035^{TM} substrate with a dielectric constant of 3.55 and a thickness of 0.8 millimeters (32 mils). The passive resonator's unloaded quality-factor is 180. An ATF-33143 pHEMT transistor from Avago Technologies is selected to implement the amplifier in the feedback loop. The amplifier provides a gain of 7 dB with 1.2 dB noise figure. The optimum active resonator's feedback-loop design parameters are found from (5.5) and the corresponding input/output coupling gaps (g_1 and g_2) are determined by using Agilent's Momentum^{TM} EM solver. The simulated and measured frequency responses of

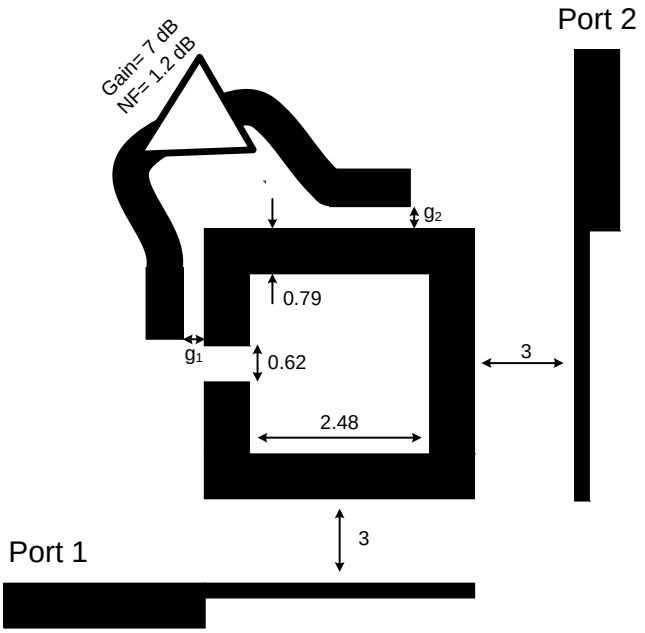

(a)

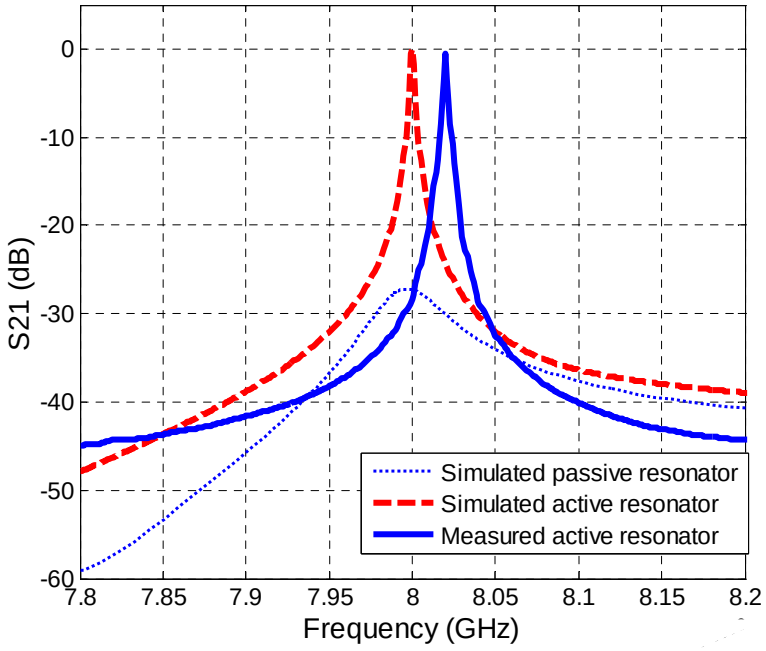

(b)

Fig. 5.9 (a) An open-square resonator with an active feedback-loop for loss compensation. (b) Measured and simulated frequency response of the loosely-coupled active resonator compared to a similar passive resonator. All dimensions are in millimeters.

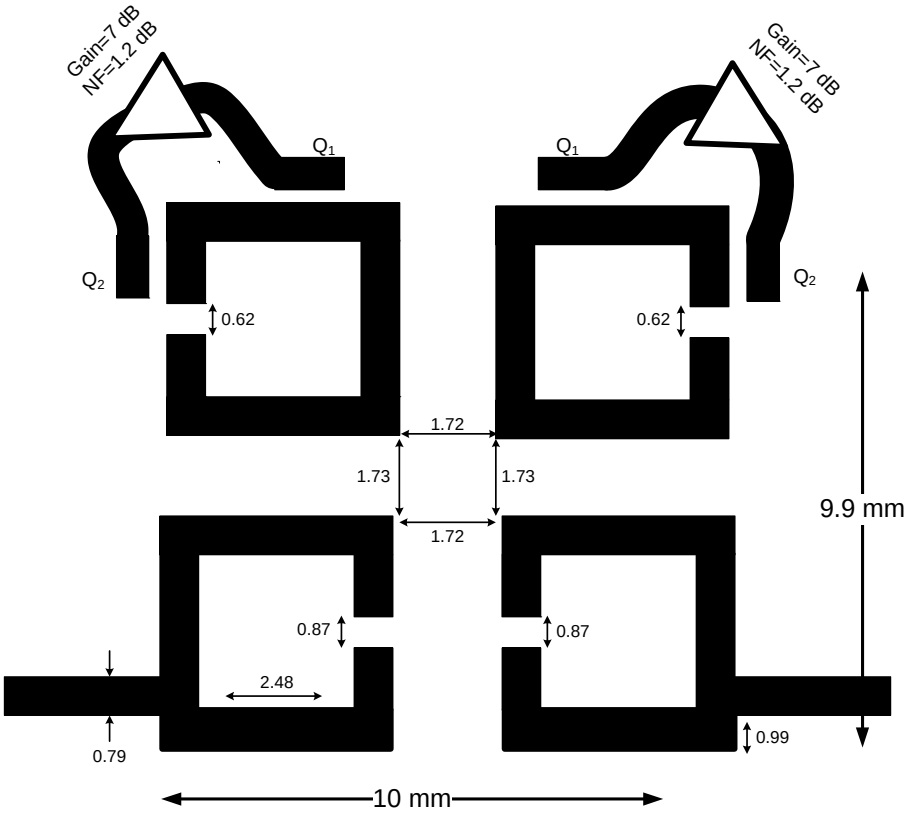

Fig. 5.10 An active four-pole elliptic-response band-pass filter designed for low phase-noise oscillator applications. The two middle resonators are loss compensated using amplifiers. Q_1 and Q_2 are resonator quality-factor due to feedback-loop's input and output loadings. All dimensions are in millimeters.

the active resonator are shown in Fig. 5.9(b). The simulation results of a passive resonator are also included for comparison. The active resonator demonstrates a measured unloaded-quality-factor of 4000. The resonant frequency of the fabricated resonator is slightly shifted due to fabrication tolerances.

Fig. 5.10 shows the circuit schematic of the elliptic filter in which the input and output resonators have been cross-coupled to realize the transmission zeros. It is not necessary to compensate for the losses of the input and output resonators since their loaded quality-factors are limited by the external loadings rather than the internal resonators' losses. In fact, in coupled-resonator filters, the unloaded quality-factors of the middle stage resonators have the highest impact on the filters' selectivity [48]. Therefore, in the filter of Fig. 5.10, only the losses of the two middle resonators have been compensated to enhance their unloaded quality-factors. This helps reduce the number of

the active devices and their associated noise in the design of the active filter. The filter design parameters, such as the bandwidth, return loss and location of the transmission-zero, are determined by optimizing the filter's *R-FOM* through the procedure introduced in chapter 4. Fig. 5.11(a) shows the simulated insertion loss and loaded quality-factor of the active filter. The simulation results of a similarly designed passive filter are also included for comparison. The active filter exhibits a peak loaded-quality-factor of 720 at the pass-band edge, which is about six times higher than that of the passive filter. The 2.2 dB insertion loss of the active filter is due to the uncompensated input and output resonators' losses. The very high loaded quality-factor of the active elliptic filter makes it suitable for the design of low phase-noise oscillators.

Noise-figure simulation results are shown in Fig. 5.11(b), where the optimized active filter (solid line) shows a slight noise-figure degradation within its pass-band compared to the passive filter (dashed line). This figure also compares the noise-figure of various other active filters designed with different feedback-loop parameters (Q_1 and Q_2). These filters satisfy the full loss compensation condition given in (5.2) and, thus, have a similar transfer characteristic as shown in Fig. 5.11(a). However, they exhibit different noise-figure performance. Simulations show that the noise-figure of the active filters will be severely degraded if the active resonators employed are not properly designed. The optimized active filter designed based on the equations given in (5.5) achieves the lowest noise-figure values over the entire pass-band.

The filter shown in Fig. 5.10 was fabricated on a RO3035^{TM} substrate. The measured insertion loss of the active filter is shown in Fig. 5.12(a). A slight shift in its center frequency is believed to be due to the fabrication tolerances. The R-FOM of the active filter is calculated based on (5.14) using the measured quality-factor and simulated noise-figure of the active filter. As shown in Fig. 5.12(b), the active filter demonstrates up to 8 dB improvement in R-FOM, compared to a passive filter with similar design parameters. This active filter is used to design a low phase-noise oscillator as described in the following section.

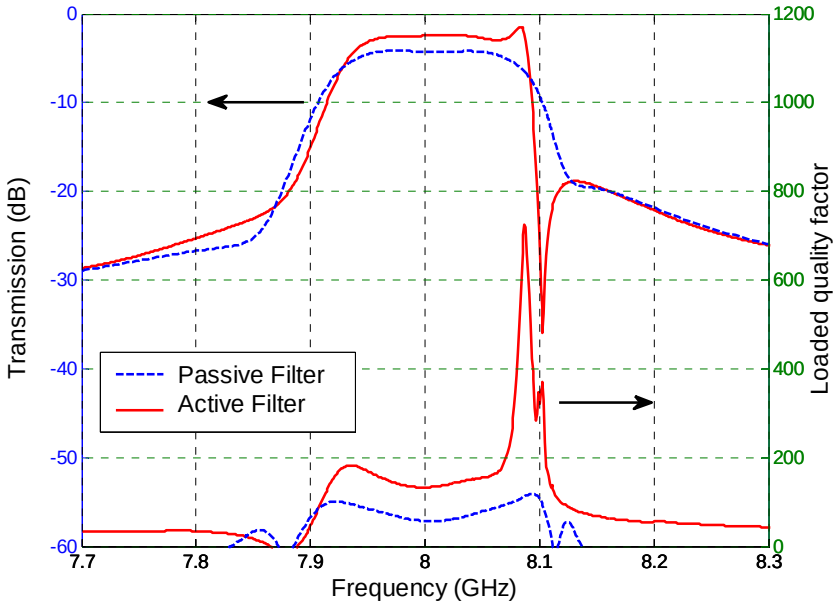

(a)

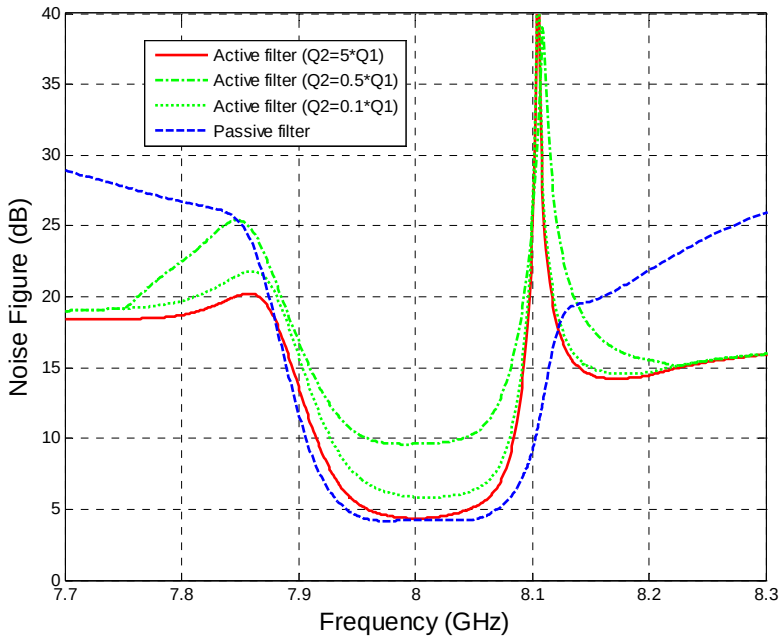

(b)

Fig. 5. 11 (a) Simulated insertion loss and loaded-quality-factor of the passive and active filter. The center frequency is 8 GHz with 130 MHz bandwidth, 10 dB return loss and normalized transmission-zero-location of 1.2. (b) Simulated noise-figure of the active and passive filters. Noise-figure simulation results of various other active filters with different feedback-loop parameters are also shown for comparison.

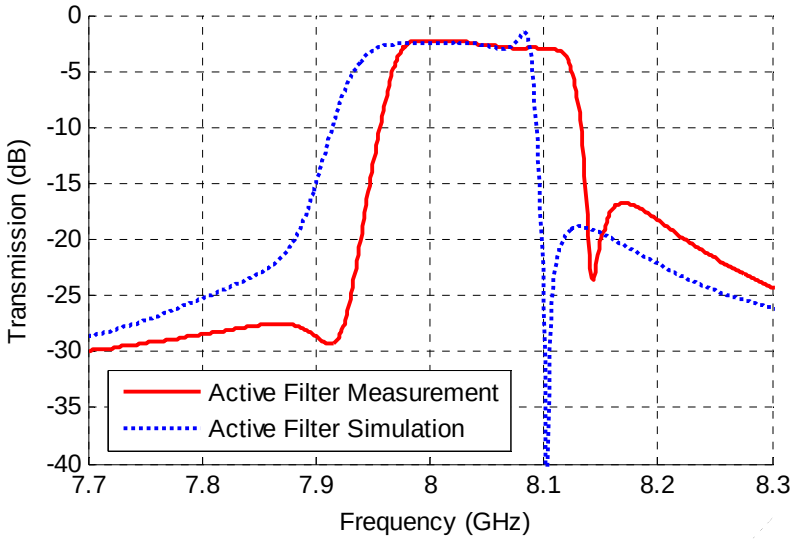

(a)

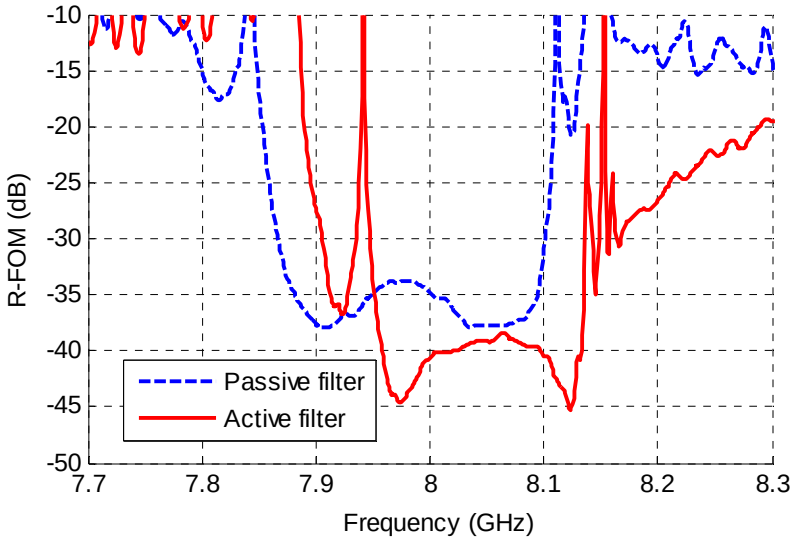

(b)

Fig. 5.12 (a) Measured and simulated insertion loss of the active filter. (b) R-FOM of the active filter. The measurement results of a similar passive filter are also shown for comparison. Lower R-FOM values are desired for low phase-noise oscillator applications.

5.3.2 Oscillator Design and Measurement

An X-band oscillator is designed using the active four-pole elliptic filter described in the previous section. The design frequency is selected at the point where the R-FOM of the filter is minimum, so as to achieve the lowest phase-noise operation of the oscillator. Fig. 5.13 shows a picture of the fabricated oscillator. The amplifier in the oscillator loop employs an NESG2030M04 HBT transistor from NEC with a gain of 8 dB. The transistor is biased at the collector voltage of 2 volts and collector quiescent current of 10 mA. A π-circuit configuration is selected to design the parallel feedback network based on the substitution theory discussed in Section 4.2.1.

The oscillator is fabricated and its measured output spectrum is shown in Fig. 5.14(a). The oscillation frequency is 7.990 GHz with an output power of 10 dBm. The total consumed DC power for the oscillator is 200 mW, corresponding to DC-to-RF efficiency of 5%. The core oscillator efficiency, not including the active resonators, is 31%.

The phase-noise of the oscillator is measured by an Agilent's E5500 phase-noise measurement system. The measurement results are shown in Fig. 5.14(b) where it shows a phase-noise of -150 dBc/Hz at 1 MHz offset from the carrier. This corresponds to an approximately 7 dB phase-noise improvement over the phase-noise of the oscillator in Chapter, 4 which uses a passive filter with similar design parameters. A similar improvement is observed in $1/f^3$ region where the flicker-noise is dominant. It is noteworthy that the phase-noise in this region is generated through a multiplicative process and does not directly depend on the carrier power level [49]. This indicates that the phase-noise improvement is due to the enhanced quality-factor of the active filter over the passive filter. Table 5.1 compares the performance of the oscillator with other reported planar oscillators. To the best of our knowledge, the oscillator described here has the lowest phase-noise among microwave planar oscillators reported to date. The FOM of the oscillator is -205 dBc/Hz, which is about 2 dB worse than the FOM of the oscillator employing a four-pole passive elliptic filter described in Chapter 4. This indicates that the active filter improves the phase-noise of the oscillator at the cost of increased power consumption compared to the oscillator employing a similar passive

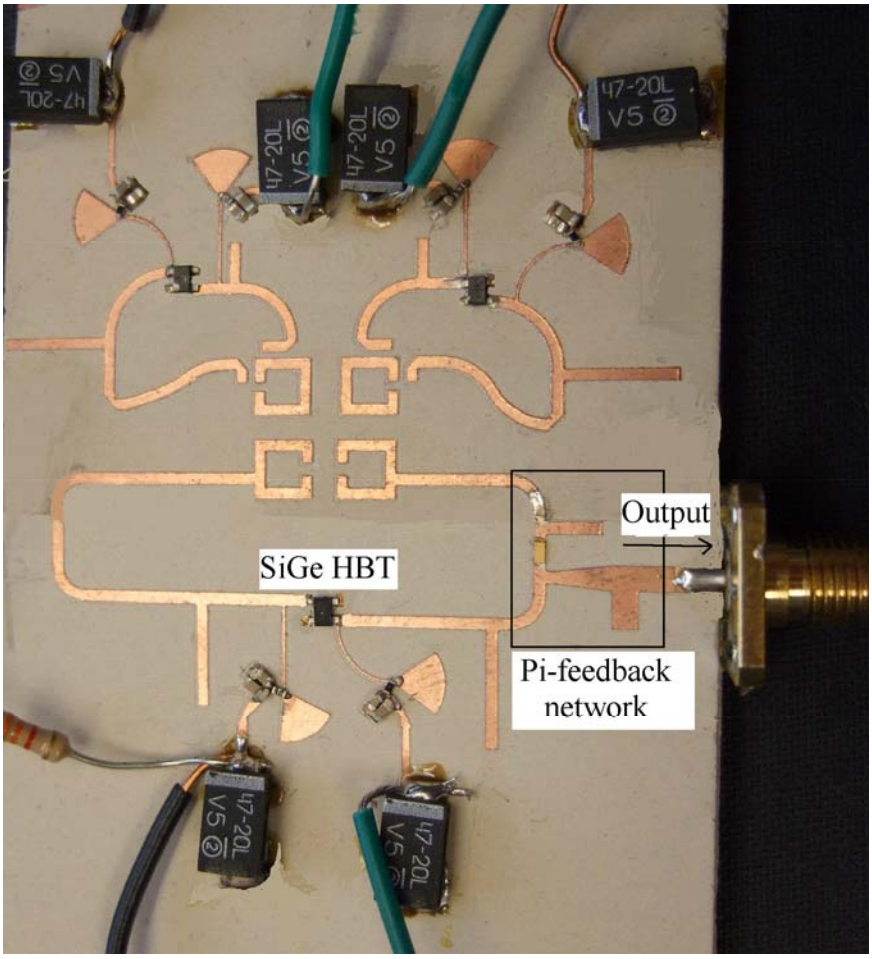

Fig. 5.13. Top view of the fabricated 8 GHz oscillator employing an active four-pole elliptic-response bandpass filter. The active device in the oscillator loop is an NESG2030M04 HBT SiGe transistor. The transistors of the active filter are ATF-33143 pHEMT devices. The π-network consists of a series capacitor and two shunt microstrip open stubs. The filter's dimensions are given the Fig. 5.10.

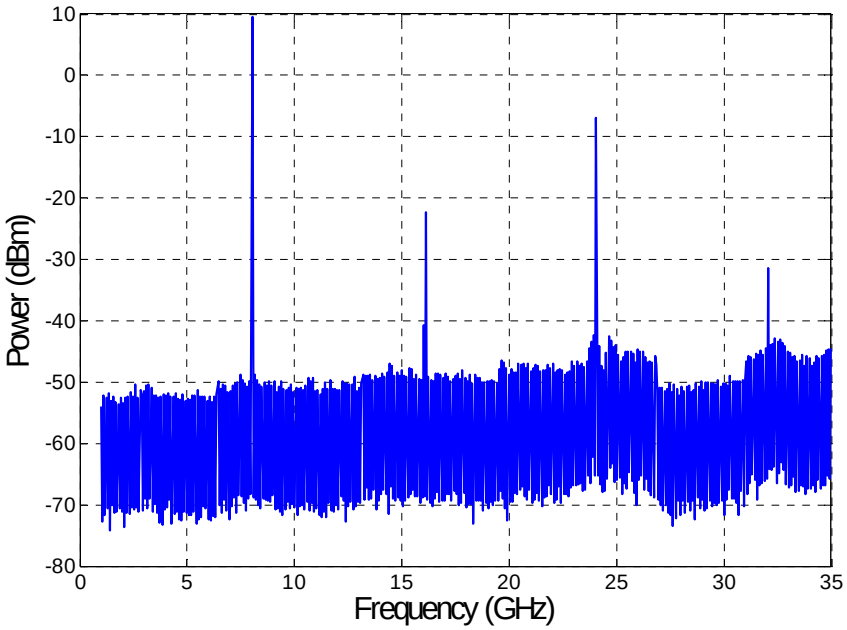

(a)

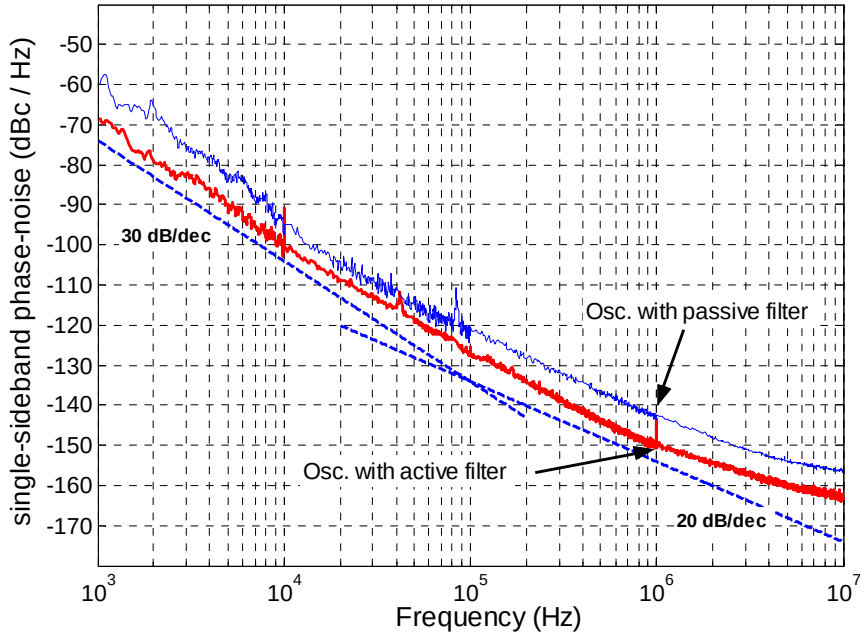

(b)

Fig. 5.14 (a) Measured output spectrum of the oscillator. (b) Measured phase-noise of the fabricated oscillator at 8 GHz. Phase-noise at 1 MHz offset from the carrier is about -150 dBc/Hz. Compared to an oscillator utilizing a similar passive filter, the oscillator with the active filter provides about 7 dB lower phase-noise at 1 MHz offset from the carrier.

Table 5.1
Comparison with other reported microwave planar hybrid oscillators

Device	Resonator	F_o GHz	P_o dBm	Eff. %	L(f) † dBc/Hz	FOM dBc/Hz
HEMT [7]	Ring resonator	12	5.3	48.7	-116.2	-189.3
Si BJT [8]	Hairpin Resonator	9	9	4.5	-129	-185.6
HEMT [26]	Active resonator	10	10	2	-134.4	-187.4
SiGe HBT [34]	Extended resonance	9.1	9.7	14	-139	-199.9
HEMT [41]	Active filter	10	1.5	-	-119	-
SiGe HBT [50] [Chapter 4]	Passive elliptic filter	8.1	3.5	10	-143	-207
This work (SiGe HBT)	Active elliptic filter	8	10	5	-150	-205

† Phase-noise at 1 MHz frequency offset.

filter.

5.4 Conclusion

High loaded quality-factors of active resonators make them attractive for the design of low phase-noise oscillators. However, active resonators introduce extra noise sources whose impact on the phase-noise of the oscillators need to be minimized. In this chapter, active resonators were analyzed and a design procedure was introduced that allows for their full loss-compensation with minimum noise-degradation. Consequently, the active resonators can achieve high loaded quality-factors while their excess-noise contribution to the phase-noise of the oscillators is minimized. It is shown, through analysis and simulation, that active resonators can significantly reduce the phase-noise in oscillators, at the cost of increased power consumption. In other words, in oscillators using single active resonators as their frequency stabilization elements, DC-to-RF power efficiency is traded for lower phase-noise.

Active elliptic filters are advantageous to single active resonators as they can generate high loaded quality-factors at lower noise figures and power consumptions. An X-band oscillator was designed using a four-pole active elliptic filter. The active elliptic filter was optimized to achieve the lowest oscillator's phase-noise. The fabricated oscillator provides 10 dBm output power with 5% DC-to-RF efficiency at 8 GHz. Its measured phase-noise achieves a record value of -150 dBc/Hz at 1 MHz frequency offset. This corresponds to an approximately 7 dB improvement over the oscillator reported in Chapter 4, which uses a passive filter with similar design parameters. To the best of author's knowledge, the oscillator presented in this paper achieves the *lowest* phase-noise among any published planar oscillator to date.

Chapter 6

Miniaturized Low Phase-Noise Voltage-Controlled-Oscillator Design Using Dual-Mode Active resonators

In Chapter 5, an X-band oscillator was designed employing a four-pole active elliptic filter in its feedback loop. The oscillator achieved a record low phase-noise performance due to the high-Q and low-noise properties of the filter. However, the oscillator is not amenable to integrated circuit fabrication due to its relatively large area and high DC power consumption. In this chapter, a new oscillator design technique is introduced that offers significant advantages in terms of size, frequency tunability and DC power consumption, while achieving a similar state-of-the-art phase-noise performance.

The oscillator's core is a reactively-terminated active elliptic filter, acting as a high-Q negative-resistance resonator, as shown in Fig. 6.1(a). In this configuration, the active filter provides high frequency-selectivity and, at the same time, initiates and sustains oscillation. Therefore, as opposed to the conventional parallel feedback technique (Fig. 6.1(b)), there is neither a need for an amplifier in the oscillator loop, nor for a coupler to deliver power to the external load, leading to a considerable DC power saving and a compact oscillator structure. To further reduce the oscillator's size, the active filter is designed using a dual-mode active resonator. As discussed in this chapter, dual-mode resonators can be configured to realize compact elliptic filters. This technique not only helps to achieve high quality-factors while occupying a small area, but also facilitates an oscillator's frequency tuning.

In Section 6.1, dual-mode resonators and their resonant properties are discussed.

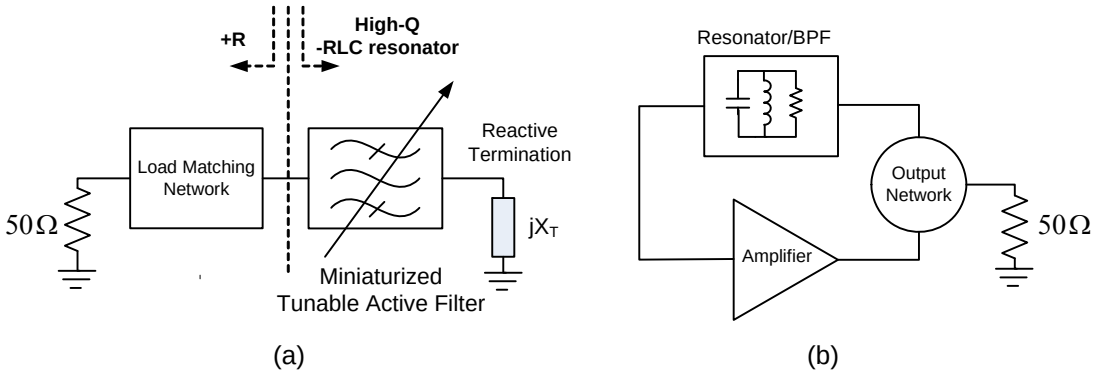

Fig. 6.1 Block diagram of (a) the proposed voltage-controlled-oscillator, and (b) a conventional parallel-feedback oscillator.

A compact pseudo-elliptic band-pass filter is designed by coupling the two resonant modes of a dual-mode active resonator. Simulation and measurement results show that the dual-mode filter can achieve very high loaded quality-factors, making it attractive for the design of compact low phase-noise oscillators. In section 6.2, the proposed very low phase-noise voltage-controlled-oscillator (VCO) design approach using a dual-mode active resonator is described. The VCO achieves a measured tuning range of 8.15-8.255 GHz with phase-noise values of less than -148 dBc/Hz, at 1 MHz frequency offset, over the entire tuning range. The VCO's figure-of-merit is -211.7 dBc/Hz. To the best of our knowledge, this is the lowest phase-noise and FOM for a planar oscillator. The output power level is 7 dBm with 12.5% DC-to-RF efficiency. The proposed VCO structure occupies a relatively small area making it attractive for integrated circuit fabrication at mm-wave frequencies.

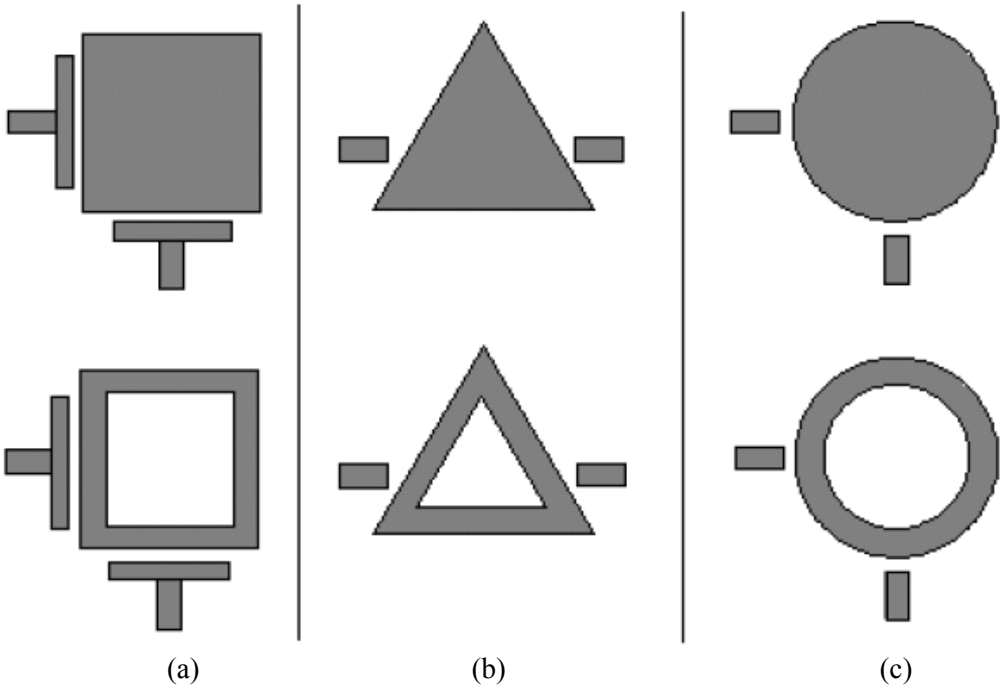

Fig. 6.2 Microstrip loop and patch resonator topologies for dual-mode operation (a) square shape (b) triangular shape (c) circular shape [52].

6.1 Miniaturized Band-Pass Elliptic Filter Design Using a Dual-Mode Active Resonator

Classical microstrip band-pass filters are designed using single-mode resonators. In recent years, dual-mode resonators have been increasingly used in wireless communication systems and other RF applications for their low-loss and compact properties [51]-[55]. Because of their double resonant behavior, a dual mode band-pass filter of a certain order requires half as many resonators when compared to a single-mode-resonator band-pass filter topology. Fig. 6.2 shows some typical resonator topologies used for dual-mode operation. These topologies possess a pair of degenerate resonant modes whose resonant frequencies are split when a perturbation element is strategically introduced. This section shows that a pseudo-elliptic band-pass filter can be designed by controlling the resonant frequencies and transmission zeros produced by the resonator in dual-mode operation.

6.1.1 Resonant Properties of Dual-Mode Resonators

A dual-mode square-loop resonator is shown in Fig. 6.3. The total periphery of the resonator is a wavelength. This allows the resonator to simultaneously sustain two orthogonal resonant modes along its vertical and horizontal axes. The electric and magnetic field patterns, shown in Fig. 6.3(b), indicate that the excited resonant mode is corresponding to TM_{100}^{z} mode when port 1 is excited, where z is the axis perpendicular to the ground plane [55]. If the excitation port is changed to port 2, the field patterns are rotated by 90^{o} for the vertical degenerate mode, which corresponds to TM_{010}^{z} mode. The two modes have the same resonant frequencies. With the presence of a small perturbation ($d \neq 0$), the modes are coupled to each other and resonant frequency splitting occurs, as shown in Fig. 6.4(a). The coupling coefficient depends on the perturbation size, *d*, and it can be calculated from the following [31]

$$k = \pm \frac{f_2^2 - f_1^2}{f_2^2 + f_1^2} \tag{6.1}$$

where f_2 and f_1 are the upper and lower resonant frequencies. Fig. 6.4(b) shows the calculated coupling coefficient versus perturbation size for a square loop resonator implemented on a 32 mils thick RO4003C substrate at 8 GHz. The sign of *k* depends on the nature of coupling which is determined by the type of perturbation. A patch perturbation, $d > 0$, results in electric coupling with positive *k*, whereas a magnetic coupling with negative *k* is created through a corner cut, $d < 0$, [56], [57].

The input/output ports can be coupled to both modes through offset-to-center feeding lines, as shown in Fig. 6.5(a). The external loading effects on the horizontal and vertical modes are represented by the external quality-factors, Q_e^{h} and Q_e^{v}, respectively. The external quality-factors are calculated using [31]

$$Q_e = \frac{f_0}{f_{+90^o} - f_{-90^o}} \tag{6.2}$$

where f_{+90} and f_{-90} are the frequencies at which the phase of S_{11} (for horizontal mode) or

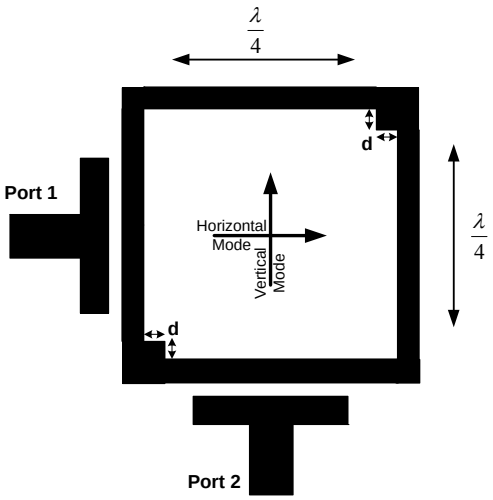

(a)

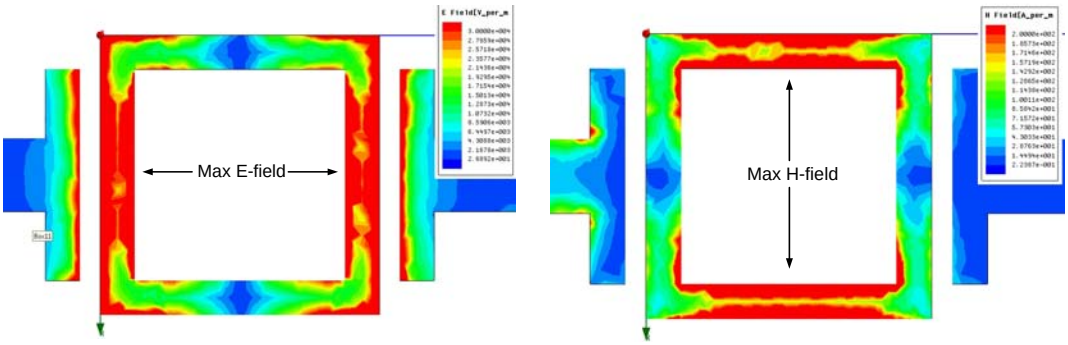

(b)

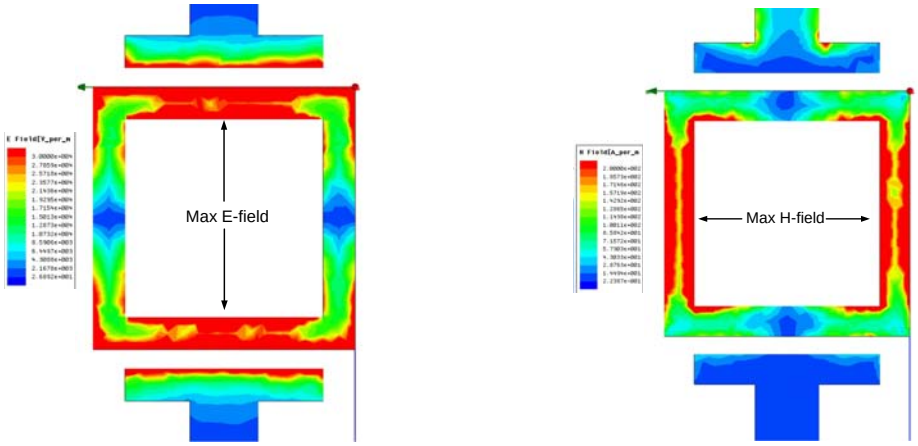

(c)

Fig.6.3 (a) A microstrip square-loop dual-mode resonator. λ is the wavelength. (b) Field pattern of horizontal mode. (c) Field pattern of vertical mode. Simulation results are obtained from Ansoft HFSS.

S_{22} (for vertical mode) shows $+90^{o}$ and -90^{o} difference with respect to the phase at center frequency, f_0. Fig. 6.5(b) shows the calculated external quality-factor curves versus the feeding line's dimensions.

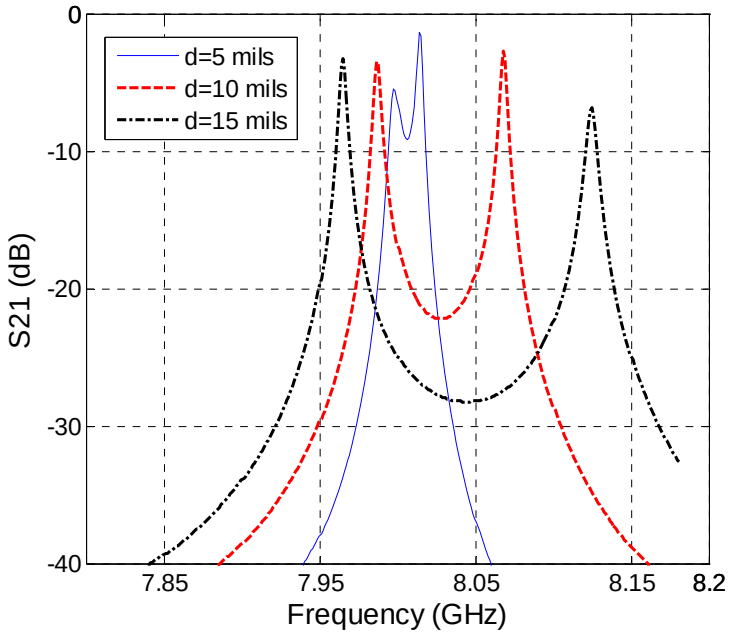

(a)

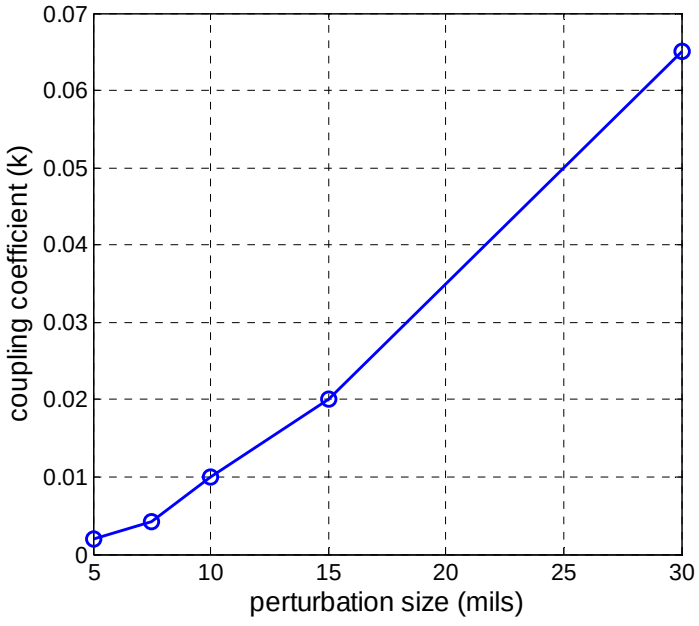

(b)

Fig.6.4 (a) Resonant frequency splitting due to mode coupling in a square-loop dual-mode resonator shown in Fig. 6.3(a). (b) Calculated coupling coefficient versus perturbation size *d*. The dual-mode resonator's square-loop periphery is 950 mils and *W*=33 mils.

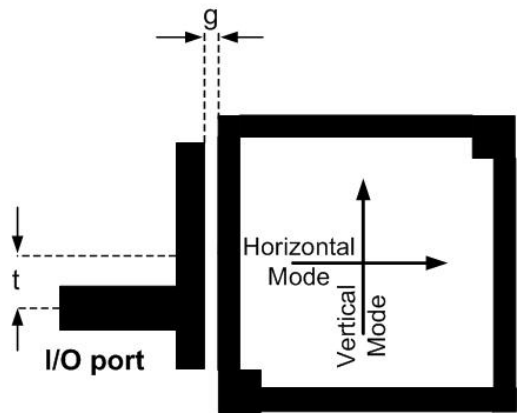

(a)

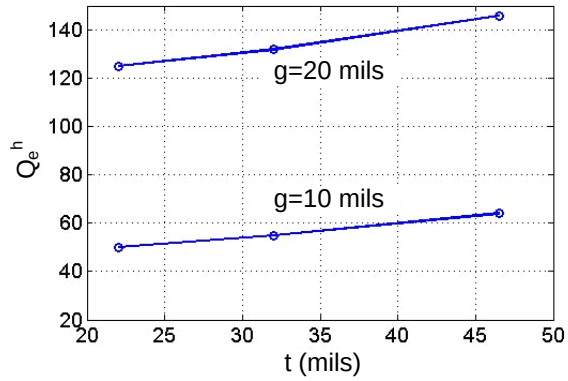

(b)

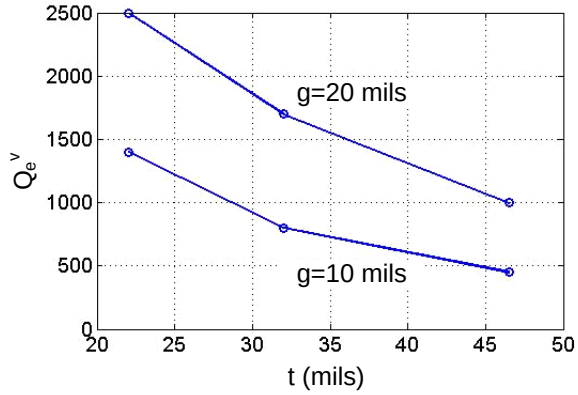

(c)

Fig. 6.5 I/O Coupling structure for the dual-mode square-loop resonator shown in Fig. 6.3(a). The I/O port is coupled to both modes through offset to center feeding line. The calculated (b) Q_e^h and (c) Q_e^v for various feeding line dimensions. Q_e^v and Q_e^h are, respectively, the vertical and horizontal modes' external quality-factors due to the loading from I/O line. The dual-mode resonator's square-loop periphery is 950 mils and W=33 mils.

6.1.2 Realization of a Compact Pseudo-Elliptic Band-Pass Filter Using a Dual-Mode Active Resonator

A dual-mode active resonator configured to realize a pseudo-elliptic band-pass filter is shown in Fig. 6.6. A compact version of the resonator employing meandered lines is given in Fig. 6.6(b), occupying a relatively small area of λ/8 × λ/8, where λ is the wavelength. Each resonant mode is coupled to a negative-resistance device for loss compensation. The negative resistances are realized using NESG2030 SiGe HBT transistors based on the procedure outlined in Section 5.1.2. The two lossless resonant modes are coupled to each other by the small patch perturbation at the two inner corners. The input and output ports are coupled to both modes through offset-to-center feeding lines. According to the filter's coupling scheme shown in Fig. 6.6(c), the multi-path connection between the input and output ports facilitates the realization of a transmission zero in order to achieve a pseudo-elliptic band-pass response.

Fig. 6.7 shows the equivalent circuit of the filter, where the shunt LC networks model the lossless resonant modes, and the quarter-wave transmission lines represent the couplings. The filter's design procedure is detailed here. First, the coupling matrices (*M*) for various filters with different bandwidths, return losses, and locations of zeros, are synthesized. In the next step, the element values of the equivalent circuit are determined in terms of the filter's parameters and coupling coefficients [31]

$$\mathrm{C_0} = \frac{1}{(M_{S1}^2 \omega_0 \mathrm{Z_0})\,(F.B.W)} \times 10^{12}\ (\mathrm{pF}) \quad \mathrm{L_0} = \frac{(M_{S1}^2 \mathrm{Z_0})\,(F.B.W)}{\omega_0} \times 10^{9}\ (\mathrm{nH}) \quad (6.3)$$

where ω_0 is the angular frequency at the mid-band frequency of the filter, and *F.B.W* is the filter's fractional 3-dB bandwidth. The quarter-wavelength transmission lines' characteristic impedances are determined by [31]

$$\mathrm{Z_{S1}} = \mathrm{Z_{L2}} = \mathrm{Z_0} \quad \mathrm{Z_{S2}} = \mathrm{Z_{L1}} = \sqrt{\frac{\mathrm{Z_0}}{(\mathrm{C_0}\omega_0 \mathrm{M_{S2}^2})(\mathrm{F.B.W})}} \quad \mathrm{Z_{12}} = \frac{(\mathrm{M_{S1}^2 Z_0})(\mathrm{F.B.W})}{\mathrm{M_{12}}} \quad (6.4)$$

where Z_0 = 50 Ω is the I/O port impedance.

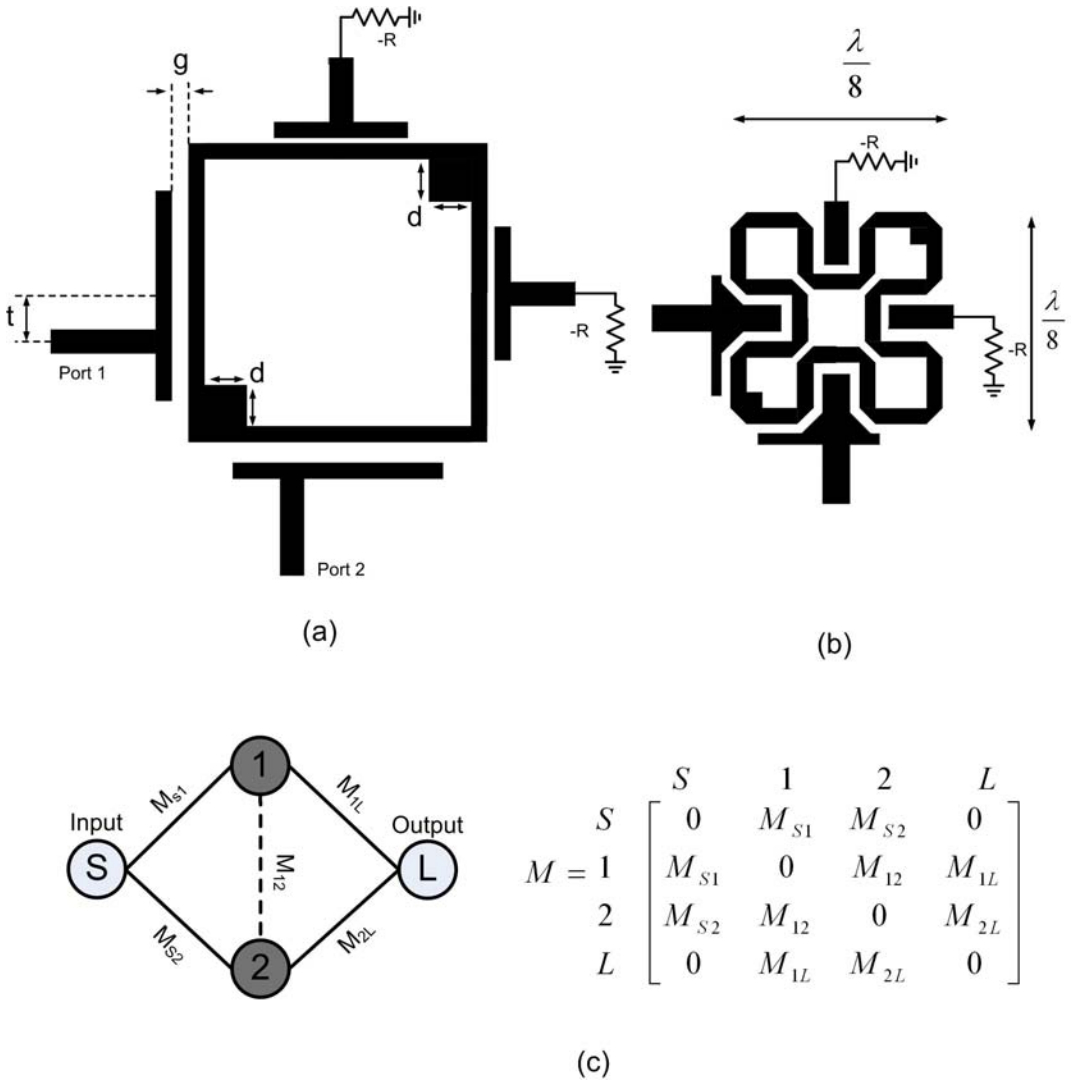

$$M = \begin{array}{c} \\ S \\ 1 \\ 2 \\ L \end{array} \begin{array}{c} \begin{array}{cccc} S & 1 & 2 & L \end{array} \\ \begin{bmatrix} 0 & M_{S1} & M_{S2} & 0 \\ M_{S1} & 0 & M_{12} & M_{1L} \\ M_{S2} & M_{12} & 0 & M_{2L} \\ 0 & M_{1L} & M_{2L} & 0 \end{bmatrix} \end{array}$$

Fig. 6.6 (a) A dual-mode active resonator configured to realize a pseudo-elliptic band-pass filter. Horizontal and vertical resonant modes are coupled to negative resistances for loss compensation. (b) Compact version of the filter using a meandered-loop resonator. (c) Coupling scheme and coupling matrix of the filter. The two resonant modes (1&2) are coupled to each other through M_{12}, and to the input and output ports through (M_{s1}, M_{1L}) and (M_{s2}, M_{2L}).

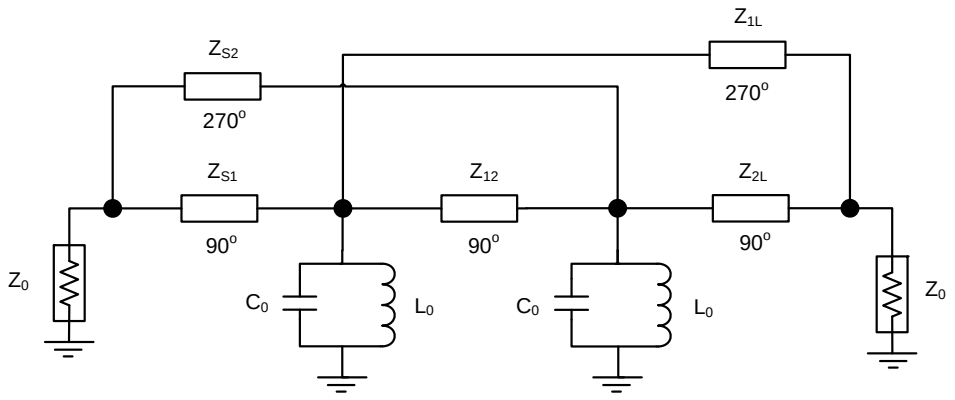

Fig. 6.7 Equivalent circuit of the dual-mode active elliptic filter.

The equivalent circuits of the filters are simulated in Agilent's ADS circuit simulator to obtain their frequency responses. Then, the resonator figure-of-merits of the filters are calculated using (5.14) and compared with each other (Section 4.1.2). Simulation results indicate that the filter with a fractional bandwidth of 1.5%, return loss of 10 dB, and a normalized transmission zero location of 1.2 yields the minimum resonator figure-of-merit for lowest phase-noise. The corresponding filter's coupling matrix is

$$\mathrm{M} = \begin{bmatrix} 0 & 0.675 & -0.258 & 0 \\ 0.675 & 0 & 0.336 & -0.258 \\ -0.258 & 0.336 & 0 & 0.675 \\ 0 & -0.258 & 0.675 & 0 \end{bmatrix}. \tag{6.5}$$

The physical dimensions of the dual-mode filter with the above coupling matrix are calculated here for implementation on a 32 mils thick RO4003® substrate at 8 GHz. The dual-mode resonator's square-loop periphery is a wavelength; corresponding to 950 mils at 8GHz and the microstrip line width is 33 mils. The perturbation size, *d*, is determined by the coupling strength between the two resonators

$$\mathrm{k} = (\mathrm{F.B.W}) \times \mathrm{M}_{12} = 0.015 \times 0.336 = 0.005 \tag{6.6}$$

which, according to Fig. 6.4(b), corresponds to $d = 8$ mils. The input port is coupled to both modes with the following external quality-factors

$$Q_e^h = \frac{1}{(F.B.W) \times M_{s1}^2} = \frac{1}{(0.015) \times 0.675^2} = 146$$

$$Q_e^v = \frac{1}{(F.B.W) \times M_{s2}^2} = \frac{1}{(0.015) \times 0.258^2} = 1001 \quad (6.7)$$

Therefore, according to Fig. 6.5(b), the feeding lines' gap and offset values are determined as $g = 20$ mils and $t = 46.5$ mils, respectively.

The dual-mode active filter is designed on a Roger's RO4003C® substrate and simulated using Agilent's Momentum™ EM solver. The simulated unloaded quality-factor of each resonant mode is 90. The resonant modes are loss compensated by coupling to negative-resistance devices realized by using two NESG2030 SiGe HBT transistors, with 8 dB gain and 2 dB noise figure. The simulated frequency-response of the active filter is shown in Fig. 6.8. The simulation results of a passive filter with similar design parameters are also included for comparison. It can be seen that the active filter provides a lossless transfer characteristic with high loaded quality-factors at its pass-band edge. At the 3-dB band edge, a loaded-quality factor of 550 is achieved. Fig. 6.8(b) shows the noise-figure simulation results where the active filter shows less than 1 dB noise-figure degradation within its pass-band, compared to the passive filter. The active filter's low-noise performance is due to minimum-noise design of the loss compensation networks. The high-Q and low-noise properties of the dual-mode active filter make it attractive for low phase-noise oscillator designs, as discussed in the subsequent section.

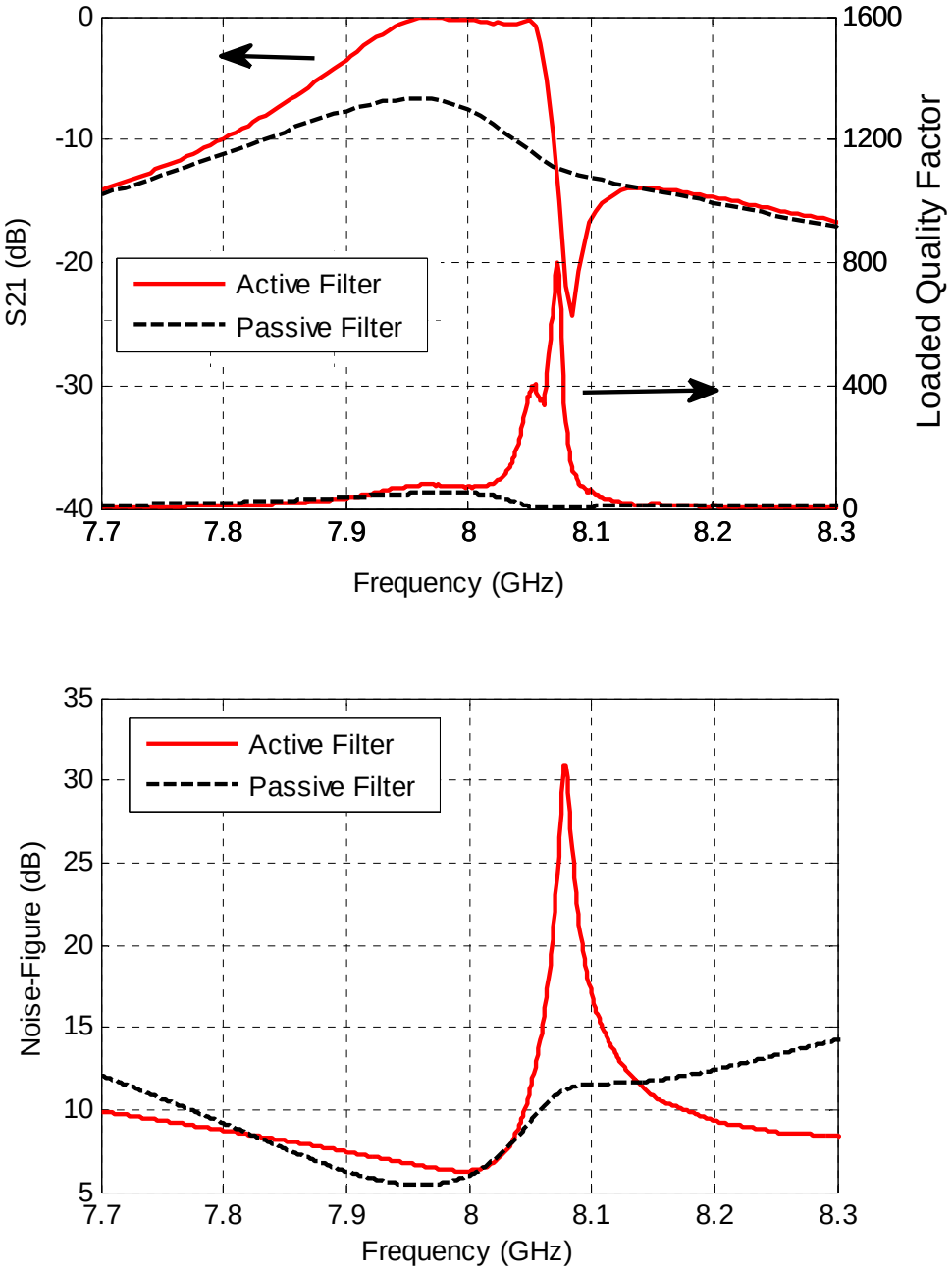

Fig. 6.8 Simulated (a) frequency response and (b) noise-figure of the dual-mode active filter. The simulation results of a similar passive filter are also included for comparison.

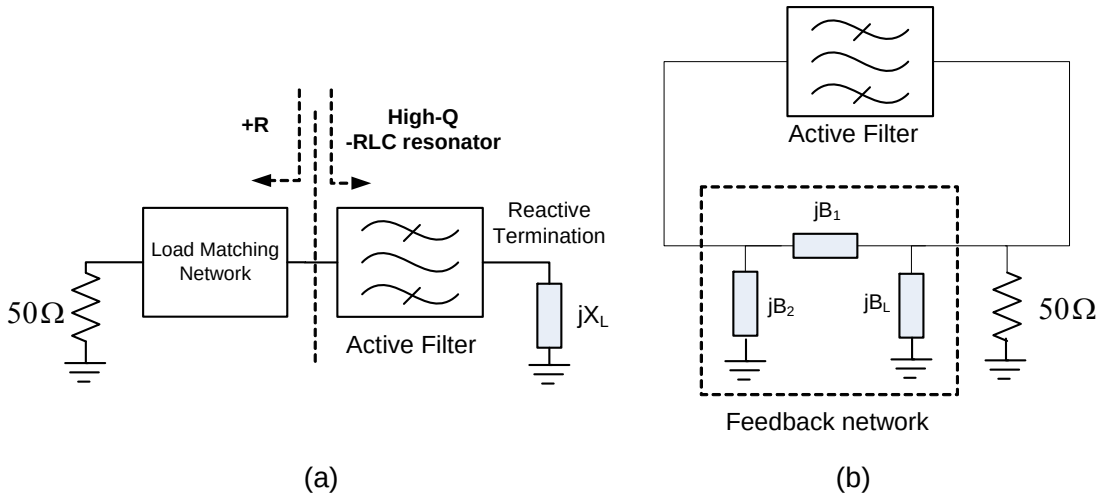

Fig. 6.9 Oscillator design using an active filter in a (a) series or (b) parallel feedback configuration

6.2 Oscillator Design Methodology

The oscillator's block diagram is shown in Fig. 6.9, consisting of an active elliptic filter and a (a) series or (b) parallel feedback network. In this configuration, the active filter provides a high frequency-selectivity for low phase-noise and, at the same time, initiates and sustains oscillation. This is achieved by designing the active filter's loss compensation networks such that they over-compensate the losses of the resonators; namely, the amount of energy produced by the active devices exceeds the energy dissipation. Therefore, the active filter becomes potentially unstable and provides a positive loop-gain required for oscillation startup. The active filter is then embedded within a feedback network to boost the instability and design an oscillator. In this section we explain the oscillator's design procedure in two steps: starting with the active filter, followed by the design of the feedback network.

6.2.1 Positive-Gain Active Filter Design

The active filter is implemented using the dual-mode active resonator discussed in the preceding section. Fig. 6.10(a) shows the filter's structure, where each resonant mode is coupled to a negative-resistance device for loss compensation. The negative-resistance

networks are designed by providing reactive terminations to the base and collector terminals of NESG2030M04 SiGe HBT transistors. The optimum reactance values are determined as X_s = -180 ohms and X_g = -50 ohms; based on the low-noise design procedure introduced in Section 5.1.2. The loading effects of the negative-resistance devices on the resonant modes are represented by the quality-factor Q_{-r}.

In order to a make the active filter potentially unstable for startup of oscillation, the couplings to negative-resistances are increased (Q_{-r} decreased) so that the losses of the resonators are overcompensated. In Section 5.1.2 of Chapter 5, it was shown that a lossless resonator is achieved when Q_{-r} is set equal to the unloaded quality-factor of the passive resonator, Q_u. Similarly, one can conclude that

$$\begin{cases} \frac{Q_{-r}}{Q_u} > 1 & \text{lossy resonator} \\ \frac{Q_{-r}}{Q_u} = 1 & \text{lossless resonator} \\ \frac{Q_{-r}}{Q_u} < 1 & \text{positive-gain active resonator.} \end{cases} \tag{6.8}$$

Therefore, once $Q_{-r} < Q_u$, the losses of the resonant modes are overcompensated and the active filter becomes unstable exhibiting positive insertion and reflection gains. This is illustrated in Fig. 6.10(b) where it shows the frequency response of the active filter for various ratios of Q_{-r} to Q_u. As it can be seen, the active filter's pass-band edge is the most unstable area suitable for the design of an oscillator. Interestingly, at these frequencies, the active filter also achieves its highest frequency-selectivity, resulting in oscillator's low phase-noise operation.

The ratio of Q_{-r} to Q_u, indicating the degree of loss compensation in resonators, is a design parameter that should be carefully selected. A small ratio indicates a tight coupling to the negative-resistance device, resulting in a highly overcompensated resonator. This enables a strong oscillation startup with high output power levels. However, the frequency selectivity of the filter is degraded since its resonators are highly loaded with the negative-resistance devices. This phenomenon can be seen in Fig. 6.10(b) where elliptic filters with less coupling to negative-resistance devices (higher Q_{-r}/Q_u

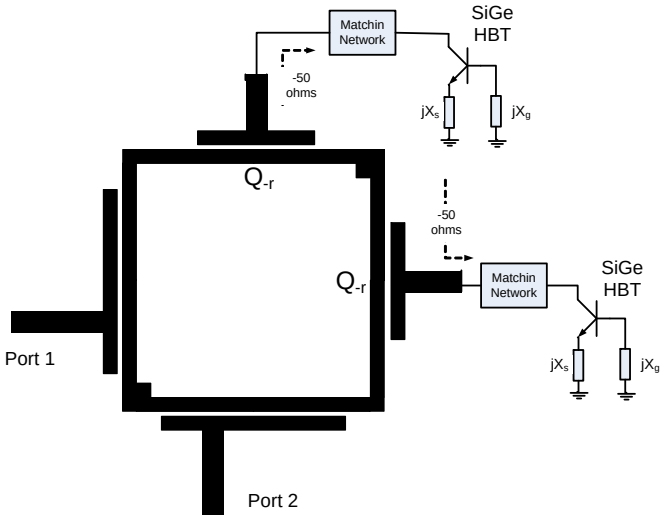

(a)

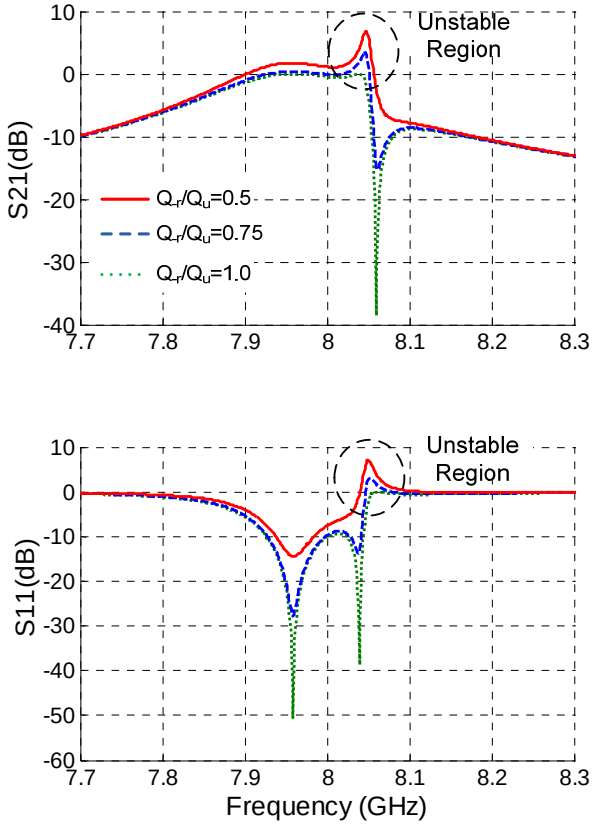

(b)

Fig. 6.10 (a) The proposed dual-mode active elliptic filter suitable for the design of miniaturized low phase-noise oscillators. Each resonant mode is coupled to a -50 Ω resistor for loss compensation. (b) Simulated frequency response of the filter. In the case of loss overcompensation ($Q_{-r} < Q_u$) the active filter shows positive gain at the upper band edge.

ratios) demonstrate sharper filtering response. Therefore, there is a trade-off between frequency-selectivity and power handling capability of active filters. The optimum ratio of Q_{-r} to Q_u depends on the specifics of the transistors and the filter design parameters, and it should be selected based on the simulations to minimize the phase-noise. For the filter under study, implemented on RO4003C® substrate and using NESG2030 transistors, the optimum ratio was determined as $Q_{-r}/Q_u=0.6$.

6.2.2 Oscillator's Feedback Network Design

The active filter with the positive gain is embedded within a parallel or series feedback network to design a low phase-noise oscillator as shown in Fig. 6.9. The design of the oscillator using a parallel feedback network is straightforward following the procedure based on the substitution theory outlined in Section 4.2.1. In this work the oscillator is designed based on the series feedback network, Fig. 6.11(a), due to its simplicity and ease of implementation.

The series feedback is realized by connecting the second port of the filter to a reactive termination, jX_T in Fig. 6.11(a), to boost the filter's instability. The simulated input reflection coefficient of the active filter is shown in Fig. 6.11(b) for two cases of matched and reactive terminations. As it can be seen the reactive termination causes a strong peak in the input reflection coefficient. The peak frequency depends on the termination value, jX_T, and is set at the filter's pass-band edge for highest frequency selectivity and lowest phase-noise. At the vicinity of the peak reflection coefficient, the reactively-terminated active filter behaves like a high-Q LC resonator having a negative resistance in shunt, as shown in the inset of Fig. 6.11(b). The resonator is then connected to the load through the matching network. The matching network is designed based on the well-known device-line theory in order to maximize the oscillation power [20].

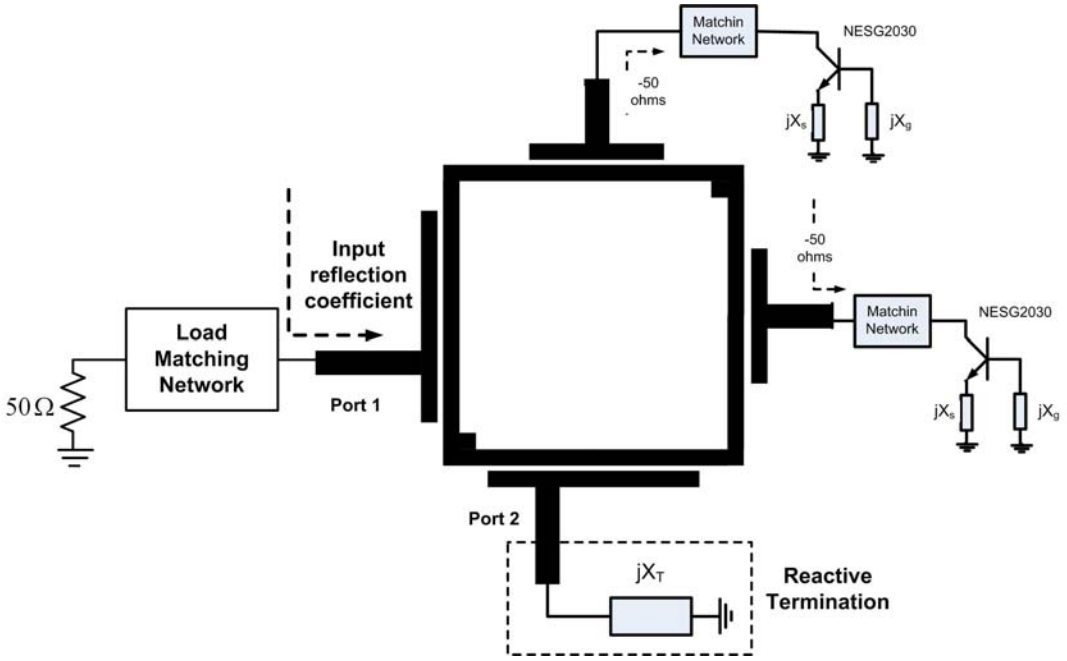

(a)

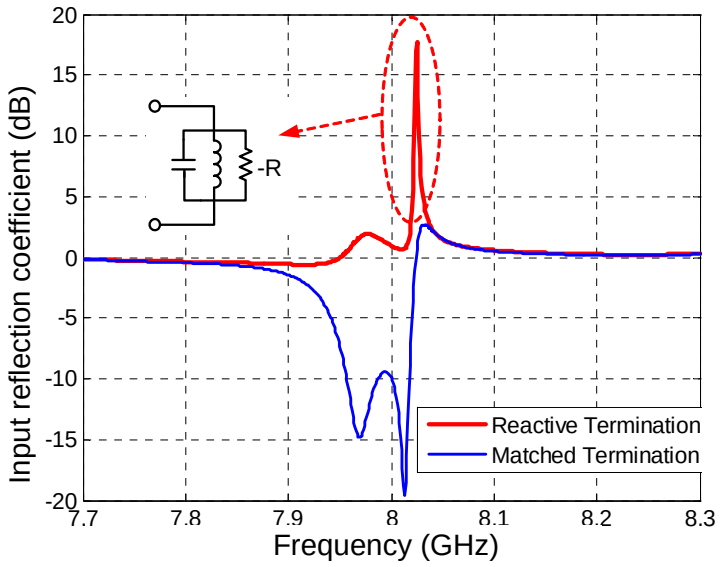

(b)

Fig. 6.11 (a) Circuit schematic of the oscillator consisting of the dual-mode active elliptic filter, reactive termination (X_T), and load matching network. (b) Input reflection coefficient of the active filter. The reactive termination causes a strong peak in the input reflection coefficient. At the vicinity of the peak the reactively terminated active filter behaves like a shunt LC resonator having a negative-resistance in shunt.

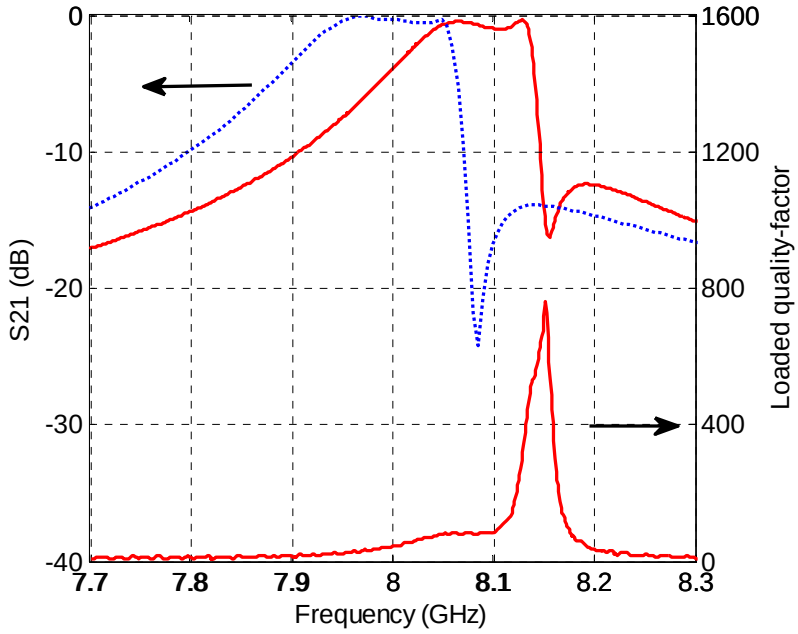

Fig. 6.12 Measured frequency response of the dual-mode active filter. Measurement results are in good agreement with the simulation results (dashed line).

6.3 Measurement Results

Dual-Mode Active Filter

The dual-mode active filter shown in Fig. 6.6 was fabricated on a 32 mils thick RO4003C substrate with a dielectric constant of 3.55. Two NESG2030 SiGe HBT transistors with the gains of 8 dB and noise-figures of 2 dB were utilized in the design of the negative-resistance devices for loss compensation. The measurement results shown in Fig. 6.12 are in good agreement with the simulation results except for a slight shift in the center frequency which is due to fabrication tolerances. As it can be seen a lossless transfer characteristic with a measured loaded-quality factor of 650 at 3- dB pass-band edge has been achieved. This high loaded quality-factor makes the active filter suitable for the design of low phase-noise oscillators. The simulated noise-figure of the active elliptic filter is shown in Fig. 6.8(b) and discussed in Section 6.1.2.

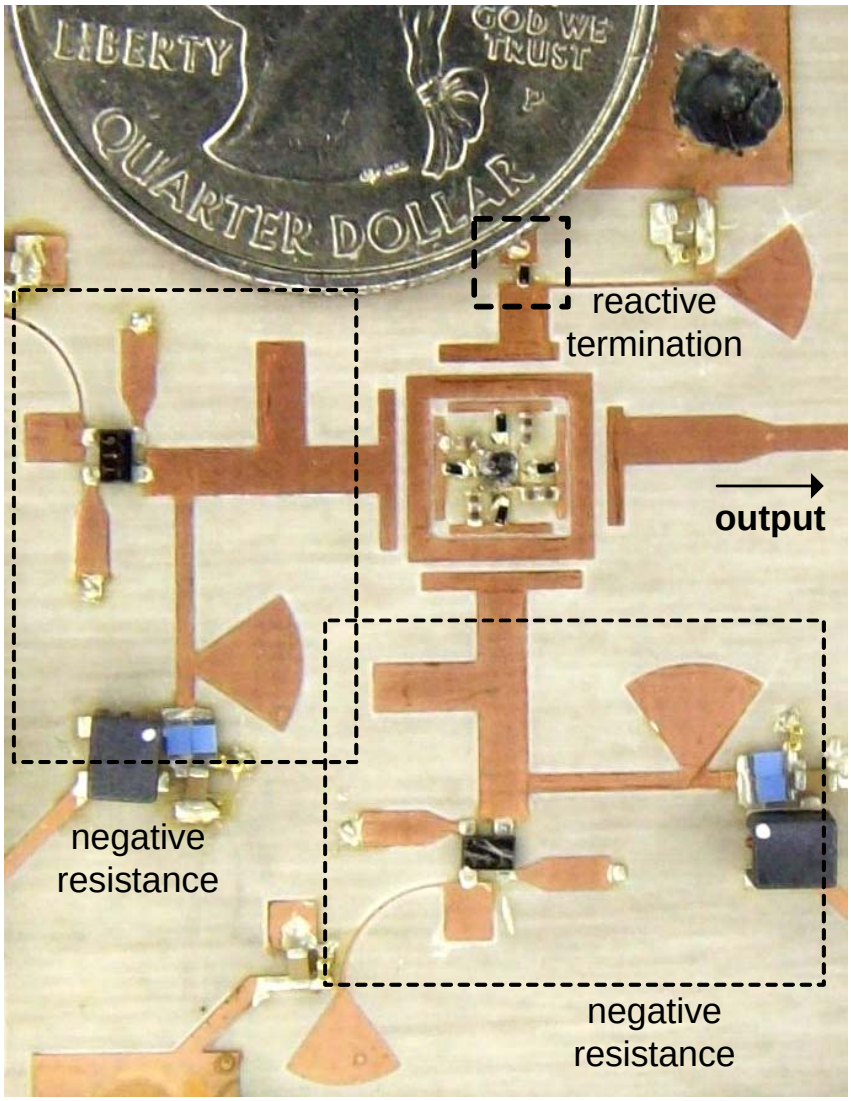

Fig. 6.13 Top view of the fabricated VCO based on a tunable dual-mode active elliptic filter. The circuit schematic of the VCO is shown in Fig. 6.11(a). The design of the dual-mode filter is discussed in Section 6.1.2.

Voltage-Controlled-Oscillator

The fabricated VCO is shown in Fig. 6.13, consisting of the high-Q dual-mode active filter described in the previous section, the reactive termination, and the external load matching network. Two NESG2030M04 SiGe HBT transistors with 2 dB noise-figure and 8 dB associated gain were used to design the negative-resistance devices for

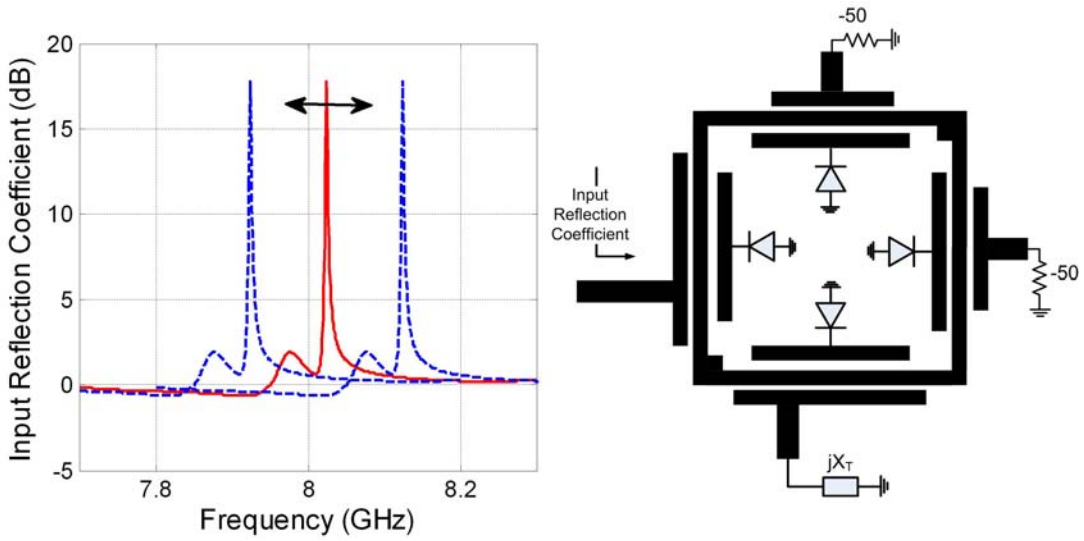

Fig. 6.14 Four diod varactors are coupled to the dual-mode resonator to provide frequency tuning. The varactors change the location of the peak reflection coefficient, hence the oscillation frequency.

TABLE 6.1
VCO's phase-noise degradation versus frequency tuning range compared to a similar free-running oscillator. Phase-noise is degraded due to diod varactors' losses.

Tuning Range	2%	5%	10%
Phase-Noise Degradation	1 dB	2.5 dB	4.8 dB

loss compensation. The physical size of the resonator is 7 × 7 mm^2. A circuit prototyping machine was used in the oscillator fabrication. The most sensitive part of the VCO to fabrication tolerances is the dual-mode filter; specially the inner corner patch perturbations. However, simulation results show that it can tolerate fabrication errors of 25 μm or less without considerable loss of performance.

Frequency tunability is achieved by coupling the dual-mode resonator to variable capacitors (varactors). Four MA46H120 hyperabrupt varactor diodes with capacitance ranges of 0.2-1 pF and quality factors of 15 were attached to the resonant modes for frequency tuning, as shown in Fig. 6.14. The varactors' control voltage of 1-10 volts changes the location of the peak reflection coefficient, thereby tuning the oscillation frequency. The tuning range depends on the degree of the coupling to varactors. A strong

coupling results in a wide tuning range, however, at the cost of phase-noise degradation. This is due to the effect of the varactors' losses which increase the noise-figure of the active elliptic filter. Since, according to the Leeson's formula, the phase-noise of the VCO is directly proportional to the noise-figure of the active filter, varactors' losses degrade the phase-noise of the VCO compared to the free-running oscillator case. Table 6.1 shows the simulated phase-noise degradation versus the tuning range of the VCO.

The measured VCO's oscillation frequency range is 8.150-8.255 GHz. The output power level varies from 6 to 8 dBm across the tuning range, while DC-RF efficiency varies from 9 to12.5 %. The output power level and DC-RF efficiency drop at lower frequencies due to the varactors' quality-factor degradation at small tuning voltages. The VCO's phase-noise is measured by the FM discriminator technique using an Agilent's E5500A phase-noise measurement system. As shown in Fig. 6.15, the VCO shows a measured phase-noise of -149.5 dBc/Hz at 1 MHz frequency offset at 8.2 GHz. The flicker phase-noise corner frequency is approximately 90 KHz. The phase-noise variations versus the tuning voltage are plotted in Fig. 6.16. Phase-noise degrades for tuning voltages below one volt due to the decreased quality-factors of the varactors. To the best of author's knowledge, the VCO presented here demonstrates the lowest phase-noise among microwave planar oscillators reported to date. The figure-of-merit (FOM) of the oscillator is calculated using [11]

$$FOM = L(\Delta f) - 20log_{10}\left(\frac{f_0}{\Delta f}\right) + 10log_{10}\left(\frac{P_{DC}}{1mW}\right) \tag{6.9}$$

where $L(\Delta f)$ is the phase-noise, Δf is the frequency offset, f_0 is the oscillation frequency and P_{DC} is the total consumed DC power. The FOM of the VCO is -211.7 dBc/Hz. Table 6.2 compares the performance of several reported VCOs. The VCO presented in this paper achieves the lowest phase-noise and FOM compared to other planar oscillators reported to date.

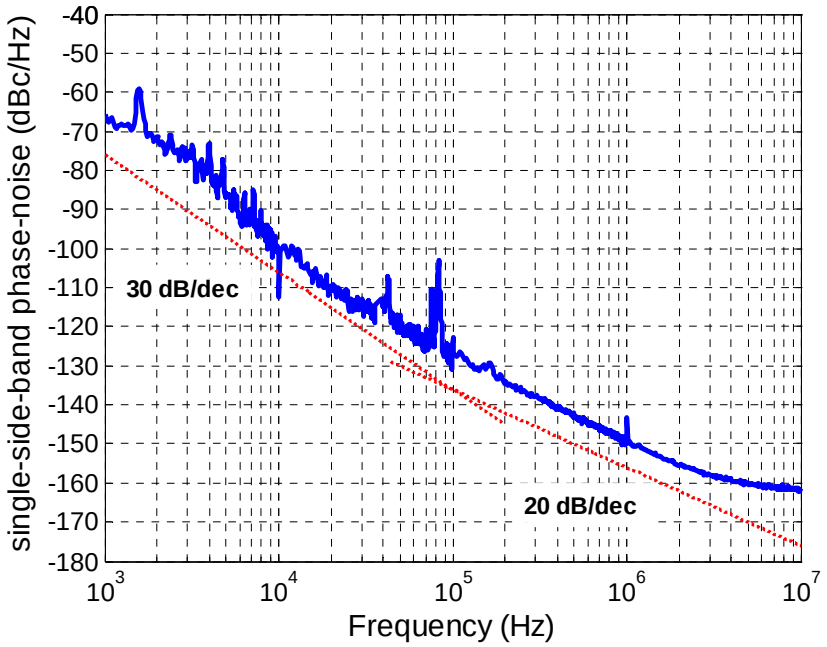

Fig. 6.15 Measured phase-noise of the fabricated VCO at 8.2 GHz. Phase noise at 1 MHz offset from the carrier is about -149.5 dBc/Hz.

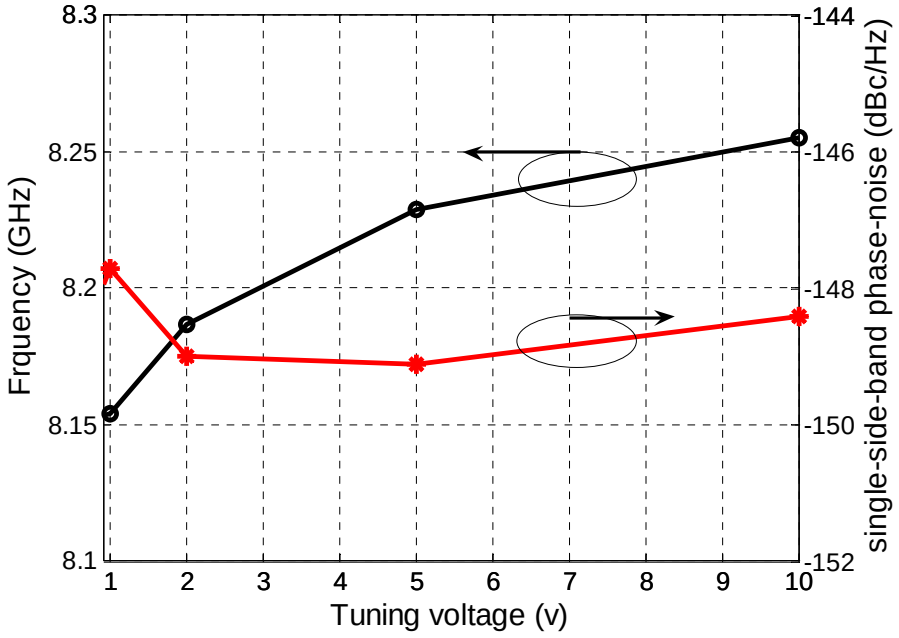

Fig. 6.16 Measured characteristics of the VCO versus varactors' tuning voltage. Phase-noise is measured at 1 MHz frequency offset.

TABLE 6.2
Comparison with other reported planar oscillators

Device	**Resonator**	**F_0 GHz**	**P_0 dBm**	**Tuning Range MHz**	**Efficiency**	**L(f)† dBc/Hz**	**FOM dBc/Hz**
HEMT [7]	Ring	12	5.3	510*	48.7%	-116.2	-189.3
Si BJT [8]	Hair-Pin	9	9	270	4.5%	-129	-185.6
HEMT [26]	Active resonator	10	10	120	2%	-134.4	-187.4
Si BJT [27]	Microstrip line	9.95	7	54	2.5%	-134	-191
SiGe HBT [50] [Chapter 4]	Passive elliptic filter	8.1	3.5	-	10%	-143	-207
SiGe HBT [58] [Chapter 5]	Active elliptic filter	8	10	-	5%	-150	-205
GaInP/GaAs HBT [59]	LC (on chip)	4.87	-4	70	8.3%	-131	-198
SiGe HBT [This Work]	High-Q negative-resistance	8.2	7	105	12.5%	-149.5	-211.7

† Phase-Noise at 1MHz frequency offset * Mechanical tuning

6.4 Conclusion

In this chapter, a low phase-noise voltage-controlled-oscillator was designed employing a compact and tunable high-Q negative-resistance resonator. The resonator is a reactively-terminated active elliptic filter which provides high frequency-selectivity and, at the same time, initiates and sustains oscillation. In this configuration, as opposed to the conventional parallel-feedback oscillators, there is neither a need for an amplifier in the oscillator loop nor for a coupler to deliver the power to the external load, resulting in a simple and compact VCO structure. The active elliptic filter was implemented using a dual-mode square-loop active resonator. The resonant properties of dual-mode resonators were discussed and it was shown that they can be configured to realize compact elliptic filters to achieve high quality-factors while occupying small areas.

The fabricated VCO operates at 8.2 GHz with 105 MHz tuning range. It shows a measured phase-noise of -149.5 dBc/Hz at 1 MHz frequency offset at 8.2 GHz. Its output power level is 7 dBm with 12.5% DC-RF efficiency. The VCO's FOM is -211.7 dBc/Hz. To the best of author's knowledge, both the phase-noise and FOM are the lowest values among published planar oscillators reported to date.

In addition to achieving very low phase-noise levels, the presented VCO possesses a planar structure, occupies a small area, and provides easy frequency tuning. The frequency tunability is particularly important in order to avoid performance degradation and frequency shifting caused by the fabrication tolerances. All these advantages make the presented VCO design technique suitable for integrated low phase-noise VCO design at microwave and millimeter-wave frequencies

Chapter 7

Conclusion

7.1 Summary of Work

This thesis presents novel techniques to design high-Q planar resonators intended for low phase-noise applications. The proposed methods can be applied to design miniaturized very low phase-noise voltage-controlled-oscillators at microwave and mm-wave frequencies.

In Chapter 2, the fundamentals of phase-noise in oscillators are discussed. Leeson's formula for phase-noise is revisited and it is generalized to oscillators with complex resonant structures. Lesson's phase-noise formula employs the term "loaded quality factor", the definition of which is critical to understanding resonator design for low phase-noise oscillators. This issue is addressed in Chapter 3 where different definitions of resonator quality-factor were discussed and compared to each other. A figure-of-merit for resonators is introduced in order to evaluate their overall effect on the phase-noise of oscillators. This figure-of-merit serves as a basis for optimizing the design of various resonators for low phase-noise applications.

A quality-factor enhancement technique based on employing multiple-resonator band-pass filters is introduced in Chapter 4. It is shown that band-pass filters, and in particular elliptic-response filters, can provide significantly higher quality factors compared to single resonators. This is due to the existence of multiple resonators and the presence of close to pass-band zeros in their transfer functions, which help increase frequency selectivity. The effect of various filter parameters, such as order, bandwidth, return loss, and location of transmission zeros, are discussed. A procedure

is introduced to optimize the design of elliptic filters for low phase-noise oscillators. The proposed method is experimentally verified by designing an 8 GHz oscillator employing a four-pole elliptic filter as its frequency stabilization element.

In Chapter 5, the application of active resonators for low phase-noise oscillators is discussed. Active resonators are analyzed and a design procedure is introduced to optimize their performance for low-noise applications. Analytical expressions for the noise figure and power consumption in active resonators are derived. These equations provide an insight into the design of active resonators for low phase-noise oscillators. It is shown that, despite their excess noise, active resonators can be used to design very low phase-noise oscillators, however, at the cost of increased power consumption. In other words, they compromise the DC-to-RF power efficiency for lower phase-noise. This problem can be mitigated by designing active elliptic filters. These filters can provide high quality-factors at lower power consumptions compared to single active resonators. An 8 GHz oscillator is designed by employing a four-pole active elliptic filter. The oscillator achieved a record phase-noise performance due to the high loaded quality-factor of the filter.

The oscillator described in Chapter 5 achieves a state-of-the-art phase-noise performance and possesses a planar structure which makes it suitable for implementation in hybrid circuit fabrication technology. However, it is not amenable to integrated circuit design due to its relatively large area and high power consumption. In Chapter 6, a new design technique is introduced that offers significant advantages in terms of size, power consumption and frequency tunability. The proposed oscillator's core is a reactively terminated active elliptic filter that acts like a high-Q negative-resistance resonator. In this configuration, the active filter provides high frequency-selectivity and, at the same time, initiates and sustains the oscillation. Therefore, as opposed to the conventional parallel feedback technique, there is neither a need for an amplifier in the oscillator loop, nor for a coupler to deliver power to the external load, leading to considerable DC power savings and a compact oscillator structure. The active filter is designed using a dual-mode active resonator. This technique not only helps reduce the oscillator's size, but also eases the frequency tunability. An X-band voltage-controlled-oscillator is

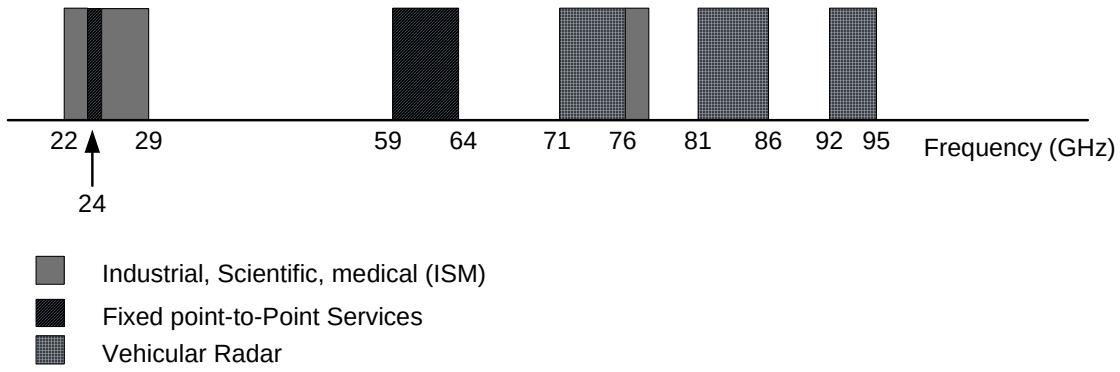

Fig. 7.1 The millimeter-wave band allocation in United States [60].

designed based on the proposed technique. The oscillator achieves a state-of-the-art phase-noise and figure-of merit (FOM) among planar oscillators reported to date. The proposed VCO structure occupies a relatively small area making it suitable for integrated circuit fabrication at mm-wave frequencies.

7.2 Future Work

Although the design techniques presented here are demonstrated at X-band in hybrid circuits, they are applicable to mm-wave integrated circuit fabrication. The explosive growth of wireless data such as Wi-Fi has triggered significant research into development of new architectures for radio transceivers that could deliver very high data rates, particularly for video and personal area networks. For these reasons, today we witness a very high interest in communication systems at millimeter-waves. Other important applications include automotive radar for safety and improved driving. The Federal Communication Commission (FCC) has allocated several frequency bands at millimeter-waves for high data rate wireless communication. Fig. 7.1 shows selected parts of the FCC-allocated frequency spectrum [60]. For example the 60-GHz band is used for unlicensed short-range data links with data rates up to 2.5 Gb/s. also shown are the frequency allocations for automotive radar at 24 GHz and 77 GHz.

Integrated low phase-noise oscillators are commonly designed using LC-tank resonators due to size considerations. Unfortunately, integrated inductors and capacitors demonstrate very low quality-factors ranging from 5 to 15. Furthermore, at mm-wave frequencies, solid-sate devices possess several fundamental limitations including low intrinsic gain, high noise-figure and low power handling, all of which make the design of low phase-noise integrated oscillators quite challenging at high frequencies. Recently, transmission-line-based resonators have received increasing attention for integrated oscillator design [61]-[63]. These resonators can provide high quality-factors while occupying a small area due to small wavelengths at mm-wave frequencies.

The VCO design technique introduced in Chapter 6 is suitable for integrated circuit designers since, in addition to achieving very low phase-noise levels, it occupies a small area and provides easy frequency tuning. The frequency tunability is particularly important in order to avoid performance degradation and frequency shifting caused by the process variations. Fig. 7.2 shows the modified version of the VCO suitable for implementation in standard CMOS circuit fabrication technologies. The loss compensation networks have been redesigned using differential negative resistances. In analog integrated circuits, differential negative resistances are preferred due to their ease of implementation, stability, and more immunity to substrate and environment noises, as compared to single-ended negative resistances used in Chapter 6. Each differential negative resistance is realized using two cross-coupled MOSFET transistors. The cross-coupled differential pair is a well-known architecture and its design for low-noise applications has been widely addressed in the literature [64]. The four differential varactors attached to the resonator provide for frequency tuning

To demonstrate the capabilities of the resonator shown in Fig. 7.2(b) for low phase-noise integrated circuit applications, it was designed and simulated at 24 GHz for IBM 0.13-μm CMOS fabrication process. The resonator is laid out on the 4 μm thick aluminum last metal layer which is 14 μm above the first metal layer used as the ground plane. The overall size of the resonator is $\lambda/8 \times \lambda/8$ corresponding to 900 μm^2 at 24 GHz. Further size reductions can be readily achieved based on the techniques introduced in [65]-[67]. The passive part of the resonator was simulated in Momentum® 2.5-D EM

solver. The resulting S-parameters were imported into Cadence SpctreRF® circuit simulator where the whole active resonator was simulated including the transistors and bias circuits. Fig. 7.3 shows the simulated frequency response and noise-figure of the active filter. At 24.1 GHz, the active filter achieves a loaded quality-factor of 325 with 17 dB noise-figure. The very high-Q characteristic of this resonator is very promising for integrated low phase-noise oscillator designs.

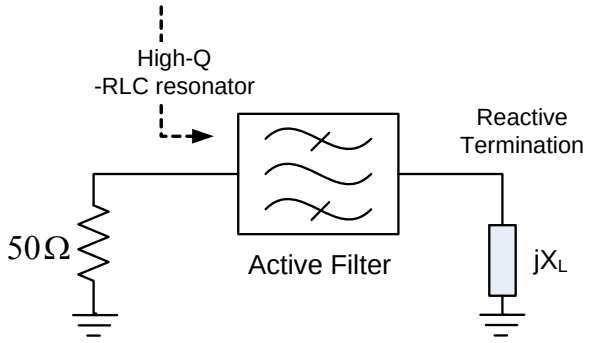

(a)

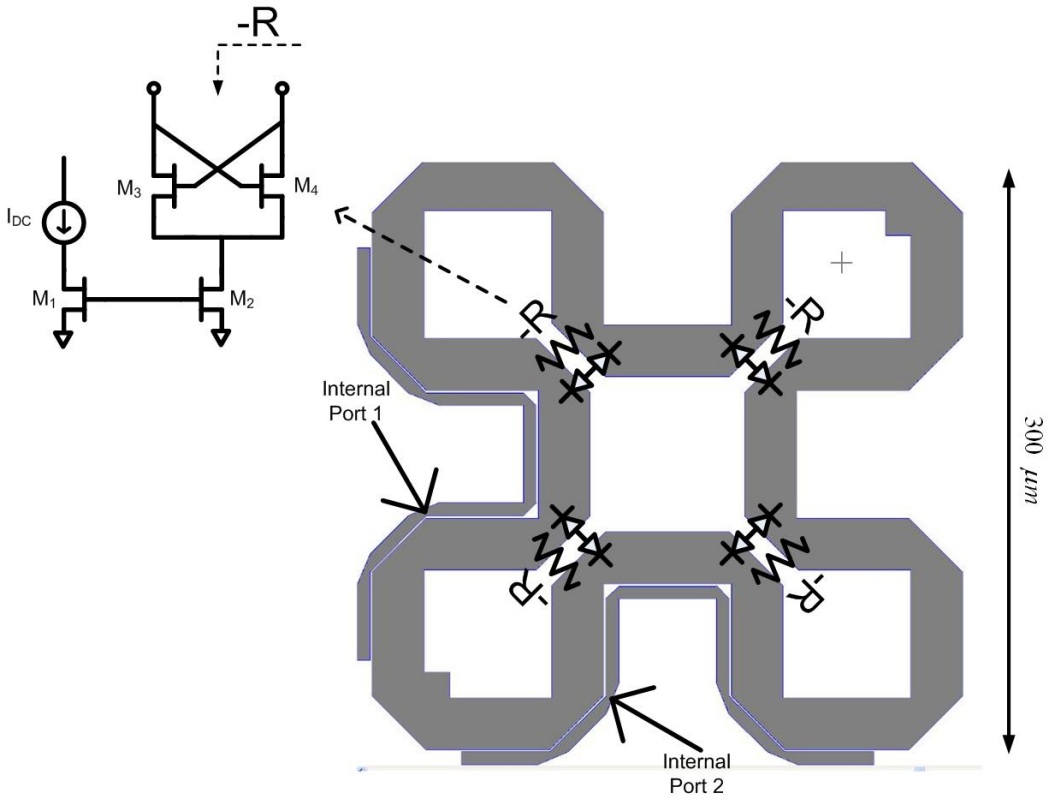

Device	M_1	M_2	M_3	M_4	I_{DC}	V_{DD}
Size	15/0.13 μm	15/0.13 μm	25/0.13 μm	25/0.13 μm	1.5mA	1.2 V

Fig. 7.2 (a) The proposed VCO block diagram, and (b) implementation of the dual-mode active filter suitable for CMOS integrated fabrication processes. The table shows the design parameters for the implementation using IBM 0.13-μm CMOS process at 24 GHz.

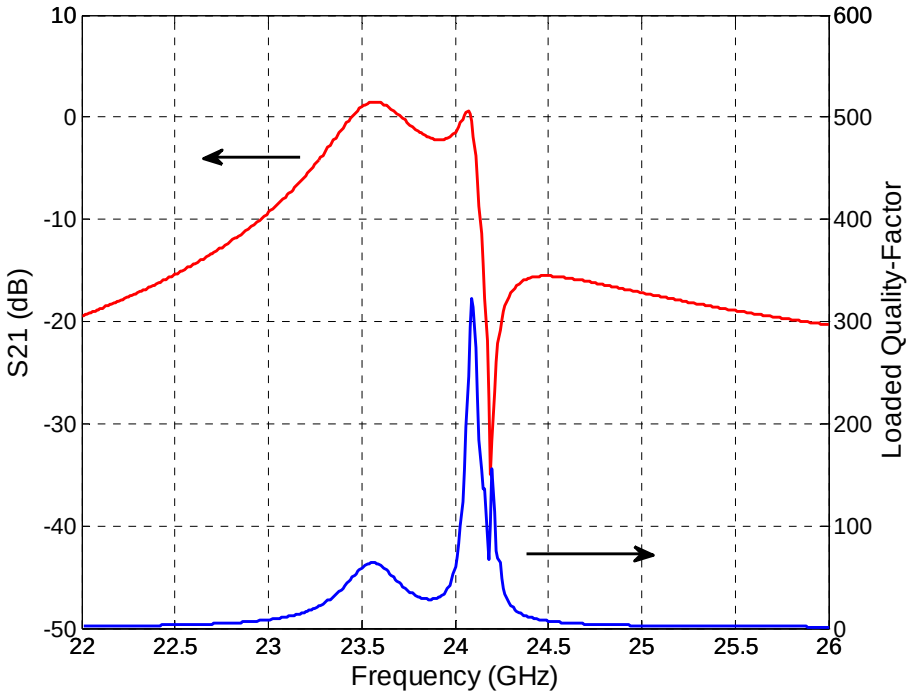

(a)

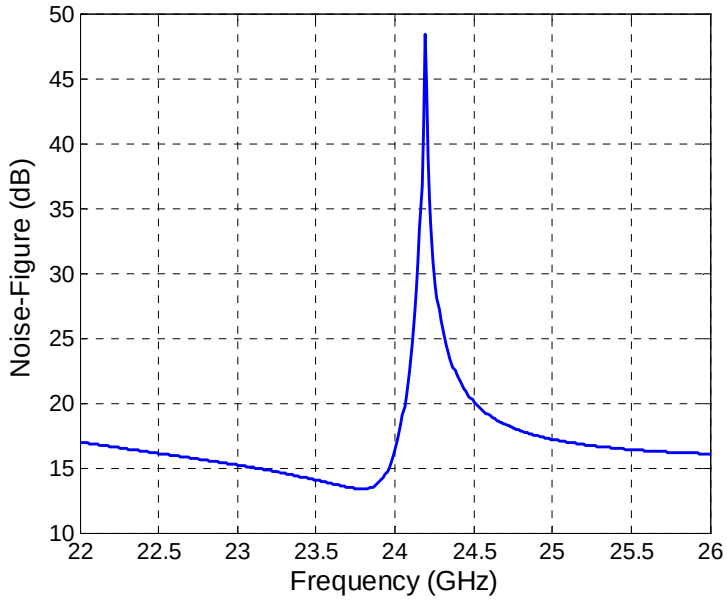

(b)

Fig. 7.3 Simulated (a) frequency response and (b) noise figure of the dual-mode active resonator designed for IBM 0.13-µm CMOS fabrication process at 24 GHz.

Bibliography

[1] T. C. W. Schenk, X. J. Tao, P. F. M. Smulders, E. R. Fledderus, "On the influence of phase noise induced ICI in MIMO OFDM systems," *IEEE Communications Letters*, vol. 9, no. 8, pp. 682-684, August 2005.

[2] L. Piazzo, and P. Mandarini, "Analysis of phase noise effects in OFDM modems," *IEEE Trans. Communications*, vol. 50, no. 10, pp. 1696-1705, October 2002.

[3] S. J. Fiedziuszko, and S. Holme, "Dielectric resonators raise your high-Q," *IEEE Microwave Magazine*, vol. 2, no. 3, September, 2001.

[4] P. Vryonides, S. Nikolaou, and H. Haralambous, "24 GHz low phase noise HBT dielectric resonator oscillator," *IEEE 11th annual Wireless and Microwave Technology Conference*, pp. 1-4, 2010.

[5] C. Perez, D. Floriot, P. Maurin, P. Bouquet, P. M. Guitierrez, J. Obregon, and S. A. Delage, "Exteremely low noise InGaP/GaAs HBT oscillator at C-band," *IEE Electronics Letters*, vol. 34, no. 8, pp. 813-814, April 1998.

[6] Hittite Microwave Corporation , "HMC-C200 Dielectric resonator oscillator module", Datasheet, http://www.hittite.com/content/documents/data_sheet/hmc-c200.pdf.

[7] L.-H. Hsieh, and K. Chang, "High-efficiency piezoelectric-transducer tuned feedback microstrip ring-resonator oscillators operating at high resonant frequencies," *IEEE Trans. Microw. Theory Tech.*, vol. -51, no. 4, pp. 1141-1145, April 2003.

[8] L. Dussopt, D. Guillois, and G. M. Rebeiz, "A low phase noise silicon 9 GHz VCO and 18 GHz push-push oscillator," in *IEEE MTT-S Int. Microwave Symp. Dig.*, vol. 2, June 2002, pp. 695-698.

[9] K. B. Ostman, S. T. Sipila, I. S. Uzunov, N. T. Tchamov, “Novel VCO architecture using series above-IC FBAR and parallel LC resonance,” *IEEE J. Solid-State Circuits*, vol. 41, no. 10, pp. 2248-2256, October 2006.

[10] D. Ham, and W. Andress, “A circular standing wave oscillator,” *IEEE Solid-State Circuits Conference*, February 2004.

[11] M. Tiebout, “Low-power low-phase-noise differentially tuned quadrature VCO design in standard CMOS,” *IEEE J. Solid-State Circuits*, vol. 36, no. 7, pp. 1018-1024, Jul. 2001.

[12] W.P. Robins, “*Phase Noise in Signal Sources*” London: IEE Telecommunications Series 9, 1982.

[13] T. H. Lee, A. Hajimiri, “Oscillatator phase-noise: a tutorial,” *IEEE J. Solid-State Circuits*, vol. 35, no. 3, pp. 326-336, March 2000.

[14] A. Hajimiri and T. H. Lee, “A general theory of phase noise in electrical oscillators,” *IEEE J. Solid-State Circuits*, vol. 33, no. 2, pp. 179-194, Feb. 1998.

[15] D.B. Sullivan , "Characterization of Clocks and Oscillators” *National Bureau of Standards Tech. Note*, TN-1337.

[16] D. B. Leeson, “A simple model of feedback oscillator noise spectrum,” in *Proc. IEEE*, vol. 54, Feb. 1966, pp. 329-330.

[17] E. Mehrshahi and F. Farzaneh, “An analytical approach in calculation of noise spectrum in microwave oscillators based on harmonic balance,” *IEEE Trans. Microwave Theory Tech.*, vol. MTT-48, no. 5, pp. 822-831, May 2000.

[18] V. Rizolli, F. Masteri, and D. Masotti, “General noise analysis of nonlinear microwave circuits by piecewise harmonic balance technique,” *IEEE Trans. Microwave Theory Tech.*, vol. MTT-42, no. 5, pp. 807-819, May 1994.

[19] A. Demir, A. Mehrotra, and J.Roychowdhury, “Phase noise in oscillators: a unifying theory and numerical methods for characterization,” *IEEE Trans. Circuits Syst. I*, vol. 47, no. 5, pp. 655 – 674, May 2000.

[20] A. Grebennikov, “*RF and microwave transistor oscillator design*,” New York: J. Wiley & Sons, 2007.

[21] K. K. Clarke, T. T. Hess, “*Communication circuits: analysis and design*,” Krieger Pub. Co., 1994.

[22] G. Sauvage, “Phase Noise in Oscillators: a Mathematical Analysis of Leeson’s Model” *IEEE Trans. Instrumentation and Measurement*., vol. IM-26, no. 4, pp. 408-410, Dec. 1977.

[23] B. Razavi, “A study of phase-noise in CMOS oscillators,” *IEEE J. Solid-State Circuits*, vol. 31, no. 3, pp. 331-343, March 1996.

[24] F. Herzel, “An Analytical Model for the Power Spectral Density of a Voltage-Controlled Oscillator and Its Analogy to the Laser Linewidth Theory”, *IEEE Transactions on Circuits and Systems – I: Fundamental Theory and Applications*, vol. 45, pp. 904–908, Sept. 1998.

[25] J. K. A. Everard, “Low-noise power-efficient oscillators: theory and design,” IEE Proc., vol. 133, Pt. G, no. 4, pp. 172-180, Aug. 1986.

[26] Y.-T. Lee, J. Lee, and S. Nam, “High-Q active resonators using amplifiers and their applications to low-phase noise free-running and voltage-controlled oscillators,” *IEEE Trans. Microw. Theory Tech*., vol. -52, no. 11, pp. 2621-2626, Nov. 2004.

[27] A. P. S. Khanna, E. Topacio, E. Gane, and D. Elad, “Low jitter silicon bipolar based VCOs for applications in high speed optical communication systems” in *IEEE MTT-S Int. Microwave Symp. Dig.*, May 2001, pp. 1567-1570.

[28] E. Park, and C. Seo, “Low phase-noise oscillator using microstrip square open loop resonator,” in *IEEE MTT-S Int. Microwave Symp. Dig*., June 2006, pp. 585-588.

[29] Y.-T. Lee, J.-S. Lim, C.-S. Kim, D. Ahn, and S. Nam, “A compact-size microstrip spiral resonator and its application to microwave oscillator,” *IEEE Microw. Wireless Compon. Lett.*, vol. 12, no. 10, pp. 375-377, Oct. 2002.

[30] M. M. Driscoll, “The use of multi-pole bandpass filters and other multiple resonator circuitry as oscillator frequency stabilization elements,” in *Proc. 50th Annu. Frequency Control Symp.*, June, 1996, pp. 782-789.

[31] J. Hong, and M. J. Lancaster, “*Microstrip filters for RF/microwave applications*,” New York: J. Wiley & Sons, 2001.\

[32] K. L. Kotzebue, “A technique for the design of microwave transistor oscillator,” *IEEE Trans. Microw. Theory Tech*., vol. -32, pp. 719-722, Jul. 1984.

[33] J. Choi, and A. Mortazawi, “*Microwave Oscillators*,” in Encyclopedia of RF and Microwave Engineering, Hoboken, NJ: Wiley, 2005, vol. 3, 2818-2827.

[34] J. Choi, and A. Mortazawi, “A new X-band low phase-noise multiple-device oscillator based on the extended-resonance technique,” *IEEE Trans. Microw. Theory Tech*., vol. -55, no. 8, pp. 1642-1648, August 2007.

[35] K. Hoffmann, and Z. Skvor, "Active resonator," *Int. Conf. Trends. Communications, EUROCON'2001*, vol. 1, pp. 164–166, Jul. 2001.

[36] P. Alinikula, R. Kaunisto, and K. Stadius, "Monolithic active resonators for wireless applications," in *IEEE MTT-S Int. Microwave Symp. Dig*., vol. 2, May 1994, pp. 1151-1154.

[37] C. Cenac, B. Jarry, and P. Guillon, "X-band active filters with half-wave or ring resonators and variable gain and phase monolithic circuits," *Microwave Opt. Techno. Lett*., vol. 11, no. 5, pp. 254–257, Apr. 1996.

[38] C.-Y. Chang, and T. Itoh, "Microwave active filters based on coupled negative resistance method," *IEEE Trans. Microw. Theory Tech*., vol. -38, no. 12, pp. 1879-1884, Dec. 1990.

[39] B. P. Hopf, I. Wolff, and M. Guglielmi, "Coplanar MMIC active bandpass filters using negative resistance circuits," *IEEE Trans. Microw. Theory Tech*., vol. -42, no. 12, pp. 2598-2602, Dec. 1994.

[40] U. Karacaoglu, and I. D. Robertson, "MMIC active bandpass filters using varactor-tuned negative resistance elements," *IEEE Trans. Microw. Theory Tech*., vol. -43, no. 12, pp. 2926-2932, Dec. 1995.

[41] J. Lee, Y.-T. Lee, and S. Nam, "A phase noise reduction technique in microwave oscillator using high-Q active filter," *IEEE Microw. Wireless Compon. Lett.*, vol. 12, no. 11, pp. 426-428, Nov. 2002.

[42] Y. Sun, J. L. Tauritz, and R. G. F. Baets, "Silicon monolithic balanced oscillators using on-chip suspended active resonators," *IEEE Radio Frequency Integrated Circuits Symp.*, pp. 149-152, June 1998.

[43] Y. Ishikawa, S. Yamashita, and S. Hidaka, "Noise design of active feedback resonator BEF," *IEEE Trans. Microw. Theory Tech.*, vol. -41, no. 12, pp. 2133-2138, Dec. 1991.

[44] H. Ezzedine, L. Billonnet, B. Jarry, and P. Guillon, "Optimization of noise performance for various topologies of planar microwave active filters using noise wave techniques," *IEEE Trans. Microw. Theory Tech.*, vol. -46, no. 12, pp. 2484-2492, Dec. 1998.

[45] H. A. Hauss, and R. B. Adler, "*Circuit theory of linear noisy networks*," New York: Wiley, 1959.

[46] P. Penfield, "Noise in negative-resistance amplifiers," *IRE Trans. Circuits Theory*, vol. CT-7, pp. 166-170, June 1956.

[47] P. Gardner, and D. K. Paul, “Optimum noise measure configurations for transistor negative resistance amplifiers,” *IEEE Trans. Microw. Theory Tech*., vol. -45, no. 5, pp. 580-586, May 1997.

[48] C.-M. Tsai, and H.-M. Lee, “The effects of component Q distribution on microwave filters,” *IEEE Trans. Microw. Theory Tech.*, vol. -54, no. 4, pp. 1545-1553, Apr. 2006.

[49] J. J. Rael, A. A. Abidi, “Physical processes of phase-noise in differential LC oscillators,” in *Proc. of Custom Integrated Circuits Conference*, pp. 569-572, May 2000.

[50] J. Choi, M. Nick, and A. Mortazawi, “Low-phase-noise planar oscillators employing elliptic-response bandpass filters” *IEEE Trans. Microw. Theory Tech.*, vol. -57, no. 8, pp. 1959-1965, Aug. 2009.

[51] C. Y. Hsu, H. R. Chuang, and C. Y. Chen, “Design of 60-GHz millimeter-wave CMOS RFIC-on-chip bandpass filter,” *Proc. of the 37th European Microwave Conference*, pp. 672-675, October 2007.

[52] J C. Lugo, and J. Papapolymerou, “Dual-Mode reconfigurable filter with assymetric transmission zeros and center frequency control,” *IEEE Microw. Wireless Compon. Lett.*, vol. 16, no. 6, pp. 499-501, Sept 2006.

[53] A. Gorur, “Realization of a dual-mode bandpass filter exhibiting either a Chebyshev or elliptic characteristic by changing perturbation’s size,” *IEEE Microw. Wireless Compon. Lett.*, vol. 14, no. 3, pp. 118-120, March 2004.

[54] A. Gorur, C. Karpuz, and M. Akpinar “A reduced-size dual-mode bandpass filter with capacitively loaded open-loop arms,” *IEEE Microw. Wireless Compon. Lett.*, vol. 13, no. 9, pp. 385-387, Sept 2003.

[55] J. S. Hong, and M. J. Lancaster, “Microstrip bandpass filter using degenerate modes of a novel meandered loop resonator,” *IEEE Microw. Wireless Compon. Lett*., vol. 5, no. 11, pp. 371-372, Nov. 1995.

[56] A. Gorur, “Description of coupling between degenerate modes of a dual-mode microstrip loop resonator using a novel perturbation arrangement and its dual-mode bandpass filter applications” *IEEE Trans. Microw. Theory Tech.*, vol. 52, no. 2, pp. 671-677, Feb. 2004.

[57] S. Amari, “Comments on “Description of coupling between degenerate modes of a dual-mode microstrip loop resonator using a novel perturbation arrangement and its dual-mode bandpass filter applications” *IEEE Trans. Microw. Theory Tech.*, vol. 52, no. 9, pp. 2190-2192, Sept. 2004.

[58] M. Nick, and A. Mortazawi, "Low phase-noise planar resonators based on low-noise active resonators" *IEEE Trans. Microw. Theory Tech.*, vol. 55, no. 5, pp. 1133-1139, May 2010.

[59] A. Victor, and M. B. Steer, "Reflection coefficient shaping of a 5-GHz voltage-tuned oscillator for improved tuning" *IEEE Trans. Microw. Theory Tech*., vol. -55, no. 12, pp. 2488-2494, Dec. 2007.

[60] Ali. M. Niknejad, and H. Hashemi, "*mm-Wave silicon technology: 60 GHz and beyond*" Springer, 2007.

[61] J. C. Chien, and L. H. Lu, "Design of wide-tuning-range millimeter-wave CMOS VCO with a standing-wave architecture, " *IEEE J. Solid-State Circuits*, vol. 42, no. 9, pp. 1942-1952, Sept. 2007.

[62] M. Varonen, M. Karakkainen, M. Kantanen, and K. A. I. Halonen, "Millimeter-Wave integrated circuits in 650-nm CMOS, " *IEEE J. Solid-State Circuits*, vol. 43, no. 9, pp. 1991-2002, Sept. 2008.

[63] W. F. Andress, and D. ham, "Standing wave oscillators utilizing wave adaptive tapered transmission lines, " *IEEE J. Solid-State Circuits*, vol. 40, no. 3, pp. 638-651, March 2005.

[64] T. H. Lee, "*The design of CMOS radio-frequency integrated circuits*," Cambridge University Press, 2003.

[65] J. S. Hong, H. Shaman, and Y. H. Chun, "Dual-Mode microstrip open-loop resonators and filter," *IEEE Trans. Microw. Theory Tech*., vol. -55, no. 8, pp. 1764-1770, August 2007.

[66] A. Gorur, C. Karpuz, and M. Akpinar, "A reduced-size dual-mode bandpass filter with capacitively loaded open-loop arms," *IEEE Microw. Wireless Compon. Lett*., vol. 13, no. 9, pp. 371-372, September 2003.

[67] B. L. Ooi, and Y. Wang "Novel miniaturized open-square-loop resonator with inner split ring loadings," *IEEE Trans. Microw. Theory Tech*., vol. -54, no. 7, pp. 3098-3103, July 2006.